NTNU – Trondheim
Norwegian University of
Science and Technology

Organic Contaminations in Sub-Marine AC and DC High-Voltage Cables

Martin Vandbakk

Master of Science in Physics and Mathematics
Submission date: June 2012
Supervisor: Jon Andreas Støvneng, IFY
Co-supervisor: Sverre Hvidsten, SINTEF Energi AS

Norwegian University of Science and Technology
Department of Physics

Abstract

In dielectric insulating materials subjected to alternating electric fields there are energy losses associated with polarization mechanisms and resistivity. A typical dielectric material used for insulation of high voltage sub-marine cables is cross-linked polyethylene (XLPE) produced from polyethylene (PE). Under production, PE can stagnate in high temperature thermal zones and consequently be subjected to thermal oxidation that introduces polar carbonyl groups to the polyethylene chain, which leads to increased energy losses, inferior insulating properties and subsequent degradation and eventually breakdown and failure of the cable.

The oxidized polyethylene can contaminate the insulating material in the form of microscopic particles embedded in the material, that are difficult to detect and separate from the polyethylene granulate. In this work the focus have been on documenting the fundamental properties of the oxidized XLPE contaminations, such as complex permittivity, associated energy losses and breakdown strengths, compared to that of un-oxidized XLPE.

In this thesis the thermal oxidation process of XLPE and PE has been studied in order to determine the degree of oxidation and carbonyl contents, using Fourier transform infra red spectroscopy. Three real contaminations was found, investigated and categorized. The contaminations was replicated through thermal oxidation of XLPE samples in a ventilated heat cabin at 170°C.

The electrical properties of replicated contaminations has been investigated using dielectric spectroscopy and breakdown strength-tests. At 50Hz the real relative permittivities is measured to be $\epsilon' = 2.30$ for un-oxidized XLPE, $\epsilon' = 2.57$ for category 1 samples, $\epsilon' = 2.72$ for category 2 samples and $\epsilon' = 4.19$ for category 3 samples.

The lossy polarization process is characterized by the imaginary part of the permittivity ϵ''. It is seen that the dielectric losses are indeed increasing with the presence of polar carbonyl group, as expected from theoretical considerations. It is also seen that ϵ'' in oxidized samples increases as the frequency decreases, which indicates that the conductive process dominates the low frequency domain, and that the DC conductivity is higher in contaminations than in un-oxidized XLPE. Breakdown tests was preformed using the ASTM D149 standard for dielectric breakdown testing.
It was observed a decrease in breakdown strength in oxidized XLPE. The breakdown strengths decreased from (55.31±31)kV/mm in un-oxidized XLPE to (24.07±12.88) kV/mm in the most oxidized category 3 XLPE sample.

As a consequence of the theories and experimental results presented in this work, it can be said that there is a causal relation between dielectric losses and breakdown strengths in oxidized XLPE material which can be sumerized as follows: The introduction of polar carbonyl groups through thermal oxidation to polyethylene causes increased permittivities and dielectric losses. Subsequently there will be a decrease in electric breakdown strength of the XLPE insulation. Contaminations of oxidized material embedded in a solid insulation system may pose a reliability issue and may eventually be the cause of breakdown and failure of the cable.

Sammendrag

I dielektriske isolasjonsmaterialer som utsettes for vekslende elektriske felt er det energitap assosiert med polarisasjonsmekanismer og elektrisk motstand. Et vanlig dielektrisk materiale som brukes i undervanns-høyspentkabler er kryssbundet polyetylen (PEX, eng. XLPE). Under produksjonsprosessen kan polyetylen stagnere i termiske soner ved høye temperaturer. Som en følge av dette kan materialet bli utsatt for termiske oksidasjonsmekanismer som introduserer polare karbonylgrupper til polymerkjeden, som kan forårsake økte dielektriske tap og forringe kvaliteten til isolasjonssystemet.

Det oksiderte materialet kan forurense isolasjonsmaterialet i form av partikler som er innkapslet i polyetylen granulatet, og er vanskelig å skille ut. I dette arbeidet har fokus vært på å dokumentere de fundamentale egenskapene til oksidert polyetylen, som kompleks elektrisk permittivitet, konduktivitet, assosierte energitap og elektrisk holdfasthet i oksidert PEX sammenliknet med uoksidert PEX. I denne oppgaven har oksidasjonsprosessen i polyetylen blitt studert for å kunne gjenskape kunstige forurensinger. Reelle forurensinger ble funnet og undersøkt ved hjelp av Fourier transform infrarød spektroskopi. Forurensingene ble gjenskapt gjennom termisk oksidasjon av PEX prøver i ventilerte varmeskap ved 170°C.

De elektriske egenskapene til de kunstige forurensingene har blitt undersøkt ved dielektrisk-respons-spektroskopi og holdfasthet-målinger. Ved At 50Hz ble den reelle relative permittiviteten målt til å være $\epsilon' = 2.30$ for uoksidert PEX, $\epsilon' = 2.57$ for kategori 1 prøver, $\epsilon' = 2.72$ for kategori 2 prøver og $\epsilon' = 4.19$ for kategori 3 prøver.

Polarisasjonsmekanismene som gir opphav til energitap er karakterisert ved den imaginære delen av permittiviteten ϵ''. Det har blitt observert at dielektriske tap øker ved tilstedeværelse av polare karbonyl-grupper i polymeren. Det er også blitt observert en økning i ϵ'' i oksiderte prøver ved lavere frekvenser , dette indikerer at DC konduktiviteten dominer tapene i lav-frekvensdomenet for oksiderte forurensinger. Holdfasthet-målinger er blitt utført i henhold til ASTM D149 standarden. Den elektriske holdfastheten sank fra (55.31±31)kV/mm i uoksidert PEX til (24.07±12.88) kV/mm i den mest oksiderte kategori 3 PEX prøven.

Som en konsekvens av teorier og resultater presentert i denne oppgaven kan en si at det er en årsakssammenheng mellom dielektriske tap og elektrisk holdfasthet i oksidert PEX materiale. Årsaken er at polare karbonyl-grupper introduseres til materialet gjennom termisk oksidering, som fører til økte permittiviteter og dielektriske tap. Forurensinger av oksidert PEX innkapslet i fast isolasjonsmateriale kan redusere pålite-ligheten til kabelen, og eventuelt være årsaken til gjennomslag og svikt.

Preface

This thesis is the finishing work for the 5 years MSc programme in Applied Physics And Mathematics at the Norwegian University of Science and Technology. This master's thesis is a continuation of a project done in the fall 2011. The work was done during the spring of 2012 in collaboration with SINTEF Energy Research AS. Research has been carried out under the supervision of Sverre Hvidsten at SINTEF.
I am grateful for getting the opportunity to write my thesis for SINTEF, and I am grateful for the guidance I have gotten from my supervisor Sverre Hvidsten. I would also like to thank Erik Bjerrehorn, Hans Helmer Sæternes and Gunnar Håkonseth for helping out with some of the experimental work and sample production.

A special thanks goes to Sverre Hvidsten and Frank Mauseth for reviewing the manuscript and providing me with advice along the whole process. I would also thank responsible supervisor associate professor Jon Andreas Støvneng at NTNU Department of Physics. A thanks to Morten Stornes for taking the time to review the manuscript.

Finally, I would like to thank my family and friends for always supporting and encouraging me.

Contents

1 Introduction

The main transmission of electrical energy from a generating power-plant to substation in the vicinity of the end-user is done by high-voltage power transmission. Because of low losses and low costs, the power transmission is usually done by high-voltage three-phase AC-lines that uses air as insulation from the ground potential.
For many purposes we need a sub-marine system for electrical power transmission. These purposes may be to transport energy to and from offshore installations, such as offshore wind-farms, oil and gas platforms and subsea-installations for oil and gas production. Sub-marine cables are also used to transport electrical energy across oceans to connect and provide stability in major power-grids in countries and continents separated by ocean-areas.

To transport large quantities of electrical energy safely through sub-marine cables, a reliable high-quality insulation-system is needed. The last 30-40 years the preferred insulation system for sub-marine cables has been solid material impregnated with an insulating liquid. The typical mass-impregnated sub-marine cable insulation is layers of paper impregnated with insulating oil.
Because of lower dielectric losses, lower production costs and less need for maintenance, it can be advantageous to use a solid insulation without impregnation. An example of this kind of solid insulation is cross-linked polyethylene (XLPE) which is the material that has been considered in this thesis.

Typical rated voltage[1] level classifications of sub-marine cables are medium voltage (MV) and high voltage (HV) at 6-36kV and 36-220kV respectively. Cables with rated voltage 220kV and above (up to 500kV) can be considered as extra high voltage (EHV) cables.

The worlds first 420kV XLPE insulated sub-marine cable system produced by Nexans was installed to the Ormen lange processing plant in 2006. The increasing trend to use mainly XLPE-insulated cables for higher voltages throughout the world was also brought up by the successful manufacturing, testing and operation of 500 kV XLPE cables. To produce XLPE cables for higher rated voltages, it is necessary to have thorough production procedures and extreme cleanliness of the polyethylene resins.

Although modern polymer materials are truly versatile materials with properties that can be designed for specific applications, they have their Achilles' heel in degradation processes that occurs in any polymer application. The degradative effects in polymers can be e.g.; cross-linking, embrittlement and chain scission. And may be caused by autoxidation,

[1] Rated voltage is the maximum AC or DC voltage that can be safely applied to the cable at operational conditions.

photo oxidation, thermal treatment, mechanical stress, hydrolysis or environmental pollutants, which always leads to an inferior material. Polymer degradation therefore remains an active area of research [2].

1.1 Background

Sub-marine cables using polymeric materials as insulation has for a long time been a subject for research and development, but there are issues still to be resolved in relation to quality, reliability and degradation in harsh environments over time.

One of the issues with XLPE insulation is organic contaminations found in the production process. This contamination is typically oxidized material found in the form of particles in the polyethylene granulate which is the raw insulation material before it is extruded onto cable-jackets and cross-linked. The particles are formed because the polyethylene can accumulate in thermal stagnation zones and thereby be exposed to high temperatures over long periods of time. This will lead to severe oxidation of the material. After a time in the stagnation-zones the oxidized particles will loosen and contaminate the polyethylene, and thereby affect the physical properties of the insulation.

One of manufacturers of polyethylene used by cable-manufacturer Nexans is Dow Chemical Company. All polyethylene material investigated in the experiments in this thesis has been kindly provided through an ongoing research project involving Nexans Norway AS, SINTEF Energy Research and Dow Chemical Company.

Figure 1.1: Installation of a sub-marine high voltage cable. (Source: Nexans Norway AS)

1.2 Common Insulation Systems

1.2.1 Conductor

The conductor in a high voltage sub-marine cable is preferably made out of copper, but aluminum can also be used. The conductor is made up from many wires twined to give the cable flexibility. Usually there are one or three conductor phases in a single cable.

1.2.2 Solid Insulation

The latest developments in cable-technology has allowed cable-manufacturers to make cables using solid insulation materials for high voltage sub-marine cables. Because of improved production techniques, solid insulation materials have become a safer alternative, and since polymeric materials have better thermal, mechanical and electrical properties than mass-impregnated cables, they have become the preferred insulation system for many applications. One of the issues and dangers with solid insulating materials is the formation of microscopic voids in the material that may cause electrical field-enhancement, gas ionization and partial discharges. Once the material has been subjected to discharges, subsequent destructive discharges may occur rapidly until complete breakdown of the insulating system.
Images of cables using XLPE insulation are shown in Figure 1.2 and 1.3
In figure 1.2 a layout of a typical design is shown.

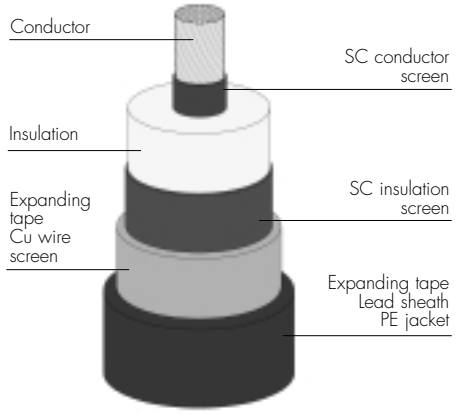

Figure 1.2: XLPE insulated cable (Source Nexans [48])

The functions of the parts of the XLPE cable design is described as follows, [48]:

- **The inner semiconductor screen** prevents concentration of the electric field at the interface between the insulation and the internal semi-conductor . It also ensures close contact with the insulation and smooth the electric field at the conductor.

- **The insulation** acts as a potential barrier which insulates the conductor when working at high voltage from the screen working at earthing potential. The insulation must be able to withstand the electric field under rated and transient operating conditions.
- **Metallic screen** is necessary when the voltage reaches tens or even hundreds of kV. Its main function is to nullify the electric field outside the cable. It acts as the second electrode of the capacitor formed by the cable.
- **The outer semiconductor** has the same function as the conductor screen: To ensure progressive transition from an insulating medium, where the electric field is non zero, to a conductive medium (here the metal cable screen) in which the electric field is zero.

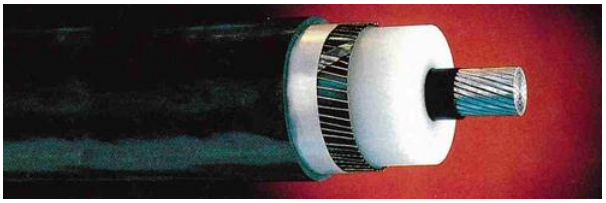

Figure 1.3: Single phase XLPE insulated cable

1.2.3 Mass-Impregnated Cables

A commonly used method for insulating high voltage cables is paper based insulation systems. Since paper is a porous material, mineral-oil is used to impregnate the insulation to prevent partial discharges that may destroy the material and cause breakdown.
The advantages of mass-impregnated cables is that they have high resistance against partial discharges.
Heat plays an important role in the degradation of the insulation system, so rapid cooling may be considered a great advantage for the mass-impregnated cable. With liquid impregnation, forced cooling can be possible.
The disadvantages of the mass-impregnated cable is that it is sensitive to moist, particles and other contaminations. The production process for mass-cables is more intricate, difficult and expensive than that of the XLPE cable. Also the process of splicing cable joints may be considered a very complicated process that has to be very thoroughly done to prevent oil-leakage and damage to the cable, [28].

1.3 Purpose

The purpose of this thesis is to investigate the dielectric properties of contaminations and thermal oxidation mechanisms in polyethylene resin used for high-voltage insulation. The polyethylene is used for extrusion and molding and then cross-linking onto cable-jackets. Issues addressed in this thesis is chemical composition of organic contaminations found in the polyethylene-granulate used by the cable-manufacturer Nexans and the effect these contaminations will have on the electrical properties of the insulating material.
As mentioned, the properties of XLPE insulating systems has been a subject for a lot of research the past years. Much of the research has been related to water-treeing, electrical-treeing, water-diffusion causing degradation during operation of the power cables [26, 25, 23]. It has also been done research on inorganic contaminations that are introduced to the insulating material [42].
Investigations done in this thesis is mainly related to contaminations that are introduced to the insulating material during production and processing. When the cable set into operation and the insulating material is subjected to stresses, the contaminations can pose a threat as a direct cause of breakdown, or as an indirect cause by accelerating degradation processes such as partial discharges, dielectric losses and eventually thermal breakdown.
Although dielectric responses and the thermal oxidation process of PE and XLPE is quite well understood, the link between thermally oxidized contaminations and dielectric properties is a quite new subject for research, and there is not much research that has been done investigating directly the correlation of the degree of oxidization of XLPE and dielectric properties. Oxidation of polyethylene and dielectric responses has previously been studied separately.
The aim of this thesis is to connect oxidation of XLPE and dielectric properties and find out what consequences the oxidized contaminations has on the properties of the insulation system.

1.4 Outline

This thesis concerns mostly experimental proof for the effect of organic contaminations in XLPE. So, the work done has been divided into different subsets of correlating experiments which is defined in the workflow shown in figure 1.4.

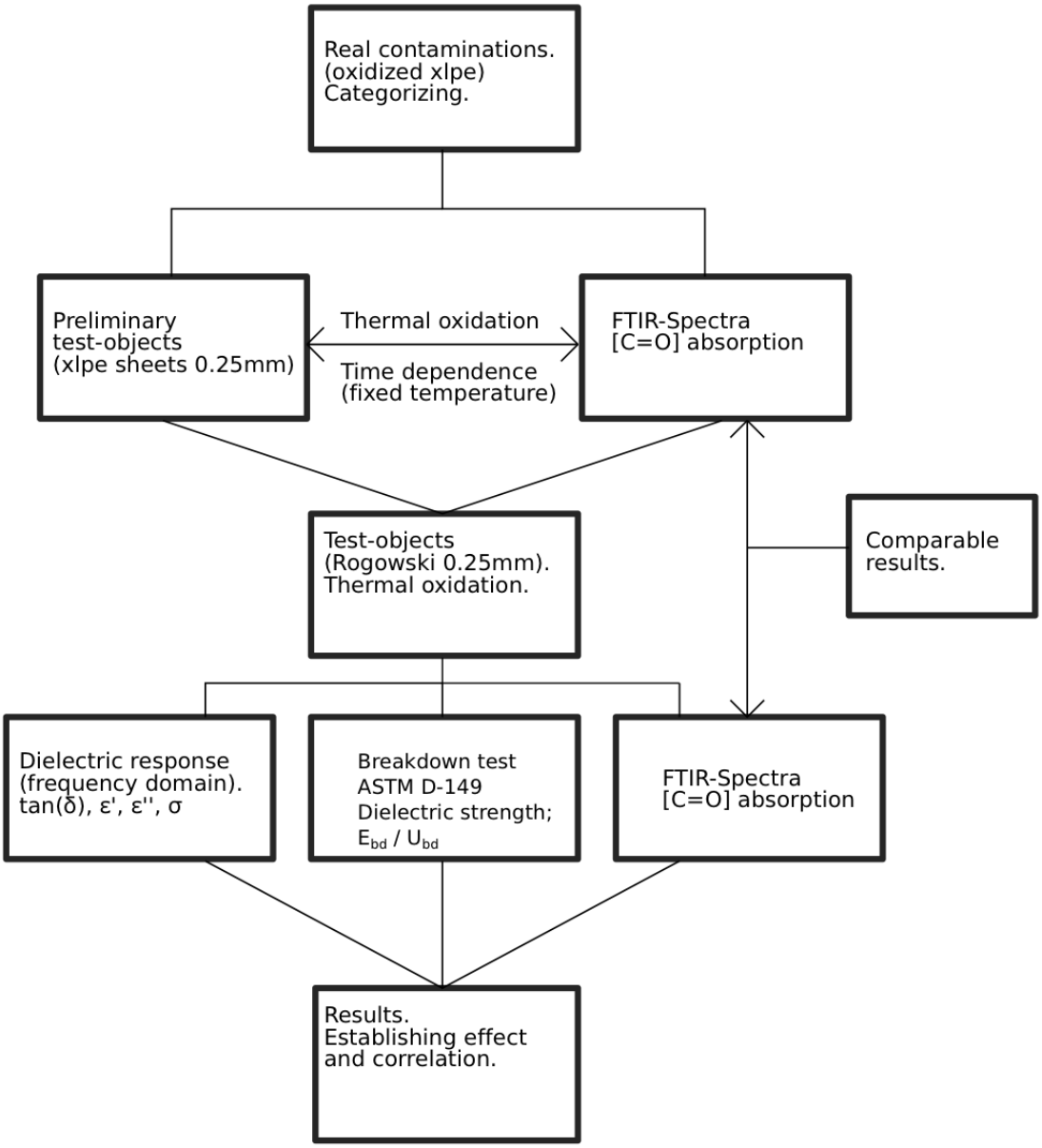

Figure 1.4: Chart of the experimental work.

2 Theory

To understand the degradation mechanisms of polyethylene, some background theory on chemical oxidation processes will be given.
Measurement techniques used in this thesis such as FITR and dielectric spectroscopy will also have a theoretical introduction in this chapter.
It is also necessary to understand how the electrical field interacts with solid state materials, therefore it will also be included a section on quite general electric properties of materials.

2.1 Introduction to Polyethylene

This section aims to give an introduction and a fundamental understanding of the physical properties of polyethylene used in electrical insulation. Emphasis will be kept on material properties that may affect the electrical properties of the polyethylene.

2.1.1 Polyolefins

Polyolefins are the volume leaders in industrial polymers. They are based on low-cost petrochemicals or natural gas and the required monomers are produced by cracking or refining crude oil. The most important monomers are ethylene, propylene, and butadiene and the four major polyolefins, polyethylene, polypropylene, polyvinyl chloride, and polystyrene are by far the least expensive industrial polymers on the market. The polyolefins derive their physical properties from the arrangement or the entanglement of the atoms in the chain molecules. Branching caused by radical transfer influences the physical properties as well as the molecular distribution, [2].

2.1.2 Polymeric Plastics

Plastics are a term used for a wide range of moldable organic solids. Plastics usually consist of long flexible chains of polymers, made of repeating units of organic molecules, which in this context are called monomers. Polymers that is made of one single monomer are called homopolymers. Copolymers are polymers that contains several types of monomers.
If the polymer is branched it will be an increased probability for the branches to be interlinked, and thereby creating a network of polymer chains. The process of linking polymer branches is called cross-linking. The process of cross-linking may affect the physical properties of the polymer considerably. [2]

The two main categories of the large and still growing family of plastics are thermosetting and thermo plastics. The two subdivisions of plastics are determined by their characteristic behavior toward heat. Thermosetting plastics soften only once under heat and do not soften again on subsequent heating. Thermo-plastics can soften under heat and be made

rigid under cooling (crystalline phase), theoretically infinitely many cycles for ideal thermo-plastics.

2.1.3 Chemical Structure of Polyethylene Insulation

Polyethylene is a polyolefin polymer. In this thesis the focus will be on polyethylene and cross-linked polyethylene and their electrical and chemical properties.

Ethylene C_2H_4 is a gaseous hydrocarbon composed of two carbon atoms and four hydrogen atoms. The two carbon atoms in ethylene are bound by a characteristic strong double-binding. By a certain process, the strong bond in ethylene can open as shown in Figure 2.5 and the ethylene molecules can react and form long polymer-chains. The C-H bonds on the left in the figure is made to indicate the 3-dimensionality of polyethylene chains, and red lines indicates C−C bonds.
The polymerization process turns ethylene into a thermoplastic polyethylene resin[1].

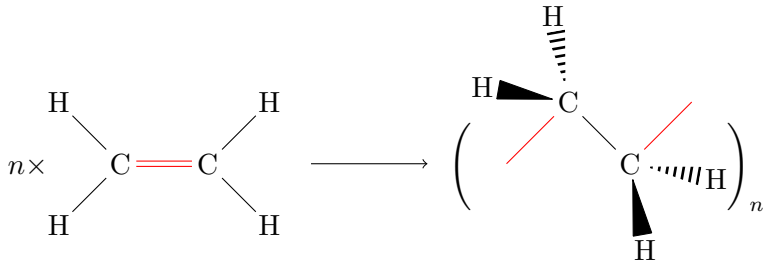

Figure 2.5: Polymerization of ethylene $n \times (C_2H_4) \rightarrow (C_2H_4)_n$.

The physical properties of polyethylene resin is not mainly dependent on the fundamental molecular properties such as short-chain branching, average molecular and molecular weight-distrubution. These fundamental properties are controlled by parameters such as size, structure and uniformity of the polyethylene molecules.

The length of a polyethylene chain can vary much. And in reality, the polymerization process will create a mix of chains with lengths of several hundred thousand carbon atoms to only 12 atoms or less. In a commercial polyethylene resin, it will never happen that the polymer chain is without branching. So each polymer chain will have several branches that will stretch out from the main chain in three dimensions. A simplified illustration of polyethylene with side-branches is shown in Figure 2.6. The side-branches is the main reason that we find variations in the physical properties of polyethylene, such as density, flexibility and viscosity upon melting. Side-branches will also be nodes where oxidation can occur.

[1]Polyethylene resin is he general term for gases, liquids and solids of polymerized ethylene chains

Figure 2.6: Polyethylene chain with branching

2.1.4 Cross-linked Polyethylene

The cross-linking process is a chemical reaction where polymer chains are linked together forming a three dimensional network. The link formed between the polyethylene molecules is a covalent chemical bond and it is practically an irreversible reaction, and the polymer can not be molten and formed to a different shape i.e the cross-links forms a rigid network of polyethylene molecules. The XLPE matrix is in it self a large macromolecule.
Cross-linking of low density polyethylene can be performed by different technologies as:

- Peroxide crosslinking.
- Silane crosslinking.
- Irradiation crosslinking.

Peroxide cross-linking is by far most the common practice for medium voltage (MV) and the only technology applied in high voltage (HV) and extra high voltages (EHV) cable manufacturing. Silane cross-linking is the dominating technology for manufacturing low voltage XLPE cable. Irradiation cross-linking is mainly used in special applications where the thickness of the polymer layer is relatively thin.[2]

2.1.5 Properties of Polyethylene

The attractive electrical properties makes robust, flexible polyethylene a very good alternative for an insulating material for electrical power cables. It is often an advantage to use polyethylene of high density for many different cable-jacket applications. High density polyethylene is tougher, and can take heavier mechanical loads. High density polyethylene also exhibit grater tear resistance and shear strength. Low conductivity and low dielectric losses are the reason that polyethylene is used in jackets for cables operating at high voltage, both DC and AC transmission.[28]

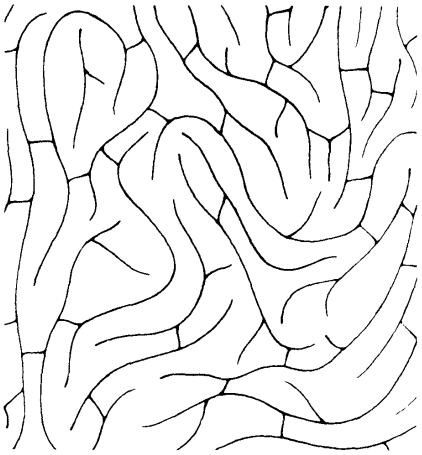

Figure 2.7: Cross-linked polyethylene

2.2 Oxidation Mechanisms

Oxidation is a chemical reaction where the oxidation number of a substance increases. There are different ways a substance can be oxidized, the most commonly known is the reaction where the substance gives off electrons and and gain an oxygen atom O^{2-} or gives off $2\,H^{+}$.
In air the dominant oxidation agent is molecular oxygen O_2. The oxidation reaction in air is called auto-oxidation.
The reason why molecular oxygen is a good oxidation-agent is that Oxygen in the ground state is a di-radical as shown in Figure 2.8. The oxygen molecule in the ground state has two electrons that occupy two degenerated molecular orbitals (MO) with spin-state $S = 1$, so the ground state is a triplet state. .

$$\dot{O}\text{——}\dot{O}$$

Figure 2.8: Oxygen in its ground state

$$O\text{═══}O$$

Figure 2.9: Oxygen in the exited singlet state.

2.2.1 Thermal Oxidation in Polyethylene

At high temperatures all polymers will oxidize and degrade at a certain rate. The oxidation rate will in most cases be increased at high temperatures and with oxygen present. Oxidation of hydrocarbons such as polyethylene is usually auto-accelerating, meaning that the oxidation-rate can be low at the beginning but gradually increase towards a con-

stant rate [49].
The oxidation is initiated by the formation of radicals on the polyethylene chain. Usually the radicals are formed by thermal excitation or by exposure to ultra-violet radiation. The energy required to excite radicals in the initiation process is denoted $\hbar\omega$ for UV-radiation and ΔH for the change in enthalpy.

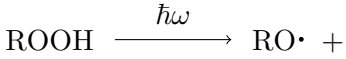

Figure 2.10: Excitation by radiation

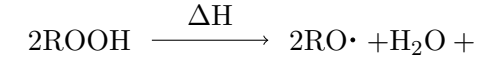

Figure 2.11: Thermal excitation

Figure 2.12: First step in the radical chain reaction

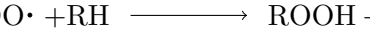

Figure 2.13: Second step in the radical chain reaction

A schematic Figure of the processes from Figure 2.12 - 2.13 is shown in Figure 2.14

In each cycle of the redox reactions shown in Figure 2.12 - 2.13 one oxygen molecule is absorbed and forms hydroperoxide. RH symbolizes the polyethylene chain (R represent the carbon-carbon chain, H are attached Hydrogen atoms etc.). The first reaction (Figure 2.12) is a radical pairing process and thereby have a low activation energy. The second step (Figure 2.13) involves breaking one carbon-hydrogen bond, so this reaction will have a higher activation energy.
In polyethylene at atmospheric pressure, the oxidation-rate will be determined by the reaction-rate of the reaction in Figure 2.13.[49].
The structure of the hydrocarbon that is oxidized and the concentration of oxygen will determine which reaction that will terminate the chain-reaction.

Since the reaction shown in Figure 2.13 defines the reaction rate in air at atmospheric pressure, alkyl-peroxyl radicals will be the dominating radicals present in the auto-oxidation, in this case the termination of the reaction happens through the reaction shown in Figure 15(c).
If the supply of oxygen is limited, the reactions in Figure 15(a) and 15(b) will be more important.[49]. The consequence of this, is that under atmospheric pressure, the oxidation rate will be determined by the reaction coefficient k_1 for reaction 2.13 and k_2 for reaction 15(c). In this case, the

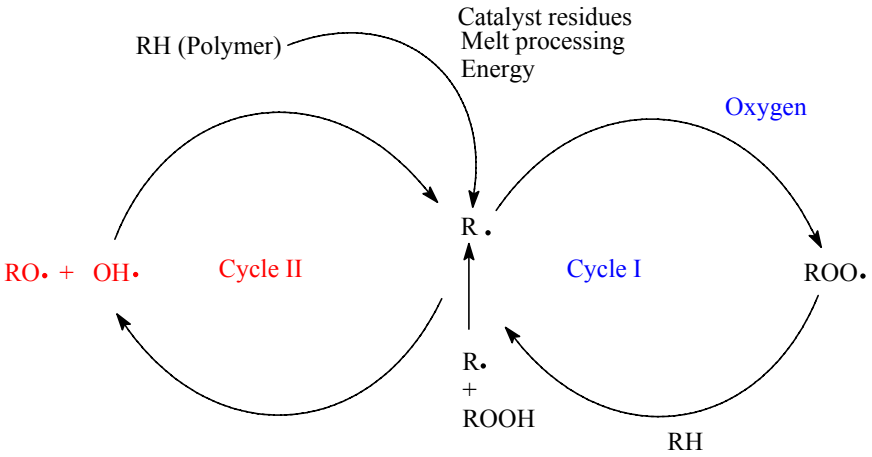

Figure 2.14: Degradation of polyolifins

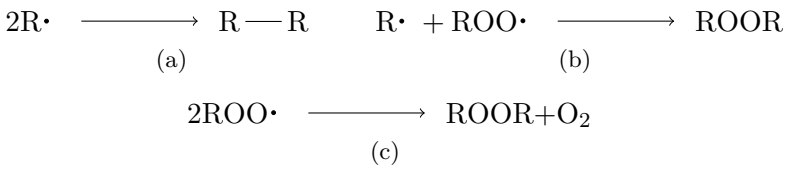

Figure 2.15: Termination of the chain-reaction

total reaction-rate is given by equation (2.1), where $[O_2]$ is the concentration of oxygen, $[RH]$ is the concentration of hydrogen peroxide and r_i is the initiation-rate [49].

$$-\frac{d[O_2]}{dt} = k_1 k_2^{-1/2} r_i^{1/2} [RH] \tag{2.1}$$

For materials that are easily oxidized under low pressure, the oxidation rate will be given by equation (2.2), where k_3 is the reaction-rate for the reaction in figure 2.12 and k_4 for the reaction in Figure 15(b). [49].

$$-\frac{d[O_2]}{dt} = k_3 k_4^{-1/2} r_i^{1/2} [O_2] \tag{2.2}$$

Most of the possible reaction mechanisms of thermo-oxidative degradation of polyethylene has been described by Hölmström and Sörvik in [24]. In this thesis, the focus will be kept on the formation of aldehydes, ketones and carbonyl compounds, as a measure of the degree of oxidative degradation. These compounds are particularly easy to identify by infrared spectroscopy. As reported by Rugg et. al in [11], the IR absorption maximum occurs at wavelength of λ =5.81μm (wavenumber k=1721cm^{-1}) and "is almost entirely due to aldehydic and ketonic

carbonyl groups". So primarily, the concentration/absorbation of the carbonyl (C=O) bands will be main measure of oxidation degree for the material.[38]

A very significant processes caused by and representing oxidative degradation of polyethylene is chain scission. Oxidative chain-scission is shown in Figure 2.16:

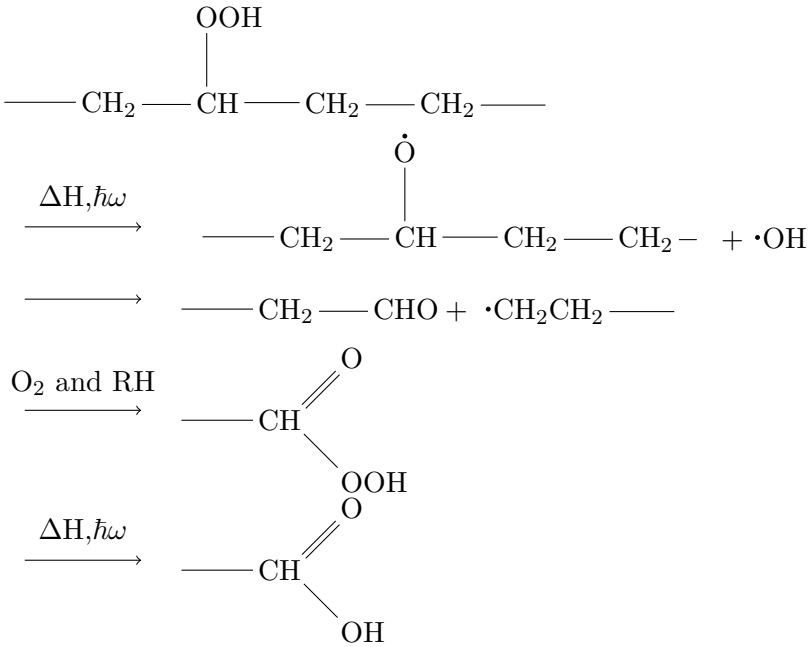

Figure 2.16: Oxidative chain-scission

Oxidative chain scission, degrades the material both mechanically by degrading the polymer chain, and electrically by introducing polar groups to the polymer matrix. [9]

2.3 Infrared Spectroscopy

By using infrared spectroscopy it is possible to determine the concentration of a chemical compound in a given sample. Since different molecules has different resonance frequencies they will absorb electromagnetic radiation at frequencies characteristic for the specific molecules. The molecules of specific compounds can also have different vibrational modes, giving the compound several absorption peaks in the IR-spectrum.
The number of vibrational modes is dependent on the number of atoms in the molecule, N. For linear molecules the number of vibrational degrees of freedom (vibrational modes) is $3N-5$. For non-linear molecules the number is $3N-6$ vibrational modes,[37]. In this sense, a polymer chain will have a very large number of atoms ($N >> 10^3$). However, the strongest vibrational modes are given by the six possible fundamental vibrational modes of the monomer unit cell (CH_2), some of which is shown in Figure 2.17 (not including wagging and twisting). The recoil of the carbon atoms is neglected in this view. In polyethylene C-C bonds and movements of the whole molecule will give rise to weaker vibrational modes, some of which are IR-active. However, the recoil effects may affect the frequency of the vibrational modes, and the macro-molecular size and structure should not be neglected when interpreting real IR-spectra.

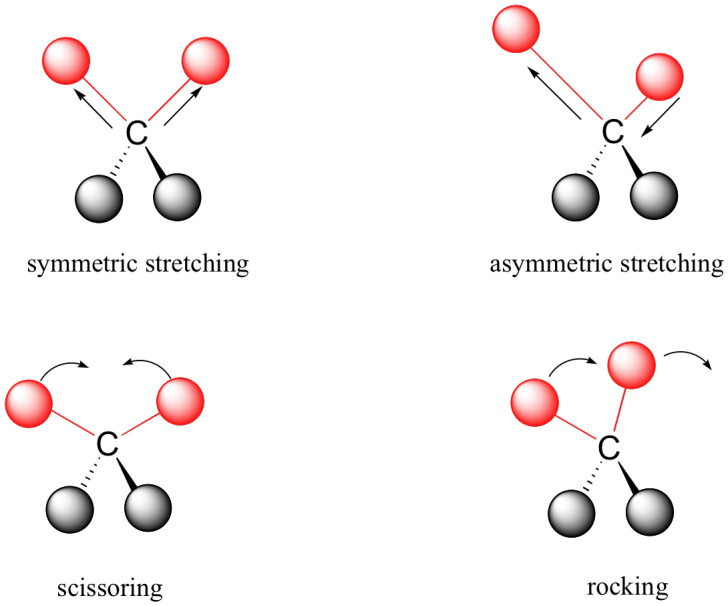

Figure 2.17: Four out of six vibrational modes of CH_2, (scissoring is not IR-active).

The energies of molecular vibrations are quantized, not continuous. This means that a molecule can only vibrate (stretch, bend etc.) at certain allowed frequencies. If a molecule is exposed to infrared radiation that matches the frequency of one of its vibrational eigenfrequencies, it will absorb energy from the radiation and jump to a higher vibrational

energy state - what this means is that the amplitude of the vibration will increase, but the vibrational frequency will remain the same. The difference in energy between the two energy states is equal to the energy of the absorbed IR-radiation.

2.3.1 IR Spectroscopy of Carbonyl Compounds

Carbonyl compounds are not only chemically important, but are also important in the interpretation of infrared spectra. The C=O absorption is almost always one of the most characteristic in the entire spectrum, and it is also most likely to be the most intense spectral feature. Table 2.1 provides an example listing of some of the common carbonyl frequencies as a function of the particular type of carbonyl group. In essence, a ketone is considered the root compound, with an aldehyde being a special case, where the carbonyl group is terminal, and only has one substituent, the other being a single hydrogen atom. All of the other carbonyl compounds, in a way, can be considered to be derived from the base ketone structure, where one or both alkyl (or aryl) substituents are replaced by another functionality, e.g. from a single hydroxy group, in the case of carboxylic acids, to two ether groups, as in the case of an organic carbonate.

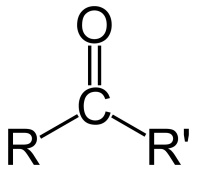

Figure 2.18: Ketone side group attached to a general organic molecule.

For carbonyl the strongest vibrational frequency is the C=O stretching (ignoring C-recoil; C=O stretching is the only mode, since $3 \times 3 - 5 = 1$). A simple calculation can be done to illustrate the origins of the infrared absorption in molecules, here is an example calculation on the carbonyl group:

The model of the simple quantum harmonic oscillator suffice to explain the origin of many of the characteristic frequencies that can be assigned to particular combinations of atoms within a molecule. The energy level n of the quantum harmonic oscillator is $E_n = (n + \frac{1}{2})\hbar\omega$.

The absorption of infrared radiation $E = \hbar\omega$ causes an excitation of the oscillator $\Delta E = \hbar\omega_e$. The vibrational eigenfrequency of the molecule or group is, as in the classical case given by Hookes' law $\omega_e = \sqrt{\frac{\kappa}{\mu}}$. Where κ is the spring constant, and μ is the reduced mass $\frac{m_1 m_2}{m_1 + m_2}$. The wavenumber of the absorption peak will be: $k = \frac{\Delta E}{\hbar c} = \frac{1}{2\pi c}\sqrt{\frac{\kappa}{\mu}}$. [4].

E.g., the fundamental absorption peak of the carbonyl group (C=O -stretching) can be approximated in the following way:
The carbonyl group is characterized by one carbon atom and one oxygen atom bound by a covalent double bond. The reduced mass of the group is $\mu = \frac{12\text{u}\cdot 16\text{u}}{12\text{u}+16\text{u}} = 6.85714\text{u} \simeq 1.1 \cdot 10^{-26}\text{kg}$. The carbonyl stretching force constant has been calculated by various authors, [30, 31, 17]. A typical value for the carbonyl stretching force constant is about 1020 ±30 N/m. [17].
So, the fundamental absorption peak will be about:
$k = \frac{\Delta E}{\hbar c} = \frac{1}{2\pi c}\sqrt{\frac{\kappa}{\mu}} = 5.3 \cdot 10^{-12}\text{s/cm}\sqrt{\frac{1020\text{N/m}}{1.1\cdot 10^{-26}\text{kg}}} \simeq 1616\text{cm}^{-1}$ The carbonyl stretching band is found experimentally to be in the region 1800 cm^{-1} - 1600 cm^{-1}. [11].

Often, the frequency ranges for the different classes of carbonyl compound overlap, and the carbonyl frequency alone is not sufficient to characterize the functional group. In most cases, spectral information from the other component of the functional group is used for the characterization. Carboxylic acids are a good example, where the C−O, C−O−H and O−H vibrations are highly characteristic. Similarly, esters (C−O−C) and amides (C−N and N−H) are other frequently encountered examples. The frequencies provided earlier for these additional functionalities (C−O, C−N, and N−H) in general apply, although the actual observed frequencies may differ slightly, being modified by the carbonyl group. It is worthwhile returning momentarily to carboxylic acids, because they are unique, in so far as the hydroxy group has direct interaction with the carbonyl group, by the formation of a stable dimeric hydrogen-bonded structure in the condensed phase (solid and liquid). Note that this structure disappears in the vapor state. A characteristic broad feature in the range 3300 – 2500 cm^{-1} , that overlaps the C−H stretching region, and with a secondary absorption close to 2600 cm^{-1}, is observed for the hydrogen-bonded O−H of most carboxylic acids. Other bands that are associated with the C−O and O−H components tend to be less pronounced, and sometimes may be overlapped with other fingerprint absorptions of the molecule. These are located in the ranges 1320 – 1210 cm^{-1} (C−O stretch) and 960 – 850 cm^{-1} (hydrogen-bonded O−H out-of-plane bending).[11],[4]

2.3.2 Beer-Lamberts law

As mentioned, infrared spectroscopy can be used to detect compounds of chemicals present in a material sample, due to the molecules characteristic vibrational signature. In addition to this qualitative analysis of the IR-spectra, the spectra can be used to analyze quantitatively the amount of a specific substance present in the material. This is done by applying Beer-Lamberts' Law, which relates the transmitted intensity through a sample to the concentration of the absorbing chemical compound.
The transmittance τ through a sample of a thickness d, molar absorptivity α and concentration c is given by Beer-Lamberts' law, usually written

Table 2.1: Carbonyl group frequencies

Absorption band (cm^{-1})	Functional group
1610 – 1550/1420 – 1300	Carboxylate (carboxylic acid salt)
1680 – 1630	Amide
1690 – 1675/(1650 – 1600)	Quinone or conjugated ketone
1725 – 1700	Carboxylic acid
1725 – 1705	Ketone
1740 – 1725/(2800 – 2700)	Aldehyde
1750 – 1725	Ester
1735	Six-membered ring lactone
1760– 1740	Alkyl carbonate
1815 – 1770	Acid (acyl) halide
1820 – 1775	Aryl carbonate
1850 – 1800/1790 – 1740	Open-chain acidd anhydride
1870 – 1820/1800 – 1775	Five-membered ring anhydride
2100 – 1800	Transition metal carbonyls

as an exponential dependence as in equation (2.3). Where the transmittance $\tau = \frac{I_{IR}}{I_0}$ is the ratio of the intensity I of a beam passing through the sample and I_0 which is the background intensity of a sample that can be either air or another reference sample.

$$\tau = \frac{I}{I_0} = 10^{-\alpha \cdot c \cdot d} \tag{2.3}$$

Equivalently, the absorbance A is given as the negative decadic logarithm of the transmittance.

$$-\log_{10} \tau = -\log_{10} \frac{I}{I_0} = \alpha \cdot c \cdot d = A \tag{2.4}$$

The value of the absorption coefficient α varies with different materials.[34], [11].

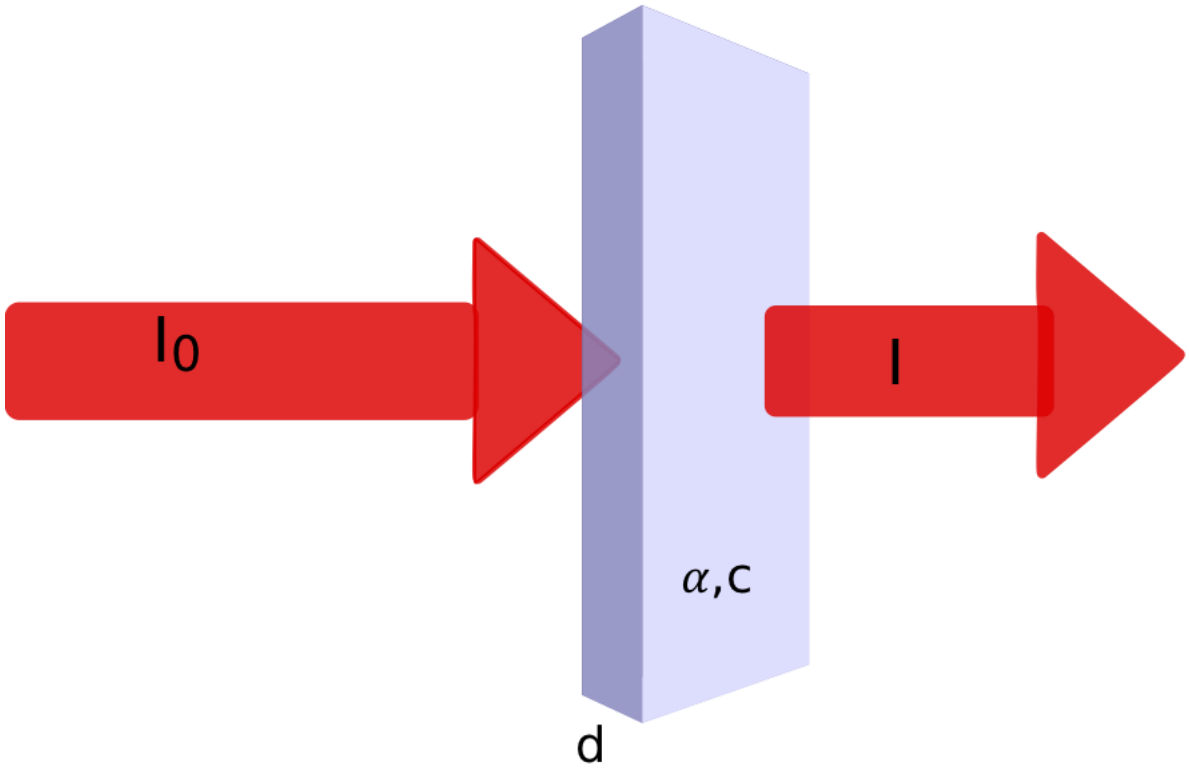

Figure 2.19: Conceptual diagram of Beer-Lambert absorption

2.4 Electrical Properties of Materials

In cable materials it is very important to know which factors that affects the physical properties of the cable, and the factors that can cause degradation, losses and eventually failure. In this chapter the focus will be on the electrical properties that may contribute to losses. One important aspect to keep in mind when losses are mentioned, is that in addition to loss of electrical energy there is a possibility for positive feedback in the system. When electrical energy is dissipated in the conductor and insulator, the energy is dissipated as heat either by resistive heating or molecular vibrations. The heating may also leave the system more vulnerable to partial discharges. The heating may affect the physical and electrical properties of the system in such a way that the losses increase even more, and furthermore heat may deteriorate the insulating-material irreversibly and eventually causing failure. In summary; the dissipation of energy in the insulating-material and conductor affects the overall quality of the insulation system.
In terms of electrical properties, materials can be categorized into three categories; conductors, insulators and semiconductors. The main focus of this chapter will be on insulators, but will also give a brief summary of the properties of conductors. This chapter should give a background knowledge in general terms used to describe the electrical properties of materials considered in this thesis. The terms introduced in this chapter will also form the basis for the measurements, observations and results related to the electrical properties investigated in this thesis. The information given in this chapter covers basic physics that may by found in a variety of textbooks [14, 28, 37], and is based on knowledge and equations that should be easily recognizable for any physicist or electrical engineer.

2.4.1 Electrical Properties of Conductors

Conductors are defined by the boundary condition of zero electrical field within the material. The reason for this boundary condition is that each atom of the conductor has one or more free electrons that are free to move through the material, and thereby making the surface of the conductor the only allowed place for electrostatic charge. To phrase the condition as Griffiths [14] does in terms of energy: *Like any other free dynamical system, the charge on the conductor will seek the configuration minimizing its potential energy.*
The conductors will act as an equipotential surface, creating an electric field around it.

The conductors ability to conduct currents is given by the conductivity σ. The conductivity arises from the fact that a current can not flow perfectly through a conductor, since the electrons will dissipate their energy through scattering of the lattice/atom-sites in the material. The conductivity σ is given by Ohms law, explained theoretically by the Drude model in appendix B.1.2:

$$\vec{J} = \sigma \vec{E} \tag{2.5}$$

Where $\vec{J}$ is the current density and $\vec{E}$ is the electric field. An equivalent way of representing a materials ability to conduct current, is the resistivity which is the reciprocal of the conductivity $\rho = \frac{1}{\sigma}$.
The empirical version of Ohms law states simply that the resistivity of a material is the ratio of the potential difference and the current applied to electrodes attached at two ends of the material.

$$R = \frac{V}{I} \tag{2.6}$$

The passage of electric current through a resistive material yields losses, and releases heat. The heating caused by the resistive losses, is named Joule heating after is discoverer. Joule observed experimentally that the heat generated by resistive losses is proportional to the resistivity multiplied by the square of the current $Q \propto I^2 R$. A general formulae for the Joule heating rendered by Ohms law, and given in terms of power is shown in equation (2.7):

$$P = V \cdot I = I^2 \cdot R = \frac{V^2}{R} \tag{2.7}$$

In addition to Joule-heating there are many interesting phenomena in conductors used for AC and DC transmission, such as the skin effect and self-induction, that needs to be taken into account when designing the cable. However, these effects lie beyond the scope of this thesis. The key property of currents in conductors considered in this thesis is the electric field it induces in the insulating material.

2.4.2 Dielectric Materials and Insulators

In dielectric materials all charges are bound to specific atoms. i.e. there are no free charges present in a dielectric material. Since a dielectric material with a high dielectric constant usually has a very low conductivity, it is commonly called an insulator. And if the dielectric material is a perfect insulator, the electric field will cause no electrical current[1]. If an electric field is applied to an dielectric material, the electric field will penetrate the material, causing polarization of the molecules.

2.4.3 Polarization Mechanisms in Dielectrics

Electronic polarization is the phenomena of polarization on atomic scale. Even though an atom might be electrically neutral, it will interact with an applied electric field. Since the atom is composed of an negatively charged electron-cloud surrounding a positively charged nucleus of protons and neutrons, the electron-cloud and nucleus will be shifted relative to each other in an electric field. The electron-cloud and nucleus will be pulled apart by the electric field and balanced by their mutual attraction at a displaced equilibrium, according to the electrostatic force law $F = qE$, leaving the atom polarized. The polarization of atoms induces a small dipole moment $\vec{\mu}$ parallel to the applied electric field $\vec{E}$. If the electric field is not too strong, the induced dipole moment is approximately proportional to the electric field.

$$\vec{\mu}_{dipole} = \alpha_p \vec{E} \tag{2.8}$$

The proportionality constant α_p is the atomic polarizability. α_p for some substances is shown in table [2.2] found in [39].

Table 2.2: $\frac{\alpha_p}{4\pi\epsilon_0}$ (in units of $10^{-30}\mathrm{m}^3$)

H	He	Li	C	O	Ne	Na	Ar
0.667	0.205	24.3	1.76	0.802	0.396	24.1	1.64

Molecular polarization is the polarization mechanism that occurs in neutral molecules in a similar manner as dipoles are induced in single atoms. But molecules may have an anisotropic polarizability, so the molecules may polarize more easily in some directions. The more general version of equation (2.8) has to be applied on completely asymmetric molecules, where the polarizability constant is replaced with the polarizability tensor α_{ij}. [37, 14]

$$\mu_i = \sum_{j=x,y,z} \alpha_{ij} E_j \quad , i = x, y, z \tag{2.9}$$

[1] As there are no perfect insulators the term "insulator" is typically used for materials with very low conductivity, and the term "dielectrics" for materials with high polarizability.

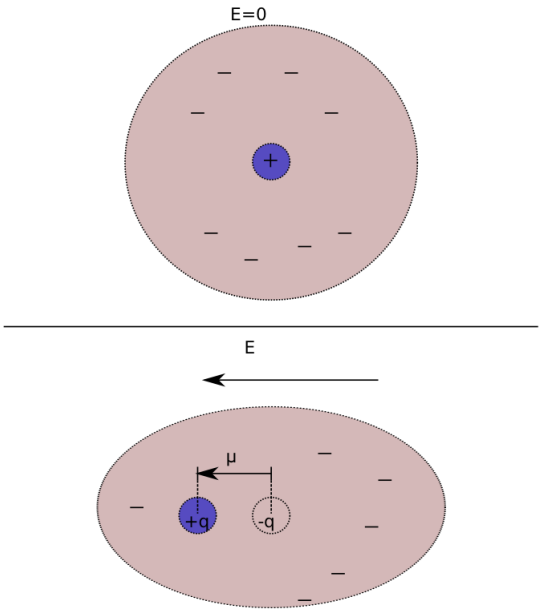

Figure 2.20: Deformation of the electron cloud and induced dipole moment in an electric field.

Dipolar/orientational polarization is a polarization mechanism that occurs in polar substances. Polar substances have molecules that are permanent dipoles that arises from asymmetric bonds and charge distributions. This means that the molecules remains polarized even though there is no applied electric field. Without an applied electric field, the dipoles will be randomly oriented, and the material will not have any net polarization. In an applied electric field, the dipoles will tend to align themselves parallel to the electric field, but the spatial charge distribution, molecular bonds, and bond angles will not change, meaning that the polarization itself rotates because of the torque $\vec{N}$ the dipole experiences from the electric field $\vec{N} = \vec{\mu} \times \vec{E}$. The response and relaxation times of this mechanism depends on the torque and the viscosity of the surrounding material. When many of the dipoles in a substance tend to align with the applied electric field the material becomes polarized.

Ionic polarization: In an ionic lattice, the positive ions are displaced in the direction of an applied field while the negative ions are displaced in the opposite direction, giving a resultant dipole moment to the whole body. The ionic polarization demonstrates only weak temperature dependence and is determined mostly by the nature of the interface where the ions can accumulate. Many cooperative processes in heterogeneous systems are connected with ionic polarization.[37]

Polarization due to **hopping charge carriers** is another important form of polarization, found mostly in solids for both bulk and surface.

This type of mechanism is something in-between on one hand induced and permanent dipoles and on the other hand free moving charges. [32]. If charge carriers can hop or tunnel through the entire dielectric, they will contribute to DC conduction.

The total polarizability can be written as a linear combination of all the contributing mechanisms.

$$\alpha_{total} = \alpha_{dip.} + \alpha_{molec.} + \alpha_{el.} + \alpha_{ion.} + \alpha_{orient.} \tag{2.10}$$

The different mechanisms has different relaxation times and resonance frequencies, so the contributions will be separated in the frequency domain, as shown in Figure 2.21. The figure is a recreation of a figure from Kittel [37].

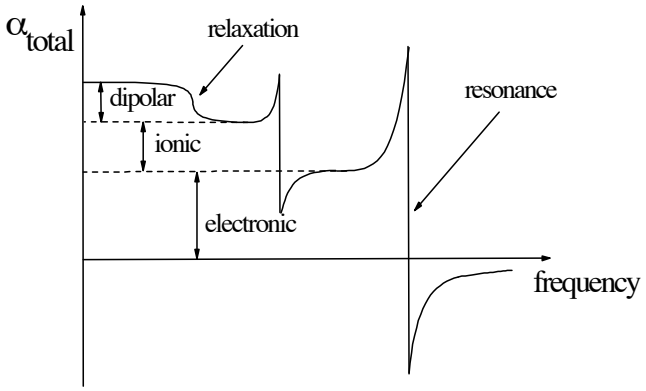

Figure 2.21: Frequency dependence of contributions to α_{total}

The dipolar, ionic and electronic polarization mechanisms have relaxation times lower and resonance frequencies higher than the part of the spectra that will be considered in this thesis (typically frequencies in the range 1mHz - 100Hz). So, even though they will all have contributions, the polarization mechanisms considered in this thesis will be dipole polarization and orientational polarization.
The polarizability is defined for each individual molecule in equation (2.9). Assuming an isotropic polarizability for the molecule, an electric field $\vec{E}_{local}$ will cause an induced dipole moment $\vec{\mu} = \epsilon_0 \alpha \vec{E}$. With N induced dipoles per unit cell, the polarizability per unit volume (polarization density) can be written

$$\vec{P} = N\vec{\mu} = N\alpha\vec{E}_{local}. \tag{2.11}$$

For the whole material the polarization density is written as

$$\vec{P} = \epsilon_0 \chi_e \vec{E}, \tag{2.12}$$

where the electric susceptibility χ_e is a proportionality parameter, telling the degree of polarization in the dielectric material subjected to an electric field $\vec{E}$. (Note that $\vec{E}$ is the macroscopic field applied to the material.)
Since the polarization affects the local charge distributions and interactions between surrounding molecules, the local electric field at the site of the individual molecule may differ from the applied electric field. Combining equations (2.11) and (2.12) we get.

$$\frac{\chi_e \epsilon_0}{N\alpha} = \frac{\vec{E}_{local}}{\vec{E}} \tag{2.13}$$

So, $\chi_e \epsilon_0 = N\alpha$, only if the local field equals the macroscopic field.
There are many formulations that relates the susceptibility and permittivity to polarization under different circumstances and assumptions, worked out by amongst others Lorentz-Lorenz, Debye, Onsager, Kirkwood and Fröhlich [6, 12, 51, 32, 37] The most famous is the Clausius–Mossotti relation, which applies to a perfectly homogenous and isotropic dielectric material:

$$\epsilon_0 \frac{\chi_e}{\chi_e + 3} = \frac{\epsilon - \epsilon_0}{\epsilon + 2\epsilon} = \frac{N}{3}\alpha, \tag{2.14}$$

where α is the polarizability, $\chi_e = \epsilon_r - 1$ is the susceptibility and N is the number of polarizable molecules per unit cell.

Because of the complicated dynamics of individual molecules and interaction between molecules, it is a bit of a challenge to calculate the susceptibility and permittivity and their time dependence analytically from the molecular structure of the material, especially in disordered solids like polyethylene. Therefore the susceptibility and permittivity is typically measured experimentally as a response function of time or frequency.

2.5 Dielectric Response

Dielectric response spectroscopy is based on the phenomena of electrical polarization and electrical conduction in materials. As discussed in the previous sections, there are a number of different dielectric polarization mechanisms operating at the molecular level. Each polarization mechanism, either a relaxation or a resonance process, is centered around its particular characteristic frequency, which is the reciprocal of the characteristic time of the process and therefore separable in frequency domain. [40]
To give a good theoretical foundation for further discussions of dielectric response spectroscopy, a short revision of Maxwells equations is necessary. In classical electrodynamics, all macroscopic phenomena are described mathematically by a set of partial differential equations know as Maxwells equations. In materials they have the form given by the equations (2.15-2.18),[14].

$$\vec{\nabla} \cdot \vec{D} = \rho_f \tag{2.15}$$

$$\vec{\nabla} \times \vec{E} = -\frac{\partial \vec{B}}{\partial t} \tag{2.16}$$

$$\vec{\nabla} \cdot \vec{B} = 0 \tag{2.17}$$

$$\vec{\nabla} \times \vec{H} = \vec{J_f} + \frac{\partial \vec{D}}{\partial t} \tag{2.18}$$

ρ_f is the free charge density, not including the bound charges. $\vec{J_f}$ is the free current density. The link from the electric field $\vec{E}$ and the magnetic field $\vec{B}$ to the auxiliary fields $\vec{D}$ and $\vec{H}$ is given by equations (2.19 and 2.20).

$$\vec{D} = \epsilon_0 \vec{E} + \vec{P} \tag{2.19}$$

$$\vec{H} = \frac{1}{\mu_0}\vec{B} - \vec{M} \tag{2.20}$$

by combining Ampéres law (2.18) and the constitutive relation (2.19). And using Ohms law $\vec{J_f} = \sigma \vec{E}$ where σ is the conductivity. The expression for the total current density is obtained and given by

$$\vec{\nabla} \times \vec{H} = \underbrace{\sigma \vec{E}}_{\text{Induced current}} + \underbrace{\epsilon_0 \frac{\partial \vec{E}}{\partial t}}_{\text{Displacement current}} + \underbrace{\frac{\partial \vec{P}}{\partial t}}_{\text{Polarization current}} . \tag{2.21}$$

2.5.1 Dielectric Response In The Time Domain

Polarisation $\vec{P}(t)$ depends on the electric field $\vec{E}(t)$ and its history. To analyze time dependence of polarization, a dielectric-response $f(t)$ is introduced. The response function $f(t)$ describes the time dependence of

polarization, assuming the material is linear and isotropic [28]. The dielectric response function represents the memory effects in a dielectric material. The relationship between $f(t)$ and $\vec{P}(t)$ can be described by the time dependence of polarization under a delta-function[33, 28]:

$$\vec{P}(t) = \epsilon_0 \cdot \vec{E}\Delta t \cdot f(t) \tag{2.22}$$

Causality demands that action precedes reaction:

$$f(t) \equiv 0 \text{ for } t < 0, \tag{2.23}$$

where $f(t)$ converges to zero at infinite time,

$$\lim_{t\to\infty} f(t) = 0 \tag{2.24}$$

and the integral has to be convergent:

$$\int_0^\infty f(\tau) \cdot e^{-i\omega\tau} d\tau < \infty \tag{2.25}$$

So, assumed that the response function $f(t)$ describes polarization, the time dependent polarization can be written

$$\begin{aligned} \vec{P}(t) &= \epsilon_0\chi_e\vec{E}(t) + \Delta\vec{P}(t) && (2.26)\\ &= \epsilon_0\chi_e\vec{E}(t) + \int_0^t f(\tau)E(t-\tau)d\tau && (2.27) \end{aligned}$$

where $\chi_e = \epsilon_\infty - 1$ is the electric susceptibility. Combining equation (2.27) with amperes law (2.21) ($\vec{\nabla} \times \vec{H} = \vec{J}$), the total current density in the dielectric can be expressed as follows:

$$\vec{J} = \sigma\vec{E} + \epsilon_0\frac{\partial}{\partial t}\left((1+\chi_e)\vec{E}(t) + \int_0^t f(\tau)E(t-\tau)d\tau\right) \tag{2.28}$$

In the equation above the term $(1+\chi_e)$ is equal to the high frequency limit of the relative permittivity ϵ_∞, [28].

It is seen from equation (2.28) that the conductivity σ, the high-frequency component of the relative permittivity $\epsilon_\infty = 1 + \chi_e$ and the dielectric response function $f(t)$ will characterize the behavior of the dielectric material. This gives in the time domain the possibility to apply an electric field, measure the current density and then try to estimate parameters that characterize the material, [33].

2.5.2 Dielectric Response In The Frequency Domain

The dielectric response in the frequency domain can be characterized by the frequency-dependent susceptibility, which is defined as the Fourier transform of the response function $f(t)$ expressed as follows [21]:

$$\begin{aligned}\chi(\omega) &= \chi'(\omega) - i\chi''(\omega) && (2.29)\\ &= \int_0^\infty f(t)e^{i\omega\tau}d\tau && (2.30)\\ &= \int_0^\infty f(t)\cos(i\omega\tau)d\tau + i\int_0^\infty f(t)\sin(i\omega\tau)d\tau && (2.31)\end{aligned}$$

The electric susceptibility is a complex function, so it contains information about both the amplitude and phase components of the polarization. The real part $\chi'(\omega)$ tells us the amplitude of the polarization, in phase with the harmonic electric field, the imaginary part $\chi''(\omega)$ gives the component of the polarization 90° out of phase with the field. The real and imaginary parts of the complex susceptibility at frequency $\omega = 0$ are

$$\chi'(0) = \int_0^\infty f(\tau)d\tau \tag{2.32}$$

and

$$\chi''(0) = 0 \tag{2.33}$$

When the Fourier transform is applied to Amperes law, it becomes

$$\vec{J}(\omega) = \sigma E(\omega) + i\omega D(\omega) \tag{2.34}$$

The displacement field $\vec{D}(\omega)$ can be expressed in terms of $\chi'(\omega)$, $\chi''(\omega)$ and $\vec{E}(\omega)$:

$$\begin{aligned}\vec{D}(\omega) &= \epsilon_0\vec{E}(\omega) + \vec{P}(\omega) && (2.35)\\ &= \epsilon_0(1 + \chi'(\omega) - i\chi''(\omega))\vec{E}(\omega) && (2.36)\end{aligned}$$

So, equation (2.34) can be expressed as:

$$\vec{J}(\omega) = \left(\frac{\sigma}{\omega\epsilon} + \chi''(\omega) + i(1 + \chi'(\omega))\right)\omega\epsilon_0\vec{E}(\omega) \tag{2.37}$$

where $(\frac{\sigma_0}{\omega\epsilon_0} + \chi''(\omega))$ is in phase with the electric field and therefore generates power loss. However $(1 + \chi'(\omega))$ is 90° out of phase to the driving field and does not contribute to the loss. Normally the material has several polarization processes coexisting but not significantly interacting. Therefore the susceptibility could be divided up, with one susceptibility representing each process:

$$\chi' = \sum_i \chi'_i \tag{2.38}$$

In many situations, it is more convenient to talk about the complex relative permittivity, which is defined as follows [21].

$$\vec{J}(\omega) = i\omega\epsilon_0(\epsilon'(\omega) - i\epsilon(\omega))\vec{E}(\omega) \tag{2.39}$$

which leads to:

$$\epsilon'(\omega) = 1 + \chi_e + \chi'(\omega) \tag{2.40}$$
$$\epsilon''(\omega) = \frac{\sigma}{\epsilon_0 \omega} + \chi''(\omega) \tag{2.41}$$

By definition: $1 + \chi' = \epsilon'_r$ and $\chi'' = \epsilon''_r$ where $\epsilon'_r$is the real part of relative permittivity, and ϵ''_r is the imaginary part of relative permittivity. Together they provide the complex permittivity $\tilde{\epsilon}(\omega)$ of the material in the following expression:

$$\tilde{\epsilon}(\omega) = \epsilon'(\omega) - i\epsilon''(\omega) \tag{2.42}$$
$$= \epsilon_0(\epsilon'_r(\omega) - i\epsilon''_r(\omega)) \tag{2.43}$$
$$= \epsilon_0\left(1 + \sum_i \chi'_i(\omega) - i\left(\frac{\sigma}{\epsilon_0\omega} + \sum_i \chi''_i(\omega)\right)\right) \tag{2.44}$$

2.5.3 Kramers–Kronig Relations

$\chi(\omega)$ is the Fourier transform of $f(t)$ defined in the previous sections, and therefore $f(t)$ can be calculated by the inverse Fourier transform of either $\chi'(\omega)$ or $\chi''(\omega)$. The relation between $\chi'(\omega)$ and $\chi''(\omega)$ is known as the Kramers-Kronig relations, which is a general mathematical formulation that connects the real and imaginary parts of any complex function that is analytical in the upper half plane. [59, 22].

$$\chi'(\omega) = \frac{1}{\pi}\int_{-\infty}^{+\infty} \frac{\chi''(\omega')}{\omega' - \omega} d\omega' \tag{2.45}$$

and,

$$\chi''(\omega) = -\frac{1}{\pi}\int_{-\infty}^{+\infty} \frac{\chi'(\omega')}{\omega' - \omega} d\omega' \tag{2.46}$$

Since the transform of a constant will be zero, a constant $\chi'(\omega)$ will not contribute to $\chi''(\omega)$. Likewise, where $\chi''(\omega) = \frac{\sigma}{\omega\epsilon_0} = \mathrm{C} \cdot \omega^{-1}$ the imaginary part of the susceptibility will not contribute to the real part.

$$\chi''(\omega) = -\frac{1}{\pi}\lim_{a\to\infty}\int_{-a}^{+a} \frac{k}{\omega' - \omega} d\omega' = -\frac{k}{\pi}\lim_{a\to\infty} \ln\left|\frac{a-\omega}{a+\omega}\right| = 0 \tag{2.47}$$

$$\chi'(\omega) = \frac{1}{\pi}\lim_{a\to\infty}\int_{-a}^{+a} \frac{\frac{\sigma}{\omega'\epsilon_0}}{\omega' - \omega} = \frac{\sigma}{\epsilon_0\pi}\lim_{a\to\infty}\left[\ln\left|\frac{\omega'-\omega}{\omega'}\right|\right]_{-a}^{+a} = \frac{\sigma}{\epsilon_0\pi}\lim_{a\to\infty}\ln\left|\frac{a-\omega}{a+\omega}\right| = 0 \tag{2.48}$$

In Figure 2.22, the graphs representing $\chi'(\omega)$ and $\chi'(\omega)+k$ are transformed to the $\chi''(\omega)$ curve below. The graphs representing $\chi''(\omega)$ and $\chi''(\omega) + \frac{\sigma}{\omega\epsilon_0}$ are transformed to $\chi'(\omega)$

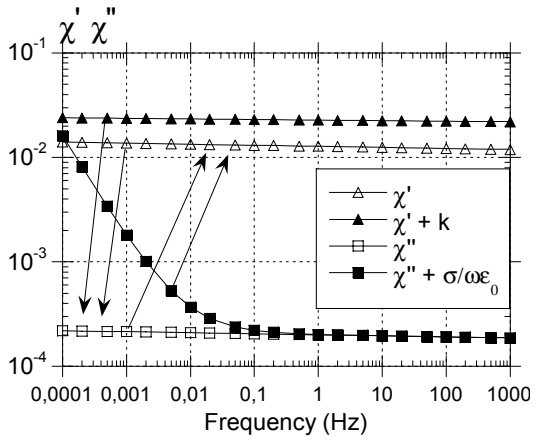

Figure 2.22: Kramer-Kronig relations.

When making frequency domain measurements the complex relative permittivity is measured. Recalling equation (2.41), the complex relative permittivity can be expressed as

$$\epsilon(\omega) = \epsilon_\infty + \chi'(\omega) - i\left(\left(\frac{\sigma}{\epsilon_0\omega}\right) + \chi''(\omega)\right) \tag{2.49}$$

2.5.4 Dielectric Loss Tangent $\tan\delta$

One of the factors usually defined to quantify dielectric losses is the dielectric loss tangent $\tan\delta$. Often called the dielectric loss tangent. It is defined as the ratio between the loss of energy due to resistive losses and polarization over one period of an applied alternating electric field and the maximum stored energy in the dielectric over the same period, [28] .

$$\text{Loss factor} = \tan\delta = \frac{\text{Dissipated energy per cycle}}{\text{Maximal stored energy per cycle}} \tag{2.50}$$

In the frequency domain equation (2.21) can be re-written as equation (2.51), given an harmonic varying applied electric field $\vec{E(t)} = \vec{E_0}\exp i\omega t$:

$$\vec{\nabla}\times\vec{H} = \underbrace{\sigma\vec{E}}_{\text{Induced current}} + \underbrace{\epsilon_0 i\omega\vec{E}}_{\text{Displacement current}} + \underbrace{i\omega\vec{P}}_{\text{Polarization current}} \tag{2.51}$$

In a uniform and isotropic material with complex electric permittivity $\epsilon' - i\epsilon''$ the polarization is proportional to the electric field $\vec{P} = \epsilon_0\chi_e\vec{E}$. So, Amperes law can be re-written as equation (2.53).

$$\vec{\nabla} \times \vec{H} = \sigma\vec{E} + \epsilon_0 i\omega\vec{E} + i\omega(\epsilon' - i\epsilon'')\vec{E} - \epsilon_0 i\omega\vec{E} \quad (2.52)$$

$$= \underbrace{i\omega\epsilon'}_{\text{Capacitive}}\vec{E} + \underbrace{(\omega\epsilon'' + \sigma)}_{\text{Resistive}}\vec{E} = \vec{J}_{tot} \quad (2.53)$$

The power-loss P_{loss} predicted by Ohms law is $P = U \cdot I$. Using equation (2.53) with Ohms law in a plane-parallel geometry, the power-loss per volume in a uniform electric field can be found. The power-loss per volume is given in equation (2.54). .

$$p_{loss} = \frac{P_{loss}}{V} = \frac{\mathrm{Re}\,(UI^*)}{V} = \frac{\mathrm{Re}\,(EdAJ_{tot})}{Ad} = (\omega\epsilon'' + \sigma)E^2 \quad (2.54)$$

The energy stored in the dielectric material per unit volume equals the capacitive reaction of equation (2.53).

$$p_{stored} = \omega\epsilon' E^2 \quad (2.55)$$

The loss tangent given in equation (2.56), is defined as the tangent of the angle between the lossy and lossless parts of equation (2.53) in the complex plane. δ is called the loss-angle.[32].

$$\tan\delta = \frac{P_{loss}}{P_{stored}} = \frac{p_{loss}}{p_{stored}} = \frac{\omega\epsilon'' + \sigma}{\omega\epsilon'} = \frac{\epsilon''}{\epsilon'} + \frac{\sigma}{\omega\epsilon'} \quad (2.56)$$

One of the great advantages by using $\tan\delta$ as a measure for dielectric losses is that the value is independent of geometry, and can be used as a loss factor even if the geometry of the insulation-system is unknown. [28], [22].

2.5.5 Frequency Domain Dielectric Spectroscopy

As expressed in equation (2.56) the dissipation factor $\tan\delta$ is dependent on the real and imaginary parts of the complex permittivity ϵ', ϵ'' and the DC conductivity σ, where the complex permittivity is frequency dependent $\tilde{\epsilon}(\omega) = \epsilon'(\omega) - i\epsilon''(\omega)$. Therefore the capacitance of the material will be complex; $\tilde{C}(\omega) = C'(\omega) - iC''(\omega)$. The complex capacitance can be related to the permittivity by a factor dependent on the geometry of the sample, as shown in equation2.57 for a parallel plate capacitor, where A is the plate area and d is the distance between the plates,

$$\tilde{C}(\omega) = C'(\omega) - iC''(\omega) = \left(\frac{A}{d}\right)(\epsilon'(\omega) - i\epsilon''(\omega)) \quad (2.57)$$

The real part of the complex capacitance represents the capacitive component of the insulation material and the imaginary part represents its lossy component. The loss factor can therefore be written as $\tan\delta = \frac{C''}{C'}$.

The complex susceptibility can also be related to the complex permittivity:

$$\tilde{\chi}(\omega) = \chi'(\omega) - i\chi''(\omega) = \frac{\tilde{\epsilon} - \epsilon_\infty}{\epsilon_0} \tag{2.58}$$

where ϵ_∞ is the very high frequency limit, and the permittivity a is purely real value, [28]. In the frequency domain the dielectric material will also have a complex conductivity $\tilde{\sigma}(\omega)$. This ac conductivity is due to the dielectric response, and is also linked to the steady state DC conductivity which has nothing to do with the dielectric relaxation phenomena. [8],[29]

Dielectric losses and conductivity are in reality two separate concepts, but is often presented together under the common umbrella of "losses". Some times it can be difficult to separate the two, since they both will add up to the measured impedance in the experimental measurements. So, to avoid confusion it should be said that $\frac{\epsilon''}{\epsilon'}$ represents the losses in an ideal insulator without conductivity (or a good insulator in the high frequency range), else wise the dielectric losses should include $\frac{\sigma}{\epsilon_0 \omega}$.

To summarize the factors contributing to energy dissipation in dielectrics:

- In alternating electric fields, polarization/depolarization currents lead to molecular vibrations and dissipation of energy through an increase in entropy/heat development (intermolecular viscosity/friction). The lossy reaction is characterized by $\epsilon''(\omega)$ or $\chi''(\omega)$ and is dependent on various polarization mechanisms in the dielectric. Sometimes called AC conductivity.
- The losses in static fields are associated with the DC resistivity which arises from Ohmic resistivity (electron scattering).

2.5.6 The Effect of Polar Groups on Dielectric Losses

The main reason why it is suspected that carbonyl compounds will have a significant effect on the dielectric response and losses in polyethylene is that carbonyl groups (C=O) has a permanent dipole moment grater than that of C−H, which have no net contribution to the permanent dipole moment in a polyethylene molecule. The carbonyl dipole is shown in figure 2.23.

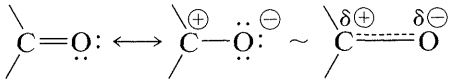

Figure 2.23: The carbonyl dipole

In terms of an atomic orbital description, the carbonyl bond can be represented as shown in Figure 2.24. The carbon is sp^2-hybridized so that the σ bonds (one of which is to oxygen) lie in a single plane (coplanar).

The last p orbital on carbon forms a π bond to oxygen. The polarity of the carbon-oxygen double bond implies that the electrons of the π- bond (and also the σ bond) are associated more with oxygen than with carbon. This is supported by the dipole moments of aldehydes and ketones, which indicate the degree of the polarization of the C=O bonds; the dipole moments are in the neighborhood of 2.7 D [1], which corresponds to 40-50% ionic character for the carbonyl bond. The σ bonds to carbon are coplanar, at angles near to 120°; the two pairs of unshared electrons on oxygen are shown as occupying orbitals n in Figure 2.24.

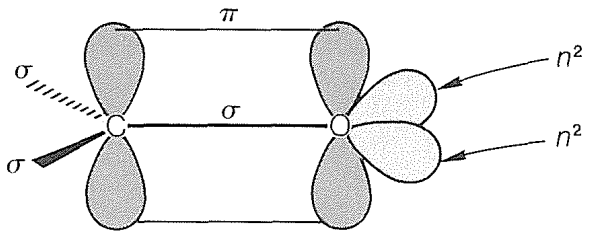

Figure 2.24: Atomic-orbital description of the carbonyl group,[46].

The dependence of $\tan\delta$ on dipolar groups in polyethylene is shown compactly as [54]

$$\tan\delta = C_f n \mu^2 \tag{2.59}$$

where n is the "polar group density" , which is the number of polar groups per thousand carbon atoms, μ^2 is the mean square of the dipole moment of the polar group, and C_f is a function derived from the Onsager reaction field and Cole-Cole law. [54].

The Cole-Cole rule states,[5]

$$\tilde{\epsilon} - \epsilon_\infty = \frac{(\epsilon_s - \epsilon_\infty)}{1 + (i\omega\tau)^\beta}. \tag{2.60}$$

Where ϵ_s and ϵ_∞ are the static[2] and "infinite frequency" dielectric constant respectively. ω is the circular frequency and τ is a general relaxation time. β is a parameter giving the degree of dispersion in the system lying between 0 and 1. $\beta = 1$ corresponds to relaxation of a system of ideal noninteracting dipoles in an AC field i.e one single relaxation time, which is known as Debye response.
Typical Debye response is shown in Figure 2.25

The imaginary part of the permittivity ϵ'' is expressed as follows:

$$\epsilon'' = \frac{1}{2}(\epsilon_s - \epsilon_\infty)\frac{\sin(\beta\pi/2)}{\cosh(\beta x) + \cos(\beta\pi/2)} \tag{2.61}$$

[1]The Debye is a cgs unit of dipole moment $1\text{D} = 10^{-18}$ statC $\cdot$ cm

[2]In the literature it is usual to use ϵ_0 for the static ($\omega = 0$) permittivity, however in this thesis ϵ_s is used to avoid confusion with the vacuum permittivity.

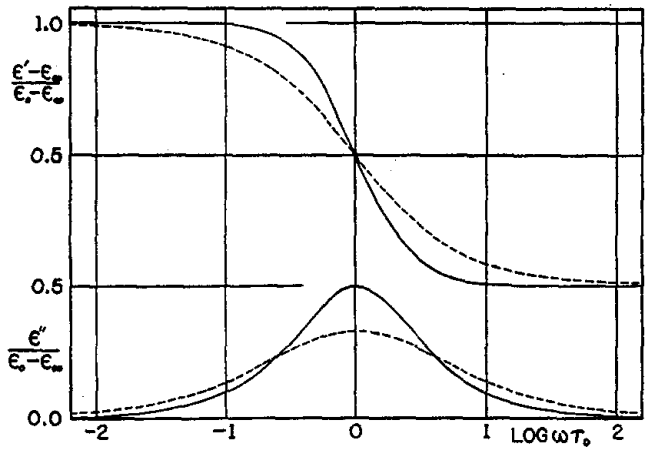

Figure 2.25: Principal behavior of Debye response (non-interacting dipoles, $\beta = 1$), theoretical (solid line) and experimental (dashed), from [54].

where $x = \ln(\omega\tau)$.
The imaginary permittivity in the cole-cole relation has its maximum value at the dispersion frequency ($\omega\tau = 1$) $\implies$ $x = 0$, so ϵ''_{max} is expressed as

$$\epsilon''_{max} = \frac{1}{2}(\epsilon_s - \epsilon_\infty)\tan\left(\frac{\beta\pi}{4}\right). \tag{2.62}$$

It is seen that ϵ''_{max} decreases with an decrease in β. For polyethylene β can vary from one single Debye relaxation ($\beta = 1$) to multiple relaxation frequencies ($\beta < 1$). If $(\epsilon_s - \epsilon_\infty)$ is small, then ϵ'' will also be a small number. $(\epsilon_s - \epsilon_\infty)$ is expressed from the Onsager reaction field [51],

$$(\epsilon_s - \epsilon_\infty) = \frac{4\pi}{3kT}\frac{3\epsilon_s}{2\epsilon_s + \epsilon_\infty}\left(\frac{\epsilon_\infty + 2}{3}\right)^2 N\mu^2 \tag{2.63}$$

where k is the boltzman constant, T is the temperature , d is the density of polyethylene and N is the number of polar groups per unit volume.
Recall that the loss tangent is $\tan\delta = \frac{\epsilon''}{\epsilon'}$. In many cases the real permittivity will be approximatively equal to the static permittivity $\epsilon' \simeq \epsilon_s$. The expression for $\tan\delta$ is calculated by using equation (2.61) and (2.63).

$$\tan\delta \simeq \frac{\epsilon''}{\epsilon_s} \tag{2.64}$$

$$\simeq \frac{2\pi}{kT}\left(\frac{\epsilon_s + 2}{3}\right)^2 \frac{N}{n}\frac{\sin(\beta\pi/2)}{\cosh(\beta x) + \cos(\beta\pi/2)} n\mu^2 \tag{2.65}$$

The relationship between n and N for polyethylene can be calculated as follwos:

$$\frac{N}{n} = \frac{d}{M} N_A \frac{M}{14 \times 10^3}, \tag{2.66}$$

where d is the density of the polyethylene, M is the molecular weight and N_A is Avegardro's number.

The expression for C_f becomes:

$$C_f = \frac{2\pi}{kT} \frac{1}{2\epsilon_s + \epsilon_\infty} \left(\frac{\epsilon_s + 2}{3} \right)^2 \frac{\sin(\beta\pi/2)}{\cosh(\beta x) + \cos(\beta\pi/2)} \tag{2.67}$$

If the polyethylene contains several polar groups, the losses can be written as

$$\tan\delta = \sum_i C_{f,i} n_i \mu_i^2 \tag{2.68}$$

The most noteworthy about equations (2.65) and (2.68) is that the loss factors ϵ'' and $\tan\delta$ increases linearly with the polar group density n and the mean square dipole moment μ^2, of a given polar group.

2.6 Breakdown

The term electrical breakdown can have several meanings. In gases such as air it is usually known it usually means that the gas becomes ionized and conductive which leads to Townsend discharges[1] and corona discharges. In solid dielectrics it occurs as momentary events like sparks and electrostatic discharges or continuous arc discharges. Common to all breakdown phenomena in insulating materials is that they eventually causes failure of the electrical apparatus or power equipment if safety devices like circuit breakers or safety protective devices do not kick in. If the dielectric is a solid, permanent physical and chemical changes along the path of the discharge will significantly reduce the material's dielectric strength, so the device will be permanently broken. However, if the dielectric material is a fluid or gas, the dielectric can recover its insulating properties when the current through the discharge channel has been interrupted by a circuit breaker. The mechanisms causing breakdown in solid dielectrics will be discussed in this section.

2.6.1 Breakdown Caused by Electrical Discharges

Electrical discharges is the cause of breakdown in many cases in solid materials. In breakdown tests discharges usually occur in the surrounding material and increases the test area and produces failure at or beyond the electrode edge. Discharges may also occur in voids or gas-bubbles that are present in the solid dielectric. These discharges may cause chemical degradation and erosion in the material, and may continue until the failure path is complete between the electrodes.

2.6.2 Thermal breakdown

Thermal breakdown occurs when materials are subjected to high electric field intensities causing dielectric and conduction losses, and subsequently develops cumulative heating within the material which generates heat more rapidly than the material can dissipate. Electrical breakdown in all materials, whether in gas, liquid, or solid phase, is ultimately due to thermal instability, leading to the destruction of the material. Thermal breakdown generally refers to the breakdown caused by Joule heating continuously generated within the dielectric specimen, due mainly to electrical conduction and polarization, which cannot be extracted fast enough by thermal conduction or convection. The general equation governing the balance of the heat generation rate and the heat loss rate is given by

$$C_v \frac{dT}{dt} = \vec{\nabla} \cdot (\kappa \nabla T) = \sigma E^2, \tag{2.69}$$

where C_v is the specific heat per unit volume, κ is the thermal conductivity, and σ is the electrical conductivity. In the case of DC fields, σ is

[1] Townsend discharge is the gas ionization process that causes an avalanche multiplication of free electrons in a strong electric field, giving rise to conduction

the DC electrical conductivity; in the case of AC fields, σ should include the conductivity due to dielectric polarization loss ($\omega\epsilon''$) in addition to the ohmic conductivity as shown in equation (2.54).

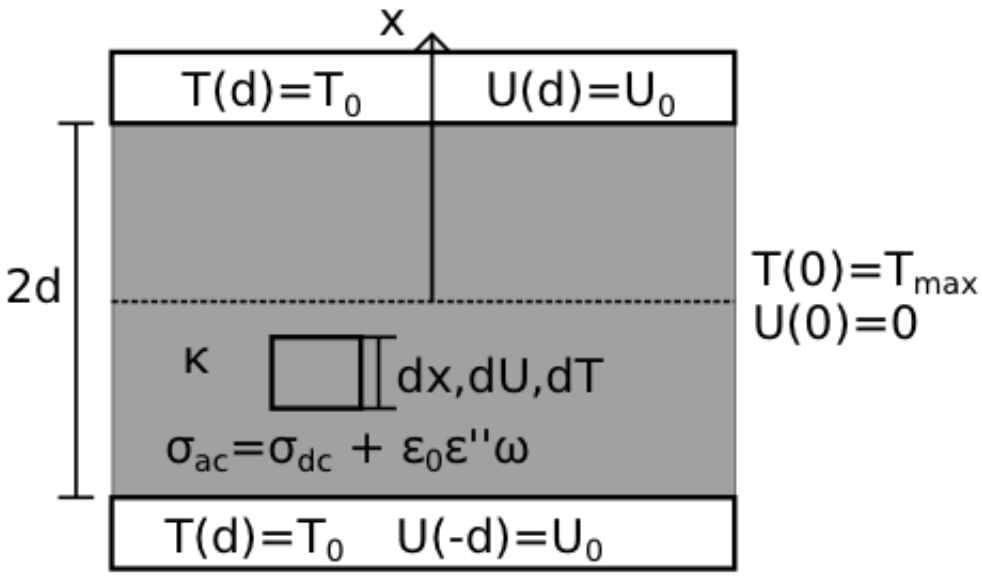

Figure 2.26: Condenser with boundary conditions

Dielectric losses will cause heating of the insulating material. This is why, for the applications of dielectric materials under AC voltage, it is important to keep the $\tan\delta$ -loss as low as possible. This loss is an essential parameter in determining the thermal breakdown voltage.[28, 35].

From equation (2.69) it is possible to derive a direct relation between the breakdown voltage and dielectric losses. And that the heat is generated only in the dielectric material by the dielectric losses $P = (\sigma + \epsilon''\omega)E^2$ .If we assume a uniform electric field (parallel plate condenser) $E = -\frac{dU}{dx}$. Then, equation (2.69) simplifies to one dimension. The parallel plate condenser with thermal and electric potential boundary conditions is shown in Figure 2.26.

$$\frac{d}{dx}\left(\kappa\frac{dT}{dx}\right) + \sigma_{ac}\left(\frac{dU}{dx}\right)^2 = 0 \tag{2.70}$$

Recognizing Ohms law $J = -\sigma_{ac}\frac{dU}{dx}$ and the continuity of the current $\vec{\nabla}\cdot\vec{J} = 0$ (no charge build up), so J = constant, using the boundary conditions $\frac{dT(0)}{dt} = 0$ (zero heat flux at the centre of the parallel plate capacitor) and integrating gives

$$\int_0^{\kappa\frac{dT}{dx}} d\left(\kappa\frac{dT}{dx}\right) = J\int_0^U dU \tag{2.71}$$

$$\kappa\frac{dT}{dx} = J\cdot U \tag{2.72}$$

Re-introducing $J = -\sigma_{ac}\frac{dU}{dx}$ gives:

$$-\kappa\frac{dT}{dx} = \sigma_{ac}U\frac{dU}{dx} \tag{2.73}$$

Integrating equation (2.73) across the capacitor, with applied voltage $V = 2U_{max}$, the expression becomes:

$$\int_{-V/2}^{V/2} U dU = \int_{T_{max}}^{T_0}\left(-\frac{\kappa}{\sigma_{ac}}\right)dT \tag{2.74}$$

When exchanging $\sigma_{ac} = \sigma_{dc} + \epsilon''\omega$, the final expression governing the thermal breakdown voltage is

$$V^2 = 8\int_{T_0}^{T_{max}} \frac{\kappa}{\sigma_{dc}+\omega\epsilon''}dT = \frac{8}{\omega}\int_{T_0}^{T_{max}} \frac{\kappa}{\epsilon'\tan\delta}dT. \tag{2.75}$$

Some observations on equation (2.75) is made:
First of all, it shows that the thermal breakdown mechanism occurs at the voltage V and is independent on insulation thickness. And that the main factors determining the thermal breakdown strength is the thermal conductivity κ and the dielectric losses ϵ'', and their dependence on temperature. Equation (2.75) also shows that T_0, which is the cooling of the object, plays a significant role.

2.6.3 Intrinsic breakdown

Intrinsic breakdown occurs if the electric field intensity becomes sufficient to accelerate electrons through the material. The mechanism may be present and involved in thermal breakdown, so the field intensity necessary for intrinsic breakdown may be higher than the critical field for thermal breakdown. The critical field intensity is called intrinsic dielectric strength.
In solid dielectrics the intrinsic breakdown strength is high, of the order of 10MV/cm. Under carefully conditions with purified materials free of imperfections the intrinsic breakdown strength may be reached. But dielectrics usually fail at electric field intensities far below the intrinsic breakdown strength, usually due to internal discharges, thermal breakdown, electro-chemical breakdown or chemical deterioration.[28].

2.6.4 Breakdown strength of polyethylene and XLPE

To figure out what effect the oxidized material has on the insulation properties it is of key importance to find what possible effects the degree of oxidation may have on the breakdown strength of the material. [13].

Dielectric breakdown strength of solid dielectric insulation has been measured and presented in [39, 57], using the ASTM D149 standard for dielectric breakdown testing. Some data for polyethylene is shown in table 2.3.

The dielectric strength of polyethylene varies based on many factors, so they range from 18.9 kV/mm to 160 kV/mm.

Table 2.3: Breakdown strength of extruded polyetyhlene insulation

Material	Dielectric strength (kV/mm)	Reference
Polyethylene	18.9	[39]
Polyethylene, low-density	21.7	[39]
Polyethylene, high-density	19.7	[39]
Polyethylene, cross-linked	21.7	[39]
Commercial Polyethylene	154-160	[61]
Polyethylene, low-density	20-160	[52]
Polyethylene, high-density	20-160	[52]

3 Experimental work

3.1 Material

All materials comes from a commercial polyethylene resin produced by Dow Chemical Company, and was provided trough by Nexans Norway AS. It was received in the form of a granulate that further more had to be processed, to make XLPE test objects. The test objects were produced at Sintef's moulding laboratory in Trondheim. Test-object geometries used was mainly of two types: XLPE sheets of thickness 0.25mm, and so-called Rogowski objects.
The XLPE sheets are circular and have a thickness of about 0.25mm, the main purpose of the sheets is to determine the aging time of XLPE trough thermal oxidation an measuring the content of oxidation products by FTIR.
Rogowski objects have a geometry similar to that of a cylindrical cup with a flat bottom that represents the insulation, it was produced test objects with an insulation-thickness of 0.25mm ± 0.02mm. Rogowski type objects has a design optimized for the experimental procedures used to measure dielectric response, conductivity and break down strength. A sketch of the Rogowski profile is shown in Figure. 3.27
The bottom is painted with conductive paint at both sides, which acts as a conductive interface between the electrodes and insulating material.

The intention of the Rogowski-profile is to ensure that the uniform field-strength in the middle of the test object is not exceeded towards the edge. More details of the Rogowski-profile are described in [16].

3.1.1 Degassing

From the preoxide cross-linking process there will be some gaseous byproducts left in the XLPE. When the cross-linking is completed, the insulation will have an approximately constant level of byproducts throughout its thickness as expected from the uniform distribution of peroxide at extrusion. The byproduct are components such as cumylalcohol, water, and acetophenone, which are polar in nature. This means they will modify the dielectric and conduction properties of the material that includes them. It was therefore necessary to degas all test objects used in this thesis. The byproducts are gaseous so they can be removed by heated diffusion trough in a low external pressure, [10]. Since the insulation thickness of the samples is relatively thin (0.25mm), it was assessed that a degassing of 3 days in a heated vacuum cabin at 70°C would give a sufficiently low level of byproducts.

3.1.2 Removing Internal Stresses

The test-objects are made by hot-pressing (melting) PE into rigid (steel) moulding shapes and subsequently cross-linking the polymer into a thermosetting phase. Then the objects are cooled down to the crystalline solid

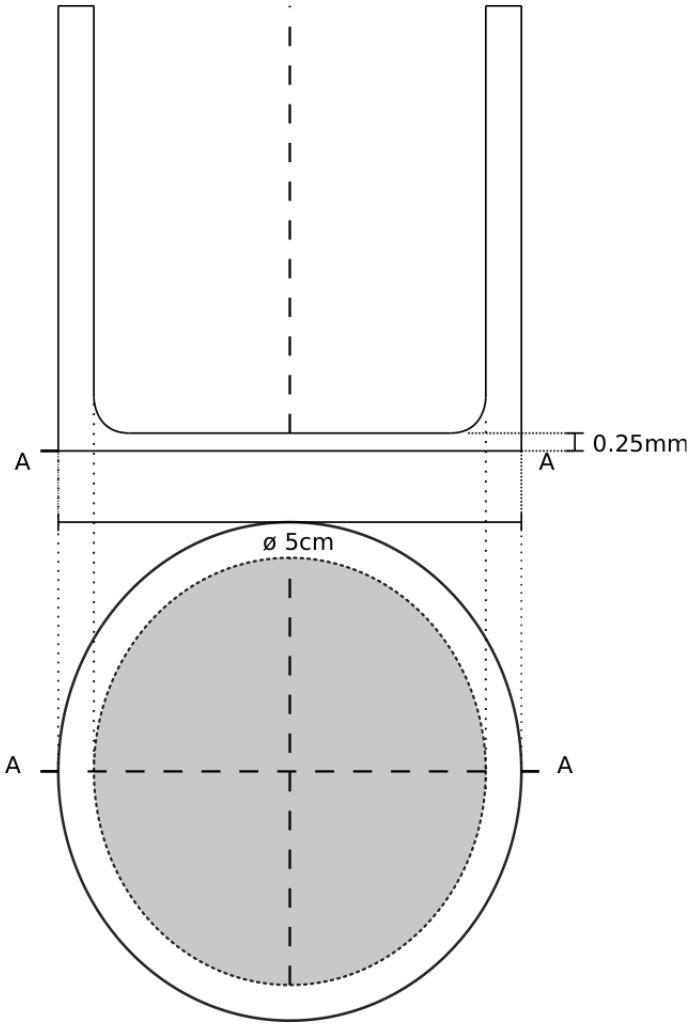

Figure 3.27: Rogowski profile, vertical cross-section and bottom view.

Table 3.4: Test objects

Type	Thickness	Intention	Additives	Degassed
XLPE-Sheets	0.25mm	Thermal oxidation, FTIR	Unknown (peroxides and stabilizers)	Yes
XLPE-Rogowski	0.25mm	Thermal oxidation, Dielectric response, Breakdown Test and FTIR	Unknown (peroxides and stabilizers)	Yes
PE - Sheets	0.25mm	Thermal oxidation, FTIR	No	No

phase whilst still in the moulding shapes. This process leaves internal mechanical stresses in the test objects that are undesirable for experimental testing, since they might cause unevenness of the insulation thickness.
The problem of internal stresses is easily solved by taking the objects out of the moulding shapes, and then heating them up again to the glass transition temperature at about 90°C. When the glass transition temperature is reached, the XLPE will be in the amorphous phase and the internal structure of the XLPE matrix will be rearranged to minimize the mechanical stresses. When cooled down to the crystalline phase, the stresses are evenly distributed. The process is done in about 30min in a heating cabinet holding a temperature of about 90°C, allowing the entire object to reach the glass transition temperature.
This process is really just necessary for the reference series of test objects, since the oxidizing temperature for the thermal aging procedure is well above the glass transition temperature.

3.1.3 Production of Artificial Oxidized XLPE Contaminations

To study the chemical characteristics of the contaminations closer, artificial contaminations were created by oxidizing sheets of XLPE. The XLPE sheets were produced by melting polyethylene granulate into 0.25 mm thick sheets. Since the the polyethylene discs was to be thermally oxidized at temperatures above the melting point of polyethylene, which is between 120°C and 130°C, the polyethylene had go trough a cross-linking process to make the thermo-plastic PE into thermosetting XLPE. The purpose of these XLPE sheets is mainly to determine the time and temperature necessary to achieve the same carbonyl-concentration in the

artificial contaminations as in the three categories of real contaminations. By oxidizing the XLPE sheets at a given temperature for different time lengths the FTIR-spectra of artificial contaminations can be tuned to match the spectra of the real. By doing this it is possible to determine the time and temperature required to oxidize realistic test-objects that will represent the real contaminations needed for experiments related to the electrical properties of the contaminations.

3.1.4 Characterization of Organic Contaminations

Contaminations in the polymeric material was found and sorted using a optical control system installed at the Nexans laboratory, which can identify inclusions of dark material in the else-wise white and transparent polyethylene pellets. The particles of darker oxidized material was furthermore investigated using optical microscopy. By visual impression the particles were categorized into three different categories, the main attribute for the initial categorizing of the particles was coloring. The first category is the lightest shade of brown. The third category is the darkest color with almost completely black and non-translucent material in its interior, and a dark shade of brown is observed at its boundary surfaces. In the second category it was observed that the lighter particles has a smoother transition of coloring at the interface between dark oxidized material and the surrounding optically transparent polyethylene material. Images of the contaminations is shown in images 3.28 (a-d).

3.1.5 FTIR Study of Organic Contaminations and Oxidized XLPE

In order to study the oxidation products found in the contaminations, a Perkin-Elmer FTIR-spectrometer was used.

It is possible to present the FTIR Spectra in several ways. In this thesis the data will be presented quantitative as absorption-spectra. The absorption-spectra is obtained by applying Beer-Lamberts law to the intensity-data (transmittance spectra) from the spectrometer. All investigations is done by comparing a reference sample to a sample from contaminations or oxidized material cut into sections of equal thickness. The absorption-spectra is adjusted by a linear factor such that the absorbance at wavenumber 1890cm^{-1} is zero. This has to be done since the intensity can vary and be attenuated because of other factors than the carbonyl contents of the contaminations, such as varying beam intensity, slight differences in sample thickness and varying detector sensitivity, and the fact that the two spectra is strictly obtained in two separate operations. It is stated that the absorption/transmission 1890cm^{-1} remains constant for XLPE in oxidized and unoxidized samples, so the intensity of the reference sample and sample will be equal $I(k = 1890\text{cm}^{-1}) = I_0(k = 1890\text{cm}^{-1})$. Hence, in accordance with Beer-Lamberts law the absorption will equal zero at $k = 1890\text{cm}^{-1}$. The constant C of the absorption spectra are worked out in the following way,

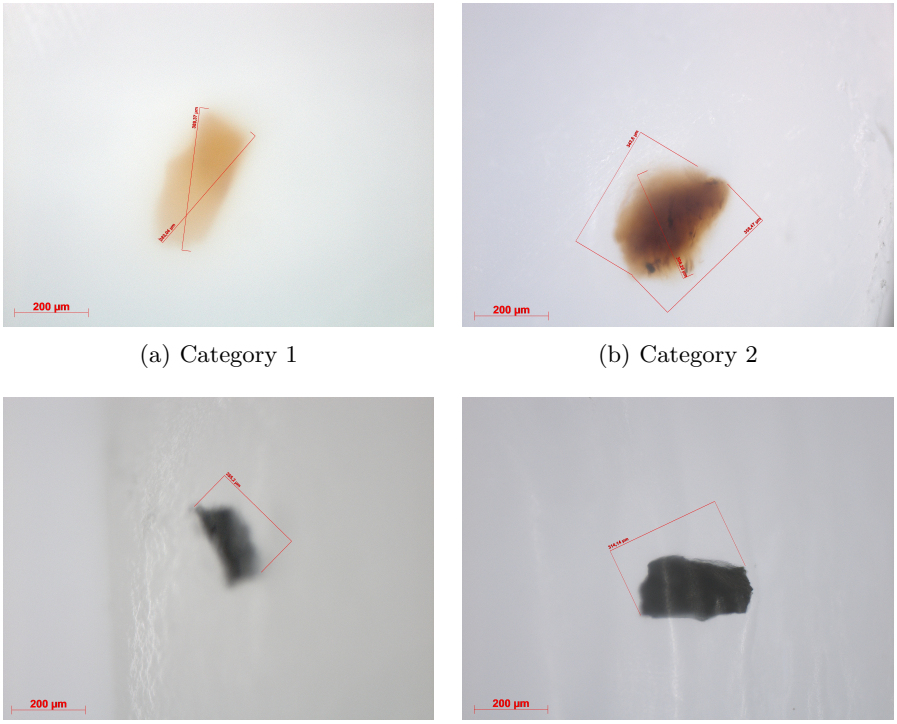

(a) Category 1

(b) Category 2

(c) Category 3

(d) Category 3

Figure 3.28: Particles from the three categories of contaminations

using I as the real intensity and I' as the measured intensity.

$$\begin{aligned} I(1890) &= I_0(1890) \\ \Rightarrow \log(I(1890)) &= \log(I_0(1890)) \\ \log(I(1890)) &= C \cdot \log(I'(1890)) \\ \Rightarrow C &= \frac{\log(I(1890))}{\log(I'(1890))} \end{aligned}$$

Applying the constant C to the entire spectrum, the measured intensity is adjusted to equate the real intensity.

$$\Rightarrow \log(I) = C \log(I') \tag{3.76}$$

The beer-lamberts law is re-written to produce the absorption spectra, in the following way:

$$\begin{aligned} A &= -\log\left(\frac{I}{I_0}\right) \\ &= \log(I_0) - \log(I) \\ &= \log(I_0) - C \cdot \log(I') \end{aligned}$$

So,

$$A = \alpha \cdot c \cdot d = \log(I_0) - C \cdot \log(I') \tag{3.77}$$

The real particles of contaminations from category 1-3 was investigated by taking microtome sections of $d \simeq 40\mu$m for category 1 and 2. The sections was placed on a KBr-disc which is transparent to infrared-light. The KBr disc was placed in a microscope mounted on the FTIR-spectrometer allowing the IR-beam to be manually aligned and adjusted to the particle. Due to particularly high infrared absorption[1] in the region of interest in the spectra from category 3 particles, the microtome sections of the category 3 particle was reduced to a thickness of $d \simeq 25\mu$. The artificial contaminations was investigated in the same manner, by taking microtome sections of $d \simeq 40\mu$m through the side of the 0.25mm thick sheets. In addition to the microscope detector the spectrometer also have a detector meant for larger samples, this was used to provide additional measurements on the oxidized films, this way a more averaged value for the concentration of oxidized material is obtained, taking into account that it is possible that the material might be un-uniformly oxidized (i.e. it is reasonable to believe that the material is more oxidized in a thin surface layer than in the bulk of the material, since the availability of oxygen is limited by diffusion in the bulk of the material)[60].

In figure 3.30 a typical view of a contamination from the FTIR-microscope is shown. It shows how it is possible to limit the IR-beam to fit the size of the particle cross section.

[1] If the absorption approaches 100% it will be impossible to determine the actual concentration of the chemical group in interest

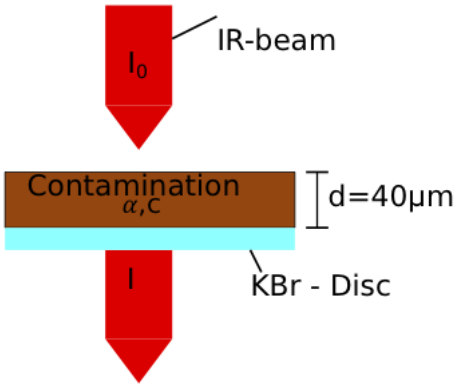

Figure 3.29: Conceptual drawing of the IR absorption in a contamination

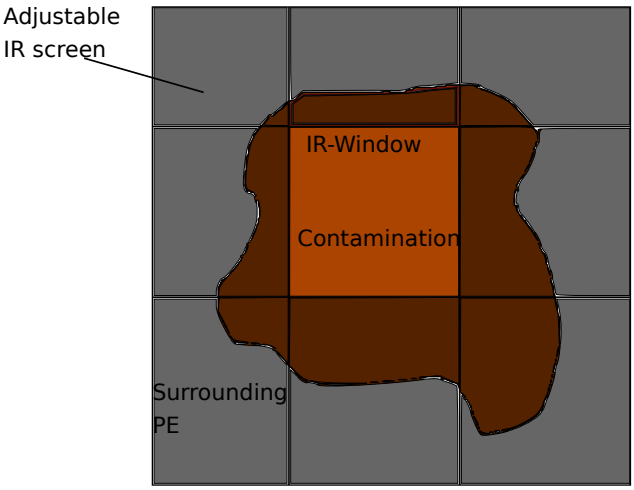

Figure 3.30: View of a contamination through the FTIR microscope

3.1.6 Thermal Ageing Procedure - Sheets

The XPLE samples were moulded to be 0.25mm ± 0.02mm thick plates. The samples were placed into a ventilated oven, heated to 170 °C ± 1°C, allowing isothermal oxidation with a constant supply of air. The temperature in the oven was monitored by a computer logger. Samples of oxidized XLPE was cut out of the samples at different times and investigated by infrared spectroscopy to determine the development of carbonyl compound concentration as a function of oxidation time at 170°C. The choice of oxidation temperature of 170°C was done on a background of the typical temperatures that will occur during production of the material and hence give rise to the oxidized contaminations.
It has also been observed in the pre-study for this thesis, that the carbonyl levels found in the contaminations are not reached in reasonable times at temperatures around 100 °C.
In an article by Langiois et. al [60] it is also shown that the oxidation surface layer is controlled by diffusion, and that the thickness of the surface layer build up of carbonyl is a decreasing function of temperature. To reach auto-accelerating oxidation for diffusion controlled thermal oxidation a high temperature like 170°C is necessary [56, 24]. The auto-accelerating oxidation is a likely candidate for the process in which the organic contaminations have occurred.

In Figure 3.31 the development of the carbonyl peak at k=1721cm^{-1} is shown. The time range of the spectra in Figure 3.31 is from 10h for the smallest peak to 340h for the highest. The peak height is shown as a function of time in Figure 3.32.

Table 3.5: Oxidized sheets and real contaminations

	t [hrs]	A/d (1721cm^{-1}) [a.u/mm]
Oxidized XLPE Sheets	10	6.05
	18	10.15
	20	18.94
	26	22.35
	48	25.03
	72	30.43
	120	32.33
	125	30.72
	143	37.03
	240	40.97
	300	44.73
	340	45.91
Real Contaminations	Category 1	10.45
	Category 2	30.36
	Category 3	31.34

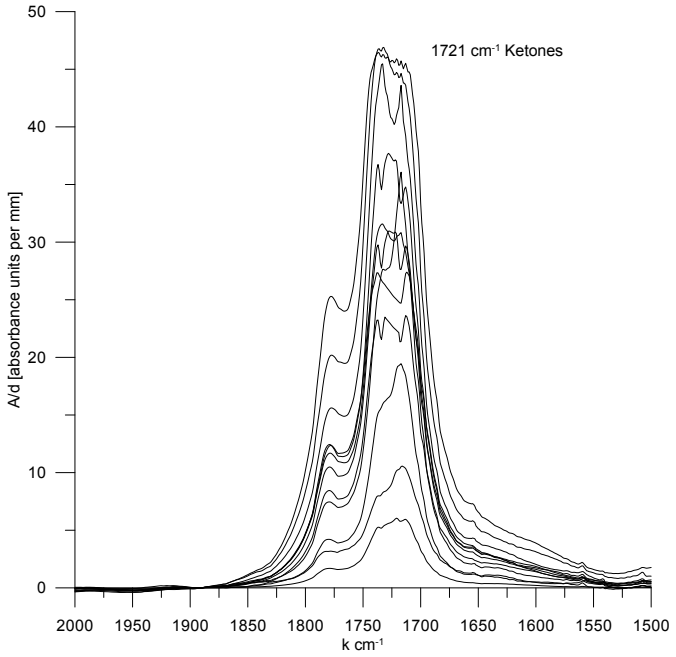

Figure 3.31: Developement of the 1721cm^{-1} carbonyl absorption peak in oxidized XLPE sheets.

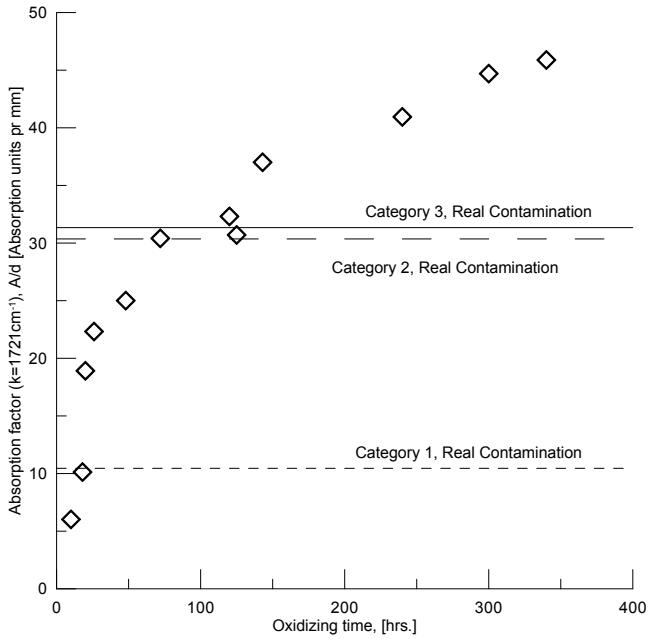

Figure 3.32: Oxidation times vs. carbonyl absorption (k=1721cm^{-1}).

3.1.7 Thermal Aegeing Procedure - Rogowski objects

In the same manner as for the XLPE plates, the Rogowski objects were thermally oxidized at 170 °C ± 1°C. The very point of this procedure is to exert the same aging conditions to the Rogowski objects, and thereby getting the same degree of oxidation as the XLPE sheets and thereby getting a carbonyl content that is comparable to the real organic contaminations that has been investigated by FTIR-spectroscopy. It was necessary to do the preliminary FTIR measurements on XLPE sheets to determine the oxidation times for the Rogowski test-objects. Figure 3.32 shows the development of the carbonyl absorption at 1721cm^{-1} with time for XLPE sheets.
Two sets of Rogowski objects were aged for 18 hrs. and 72 hrs, corresponding to the carbonyl content of the contaminations of category 1 and 2. The dynamics of the oxidation and issues of category 3 contaminations are to be discussed in the results section. The results of the investigation of the XLPE plates had to be taken into consideration for the thermal oxidation procedure for the Rogowski objects. So for reasons discussed in the results section, it was produced one set of thermally oxidized Rogowski objects that were aged for 2 weeks at 170 °C ± 1°C, to represent a degree of oxidation that is well above that of category 1 and 2 contaminations (even though the dynamical change in the FTIR-spectrum is not the same as category 3 contaminations).

3.2 Dielectric Response Measurements

The dielectric response measurements is obtained by using a Insulation Diagnostic System IDA-200.
For the dielectric response measurements, all test objects were painted with a thin carbon based conducting paint, which allows a thin even interface between the electrode and insulating material.

IDA-200 measures impedance. By measuring the impedance at one point, i.e. at a specific frequency and amplitude, parameters such as resistance, capacitance and loss can be calculated.
The impedance of a sample is measured by applying a voltage across the sample. This voltage will generate a current through the sample. By accurately measuring the voltage and the current, the impedance can be calculated, see Figure 3.33.

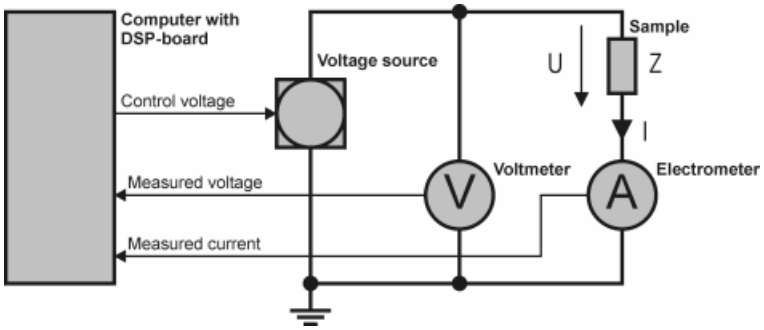

Figure 3.33: Measurement of electrical impedance

The impedance is calculated using Ohm's law: $Z = \frac{U}{I}$, where Z, U and I are complex entities.

The voltage (and the current) is generated by an external voltage source. The voltage is measured by means of a voltmeter and the current is measured by an amperemeter or electrometer which acts as a current-to-voltage converter. The analogue signals (voltages) are then converted to digital samples of the signals that are used in subsequent calculations.

In dielectric response measurements, the basic parameter measured is the complex ratio of voltage and current in the AC circuit that is formed by the voltage source, electrodes and test specimen. The test specimen is basically represented by a capacitance and resistance. And it is this capacitance and resistance that is used in the material model to calculate parameters such as permittivity, $\tan\delta$, and conductivity. The biggest issue with this measurements is that there is stray capacitance in the entire system, not just limited to the insulation part of the test specimen. E.g.

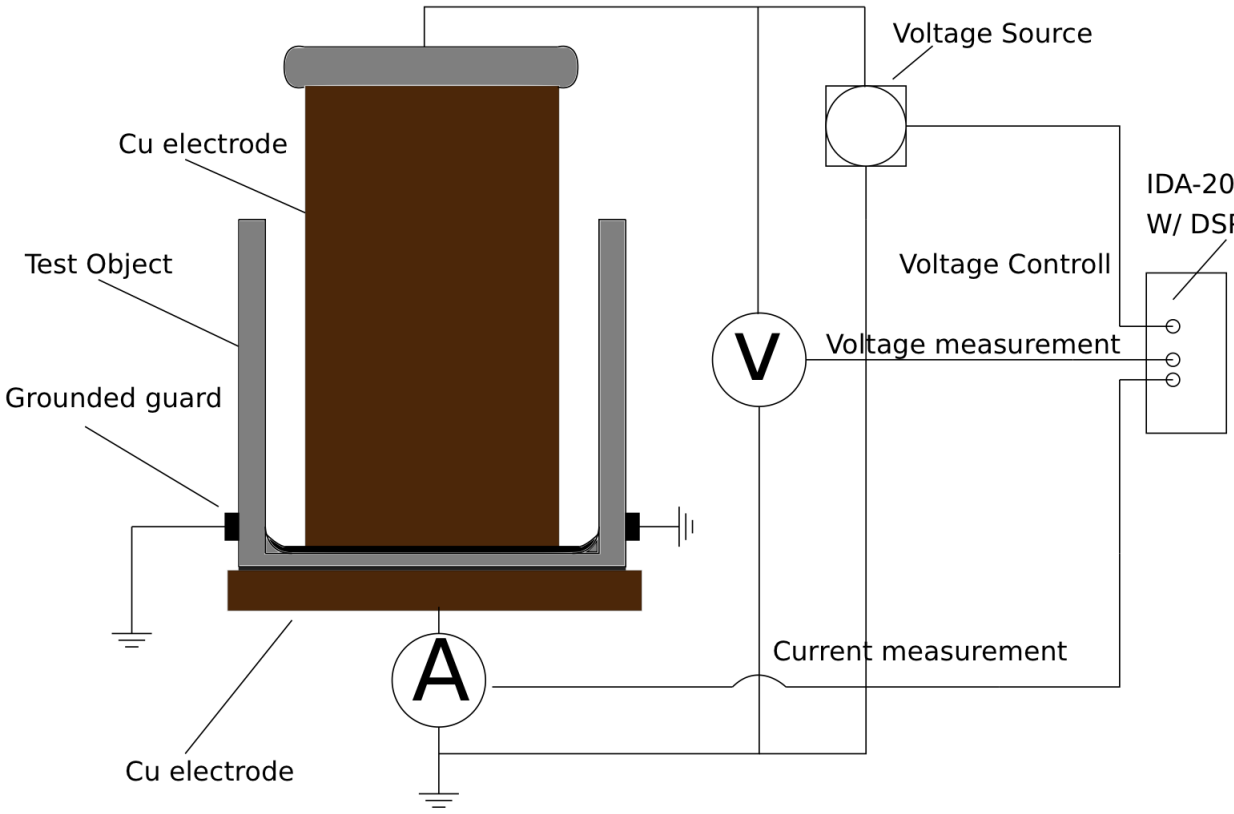

Figure 3.34: Set-up for dielectric response measurements on Rogowski objects.

there will be a capacitance in the air between the connector at the top and bottom electrodes that is attached. This is caused by the fact that the entire electrode is a equipotential surface and although the electrodes form parallel plate condenser at the test specimen there will be a fringing of the electric field at all for the edges of the electrodes. The issue has been limited by using tori with round edges to screen the fringing field from sharp edges. The stray capacitances will be more or less the same for all measurements, since the set-up of the system remains unchanged from one measurement to another. So, even though it introduces uncertainties, the uncertainty introduced by stray capacitance in the system will be the same for all test object.
In addition to stay capacitances in the system, there is also the possibility that there are surface currents going along the sides of the test object. In other works, it has been observed that the surface conduction current of oxidized polyethylene increases in proportion to the square of voltage in the high voltage range, [3], [55]. To minimize the interferences from surface conduction, the set-up includes a grounded screen that is a strip of thin aluminum foil tightly around the circumference of the test object and grounded by a conducting steel wire. By trial measurements it was found that the optimal placement of the aluminum strip was about 0.5mm above the bottom of the test object.
But indeed, there is still a possibility that some of the surface current will carry over the surface of the guard and reach the other electrode causing an error in the current measurement. It was found that the optimal placement of the guard was about 50mm above the bottom of the test object. It was seen that the role of the guard affected the measurement of the permittivity and $\tan\delta$ by 1-2 orders of magnitude.
The effect of the stray capacitance and surface conductivity can be described as in Figure 3.35 as an equivalent capacitance and resistance coupled in parallel with the test object. However, since the stray capacitance and surface conductivity may have non-trivial dependence on frequency and applied voltage these parameters may be difficult to quantify. So, rather than trying to calculate and subtract the effects from the measurements, the remedy is to limit the surface conductivity and the fringing of the electric field by shielding and improving the set-up by trial measurements.

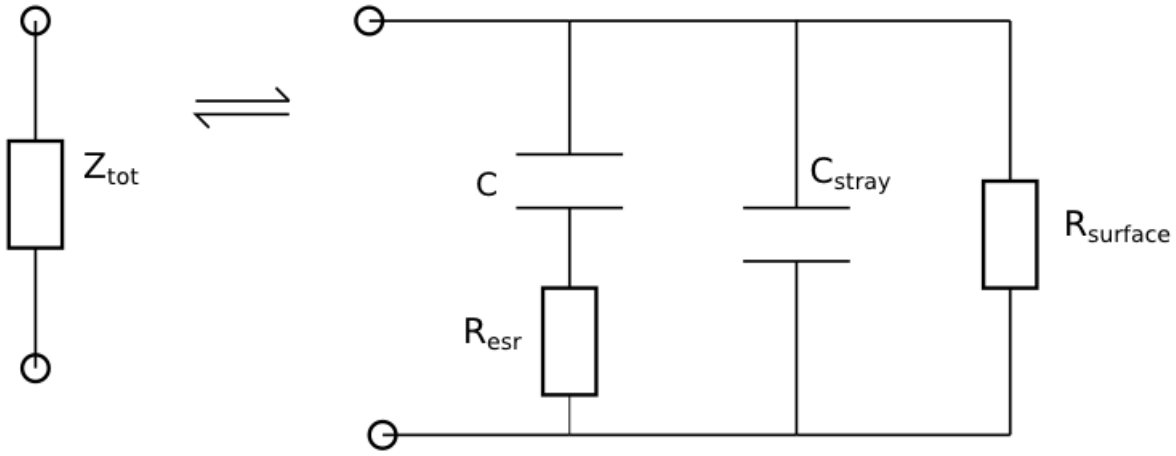

Figure 3.35: Equivalent of impedance of test object with stray capacitance and surface conductivity

3.3 Sample modeling

The insulation impedance Z can be presented directly or by using different impedance models. Two ways of presenting Z directely are the polar: $Z = Abs\{Z\}$, $\phi = Arg\{Z\}$, and rectangular: $Z_{Re} = \Re(Z)$, $Z_{Im} = \Im(Z)$.

The coplex capacitance is defined as follows.

$$C = C' - iC'' \tag{3.78}$$

The impedance Z of the capacitor is:

$$Z = \frac{1}{i\omega C} \tag{3.79}$$

The real and imaginary part of the comlex capacitance is:

$$C' = \mathrm{Re}\left(\frac{1}{i\omega Z}\right) \tag{3.80}$$

$$C'' = -\,\mathrm{Im}\left(\frac{1}{i\omega Z}\right) \tag{3.81}$$

To determine parameters like ϵ', ϵ'' the geometrical capacitance C_0 needs to be entered into the material model IDA uses. The geometrical capacitance is the capacitance between the electrodes when the medium is vacuum.
For a $\tan\delta$ measurement; δ will represent the angle between the impedance of a equivalent ideal capacitor (lossles) and an equivalent series resistance (ESR). The phasor diagram of such a circuit is shown in Figure 3.36, where $-jX_c$ is the impedance for the ideal capacitor. Evidently $\tan\delta = \frac{ESR}{|X_c|}$.

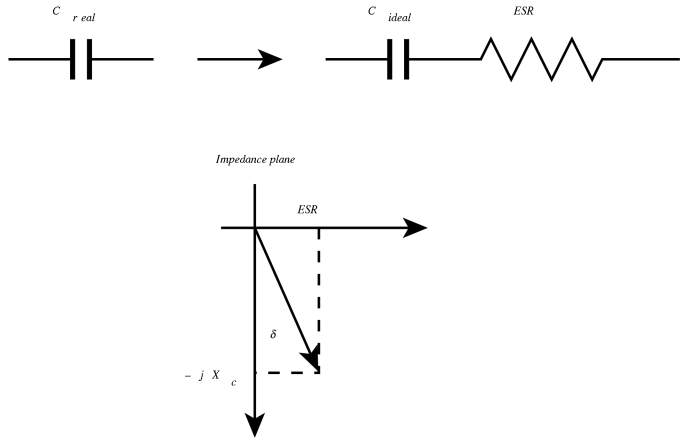

Figure 3.36: Impedance plane of a lossy capacitor (equivalent series model).

3.4 Breakdown Test of XLPE Insulation

The dielectric breakdown strength of the test objects is measured by a simple experimental setup. The measurements are obtained by following the procedure given in the ASTM D149 standard for dielectric breakdown testing. Using a step-by-step voltage increment. A total number of 5 test object from each category in addition to the reference objects is needed for this test. [29].

Since the carbon based electrode paint dissolved in silicone oil, all the test-objects used in the breakdown test was painted with electrically conductive silver epoxy instead. The silver epoxy was of the type EPO-TEK E4110, which is a two component epoxy mixed according to the data sheet in appendix C , and was cured 6h at 60°C.

Breakdown measurements are sensitive to imperfections in the insulation. This is because electric breakdown is a failure mechanism of the weakest point in the insulation, so if there are irregularities in the insulation specimen, these are most likely the reason that the breakdown occurs. The samples are of course prepared as carefully as possible, but at least 5 samples is needed to evaluate the breakdown strength with some statistical accuracy, inn accordance with ASTM D149 breakdown strength testing standard [29].
The breakdown strength is determined from the last 60s rms voltage level that the test object passed. The voltage increment is about 0.5kV for each step (electric field stress 2kV/mm), so the breakdown strength of each object can only be determined within ΔV_{rms} =0.5kV (ΔE_{rms} = 2kV/mm).
Because of varying breakdown strengths within each category of test objects, the standard deviations of the breakdown tests are quite significant, and as in every statistical experiment there would ideally be larger sample sizes than 5.

For this test a voltage regulator is used to produce 50Hz AC voltages in the range 3-230V which are stepped up using two test-transformers. A voltmeter is connected to the primary side of the step up transformer system, and a voltage probe is connected to the secondary side of the transformers at the same potential as the test electrode. The test electrode and the material specimen is all together immersed in a chamber of silicone-oil during the testing. The silicone oil will prevent breakdown and flashover that would occur in air at high voltages.

The voltage levels are incremented manually every 60s, and the exact voltage is recorded. When breakdown occurs the circuit will short circuit and an automatic circuit breaker will break the current. The last completed voltage level is the breakdown strength of the test object.

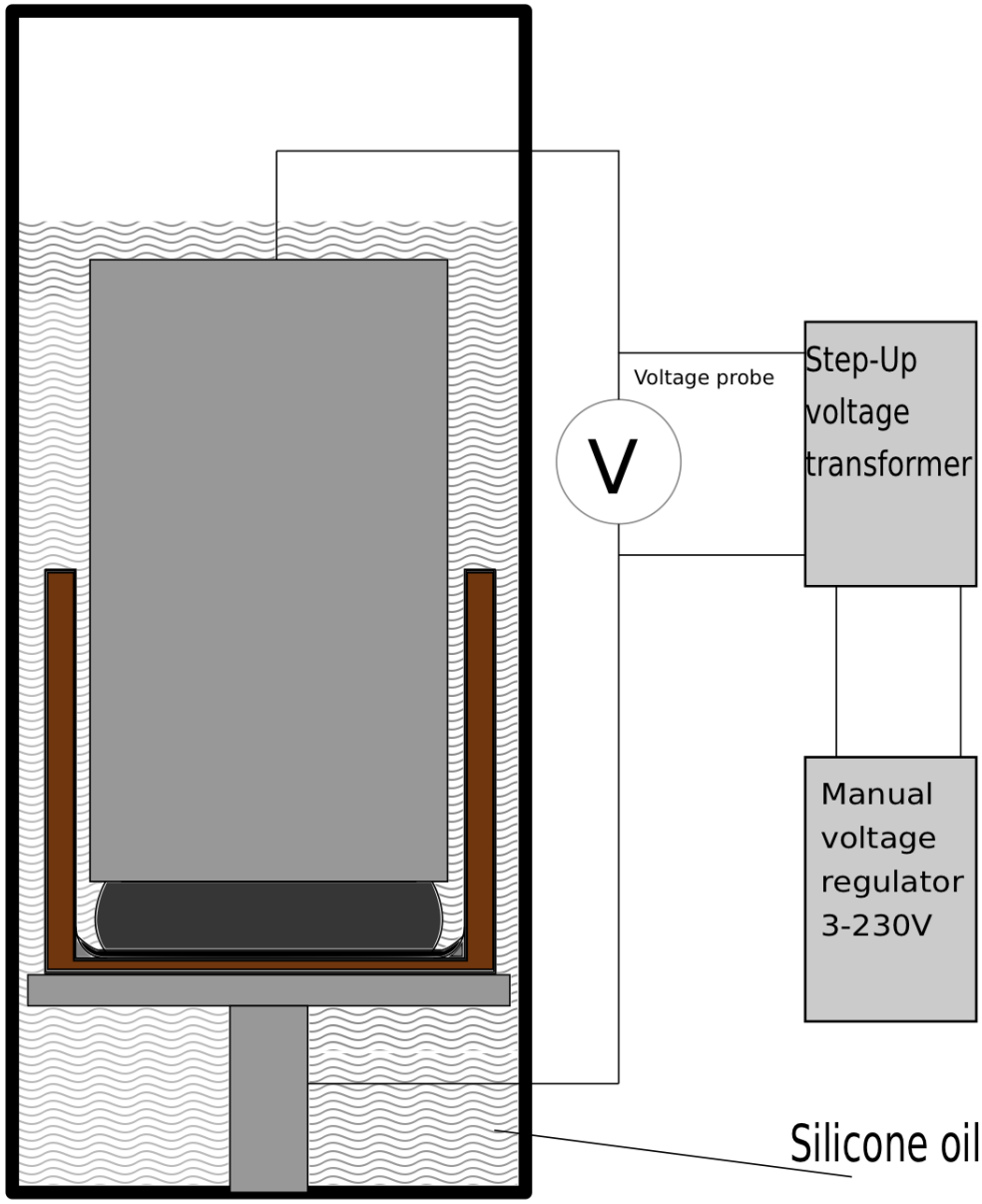

Figure 3.37: Set-up for breakdown test of Rogowski objects.

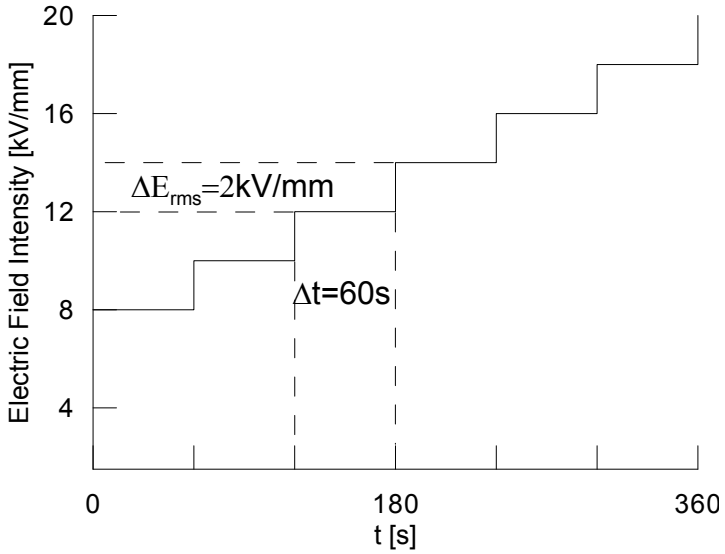

Figure 3.38: Electric field profile of step-by-step test

4 Results

4.1 FTIR Analysis

In figure 4.39 the transmittance spectra form contaminations of category 1 is shown together with the transmittance of uncontaminated polyethylene. This is so to speak the raw data produced by the FTIR, i.e the transmittance is the percent-wise transmitted intensity. The transmittance spectra uses air as reference i.e measurement without sample means 100% transmittance. It is assumed that air humidity and composure remains constant between the measurements. Common to all transmission spectra in the Figures (4.39 - 4.44) is the absorption band from about 2800cm^{-1} to 3000cm^{-1} is assigned to C−H stretching, and seems to be present in all spectra from aged and un-aged polyethylene without any particular change in.
Another feature in all the spectra is the 1890cm^{-1} edge that remains constant from un-aged to aged sample, this is used to normalize the absorbance when calculating the absorption spectra so that the absorbance at this wavenumber is zero.
The absorptions below 1300cm^{-1} has not been assigned to any particular substance, but is most likely due to C−O bonds like alcohol, esters or carboxylic acids that have relatively strong absorption over a broad band.
The absorption band for ketones centered around 1721cm^{-1} (C=O stretching) is clear in all the spectra, and is the most pronounced sign of oxidation.

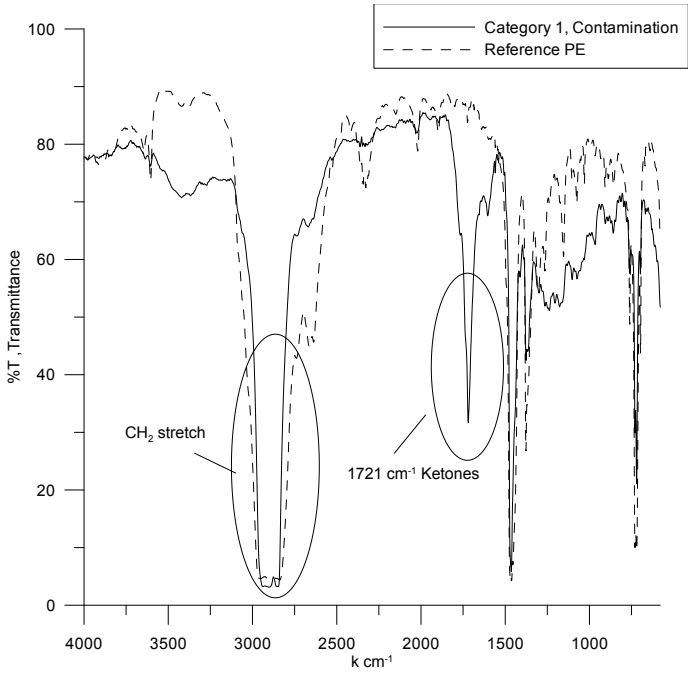

Figure 4.39: FTIR transmittance spectra of real organic contamination from category 1. Transmittance for ketones at 1721cm^{-1} is 32.3 % and 84.5% for the uncontaminated PE reference.

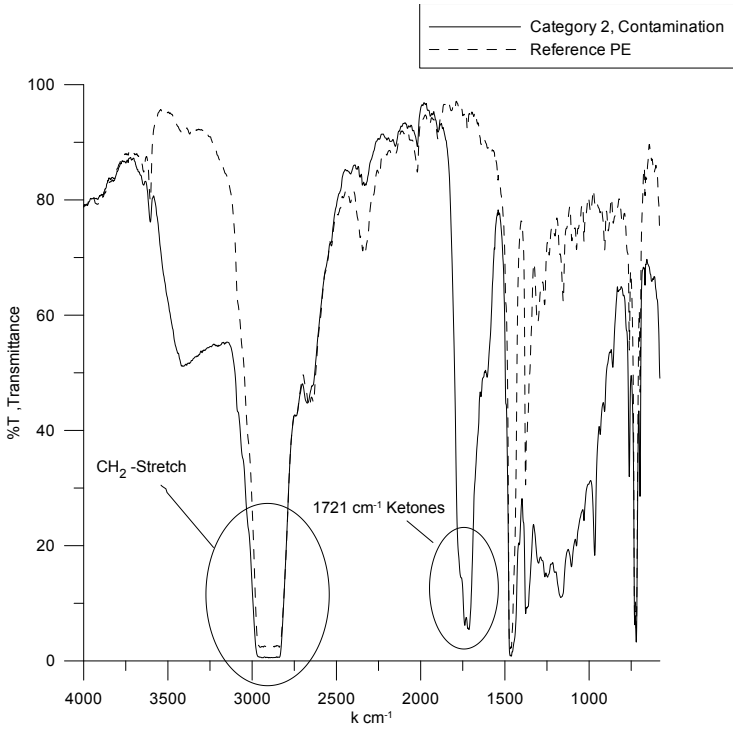

Figure 4.40: FTIR transmittance spectra of organic contaminations from category 2. Transmittance of 5.7% and the reference has 92.7% at k =1721cm^{-1}.

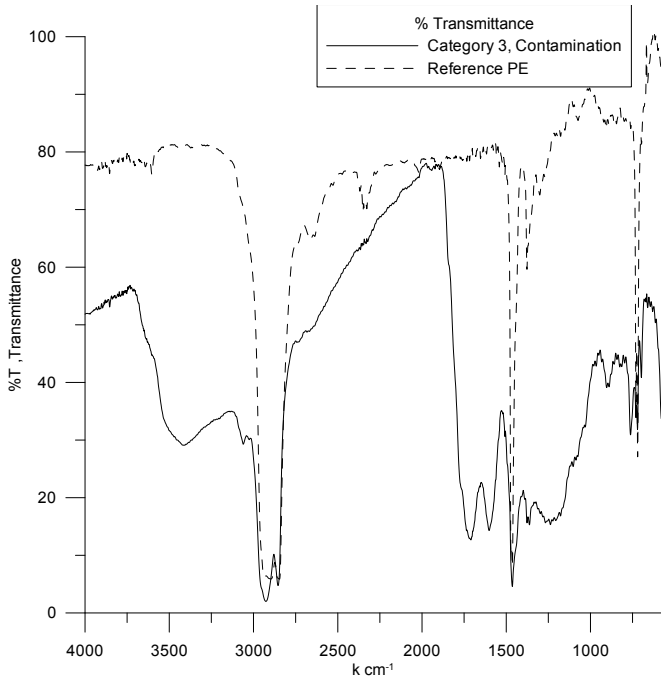

Figure 4.41: FTIR transmittance spectra of organic contaminations from category 3. The category 3 contamination has a transmittance of 12.9% and 78.4%. Bear in mind that the samples here is half the thickness 25μm for category 3, and 40μm for the other samples. Which explains slightly higher transmittance for the category 3 particle.

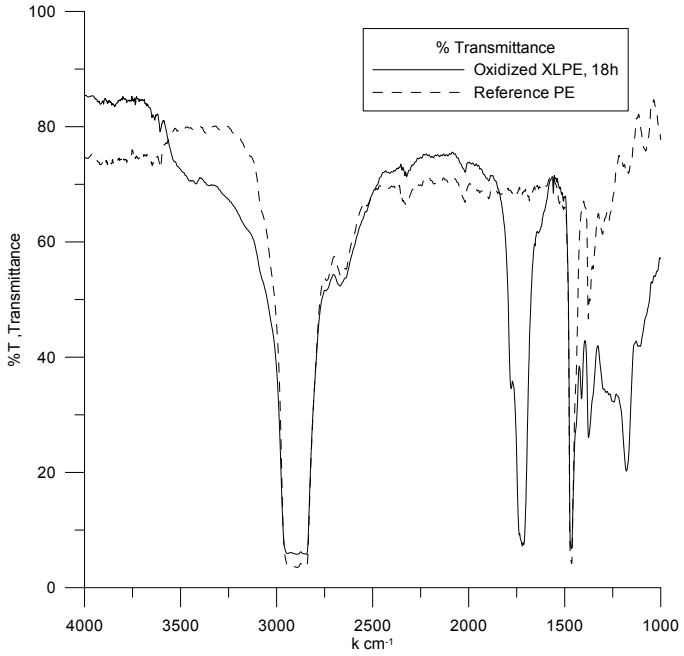

Figure 4.42: FTIR transmission spectra of oxidized XLPE sample, aged 18h. Transmittance of 7.2% and the reference has a transmittance of 68.4% at k =1721cm^{-1}.

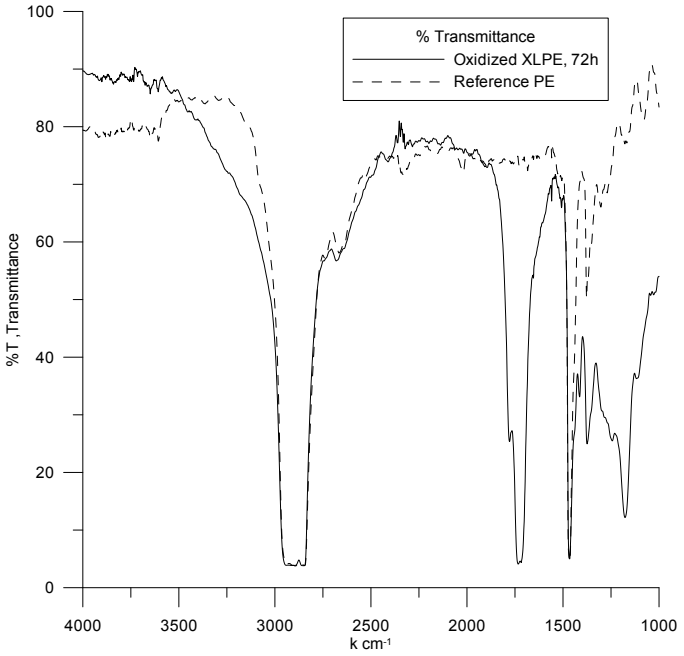

Figure 4.43: FTIR transmittance spectra of oxidized XLPE sample, aged 72h, transmittance of 4.5% and 73.1% for the reference, at k =1721cm^{-1}.

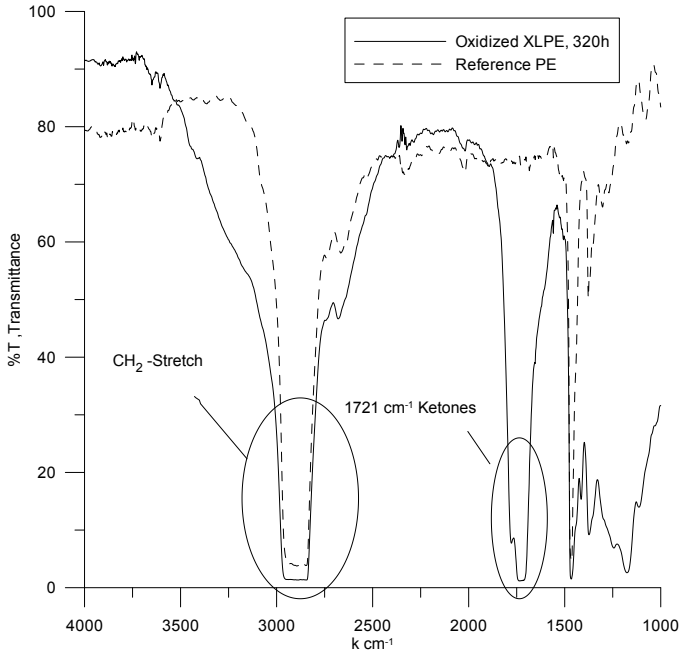

Figure 4.44: FTIR transmittance spectra of oxidized XLPE sample, aged 340h. The 340h aged contamination has a transmittance of 1.2% and 73.7% for the reference, at k =1721cm^{-1}.

The reason why the reference transmittance varies from spectra to spectra, is that the thickness of the samples can have a slight variation and the incoming intensity and detector sensitivity can change somewhat from measurement to measurement (several days timescale). This is unavoidable, but have been taken into account and corrected for when calculating the absorbance in accordance with Beer-Lamberts law mentioned in the experimental section.

4.1.1 Carbonyl Compounds

As previously mentioned, the organic contaminations has been determined to be byproducts of oxidized material that occurs in the polyethylene material used in cable-insulation. As a qualitative measure of degree of oxidation, the contaminations has firstly been categorized by their color ranging from lightly oxidized material with a light translucent brown color to very oxidized material with a black non-translucent color.
To quantify the degree of oxidation, FTIR-spectra of microtome sections cut from the contaminations has been investigated. Since the most distinctive products from thermo oxidation of polyethylene is aldehydic, ketonic and carbonyl compounds the region of interest has been chosen to be where these compounds are known to occur in the FTIR-absorption spectrum. The ROI of the FTIR experiments has been chosen to be from wave numbers $k = 2000 - 1500\text{cm}^{-1}$. By convention, the FTIR absorption spectra is usually shown with descending wave numbers along the x axis. Naturally, an equivalent way of presenting FTIR absorption and transmission spectra is with increasing wavelengths along the x-axis. These compounds are particularly easy to identify by infrared spectroscopy. As reported by Rugg et. al in [11], the IR absorption maximum occurs at wavelength of λ =5.81μm (wavenumber k=1721cm^{-1}) and "is almost entirely due to aldehydic, ketonic and carbonyl groups".

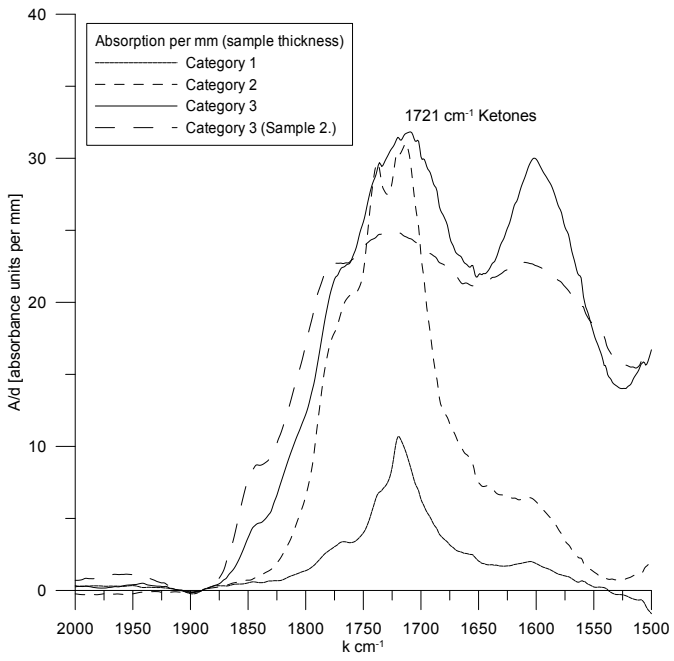

Figure 4.45: FTIR absorption spectra of organic contaminations

In figure 4.45 the results from FTIR-spectroscopy of the contamina-

tions is shown. The most distinctive peak for category 1 and 2 contaminations is at $k = 1721\text{cm}^{-1}$, and may be assigned to ketonic compounds. For category 3 contaminations, the most distinctive peaks is at $k = 1721\text{cm}^{-1}$ which indicates the same ketonic compounds as for category 1 and 2 contaminations. In addition there is a absorption peak at $k = 1610\text{cm}^{-1}$ for category 3 contaminations that may be assigned to carboxylic acids/ carboxylate ions. Whether the $k = 1610\text{cm}^{-1}$ absorption peak is due to thermal oxidation or not, is to be discussed further.

4.1.2 Ketones in Contaminations and Oxidized XLPE Samples

It is observed that in category 1 and category 2 contaminations the absorption peak at $k = 1721\text{cm}^{-1}$ is dominant and distinguished, the difference of category 1 and 2, is that the peak of category 2 has a higher absorption and also a broader band of absorption frequencies. This indicates that category 2 contaminations has a higher concentration of ketones. The broadening tells us that the ketones consist of several different ketonic molecules (C=O).The ketonic groups attached to the polymer chain has slightly different vibrational modes, dependent on the size of the molecule it is attached to, and will thereby give rise to a broadening of the absorption peak. The location of the oxygen atoms on the polyethylene-chains will also give rise to slightly different vibrational modes. In general, the vibrational eigen-frequencies of oxygen-carbon bonds located near the edge of the chain will be higher than for those located near the center of the chains [11].

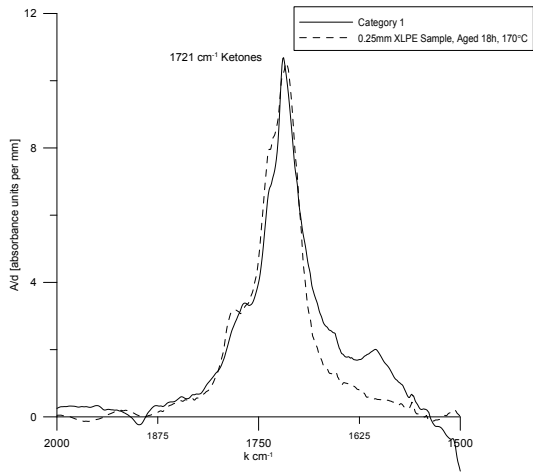

(a) Category 1 contamination and 18h oxidized XLPE sampe

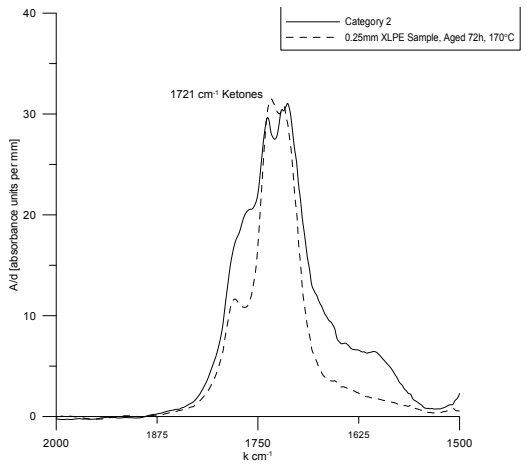

(b) Category 2 contamination and 72h oxidized XLPE sample

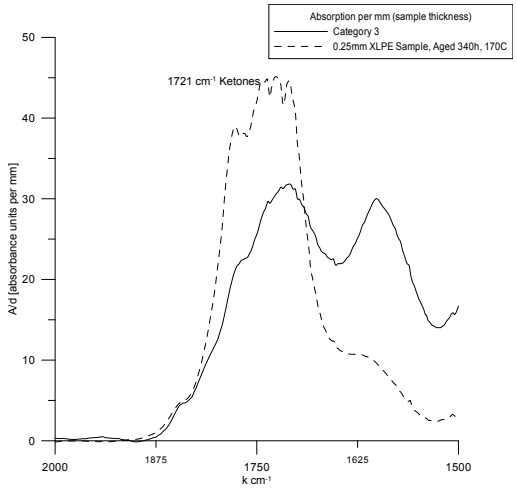

(c) Category 3 contamination and 320h oxidized XLPE sample

Figure 4.46: Comparison of FTIR absorption spectra of contaminations and oxidized XLPE samples.

4.1.3 The Category 3 Contamination

A trial PE sample was thermally oxidized for 340h to try to replicate the $k = 1610\text{cm}^{-1}$ peak, only to a moderate success, the spectra in Figure4.47 shows similarities, however there is not the same distinguished peak in the PE sample, rather a quite constant absorption-band reaching from about $k = 1850\text{cm}^{-1} - 1550\text{cm}^{-1}$.

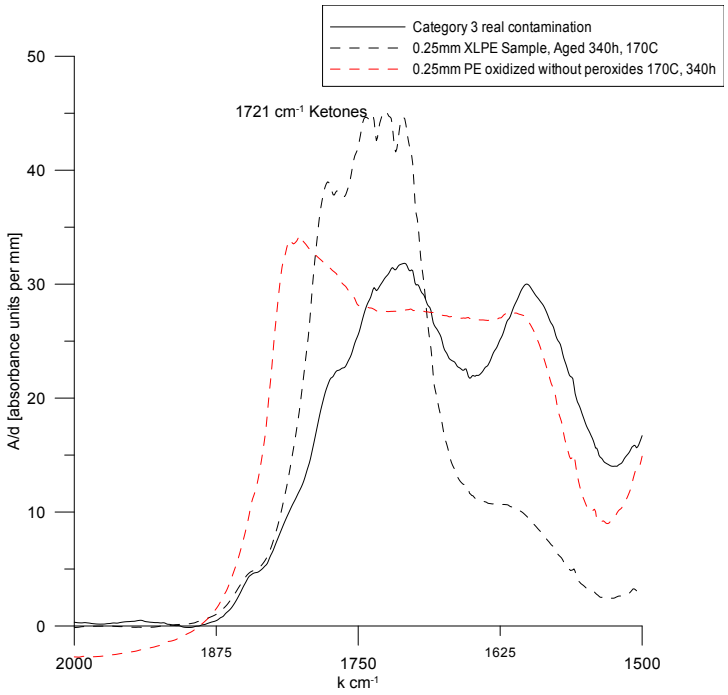

Figure 4.47: Absorption spectra of PE oxidized without peroxides and stabilizers compared with oxidized XLPE and a real contamination of category 3.

4.2 Dielectric Response Measurements

4.2.1 Permittivity

The dielectric response measurements shown in Figure 4.48 is taken at an RMS electric field of 4kV/mm (corresponding to a voltage of 1kV). For the relative real permittivity measurements there was seen no field dependence. The figure in show that the real permittivity ϵ' has a tendency to increase with the degree of oxidation. The reference samples has as normally for PE and XLPE a relative permittivity of $\epsilon' = 2.3$. For XLPE samples thermally oxidized for the category 1 contamination the permittivity was found to be $\epsilon' = 2.57$, for category 2 $\epsilon'(50\text{Hz} = 2.71$ and category $\epsilon'(50Hz) = 4.19$.

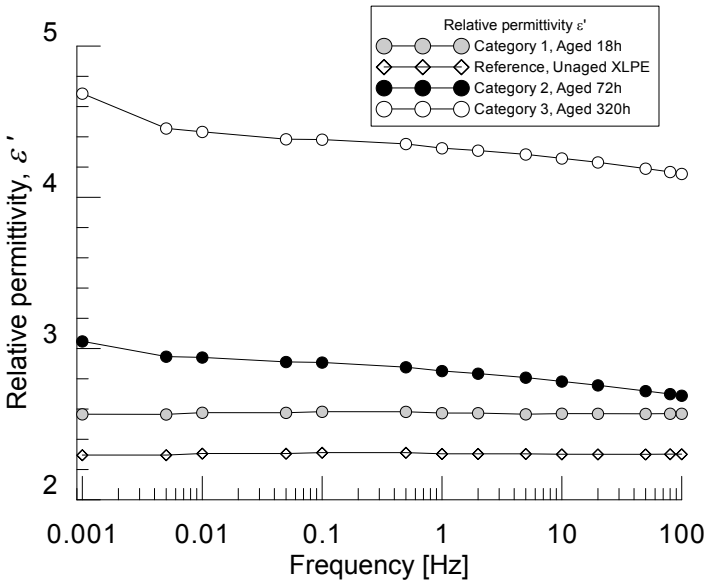

Figure 4.48: Relative permittivity measurements

Permittivities of category 2 and 3 contaminations shows a slight frequency dependence. Reference and category 1 contaminations has a quite constant real relative permittivities. The slight frequency dependence of ϵ' can be explained by polarization mechanisms other than the dipolar, such as hopping charge carries, or it can be explained by the uncontrolled surface currents which may have a frequency dependence and subsequently leads to false measurements. In Figure 49(a) real and imaginary parts of the complex permittivity of un-oxidized XLPE is shown. In Figure 49(b) real and imaginary parts of the complex permittivity of a category 1 XLPE-sample is shown. It is seen that losses are lower for the reference and category 1, and has a slight decrease with lower frequencies rather than a increase, this means that the conductivity is very low for

the reference and category 1. It is noteworthy that category 1 has such a low ϵ'' and low conductivity.

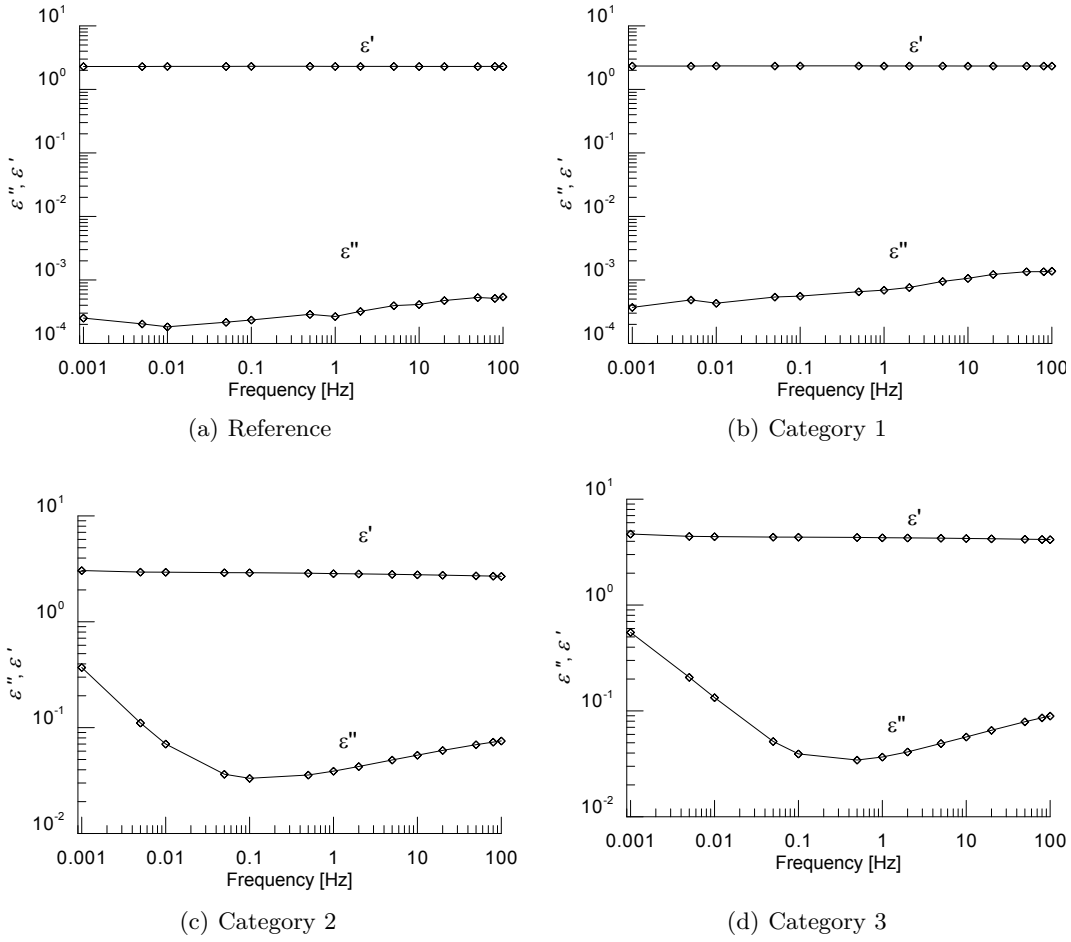

(a) Reference

(b) Category 1

(c) Category 2

(d) Category 3

Figure 4.49: Real and imaginary part of the complex permittivities

Measurements of the imaginary part of the permittivity ϵ'' shows that this value also is increasing with degree of oxidation. The imaginary part of the permittivity represents the lossy reaction mechanism in the polarization-depolarization of the material, and has been shown to have a significant dependence on frequency in the oxidized samples, especially for category 2 and 3. The lower frequency range (0.1Hz - 1mHz) shows a strong frequency dependence of ϵ'', which is increasing with decreasing frequencies. From theory and the Kramer-Kronigs relations to the real permittivity, the frequency dependence of the imaginary permittivity can be explained by the DC conductivity σ of the material, which has the dependence $\sigma \propto \omega\epsilon''$ and will pay no contribution to the frequency dependence of ϵ' which matches the data good.

Table 4.6: Values for relative permittivity at different frequencies.

	ϵ'(100Hz)	ϵ'(50Hz)	ϵ'(1Hz)	ϵ'(1mHz)
Reference	2.3018	2.3007	2.3041	2.2958
Category 1	2.5696	2.5686	2.5736	2.5659
Category 2	2.6889	2.7194	2.8519	3.048
Category 3	4.1554	4.1902	4.3251	4.6863

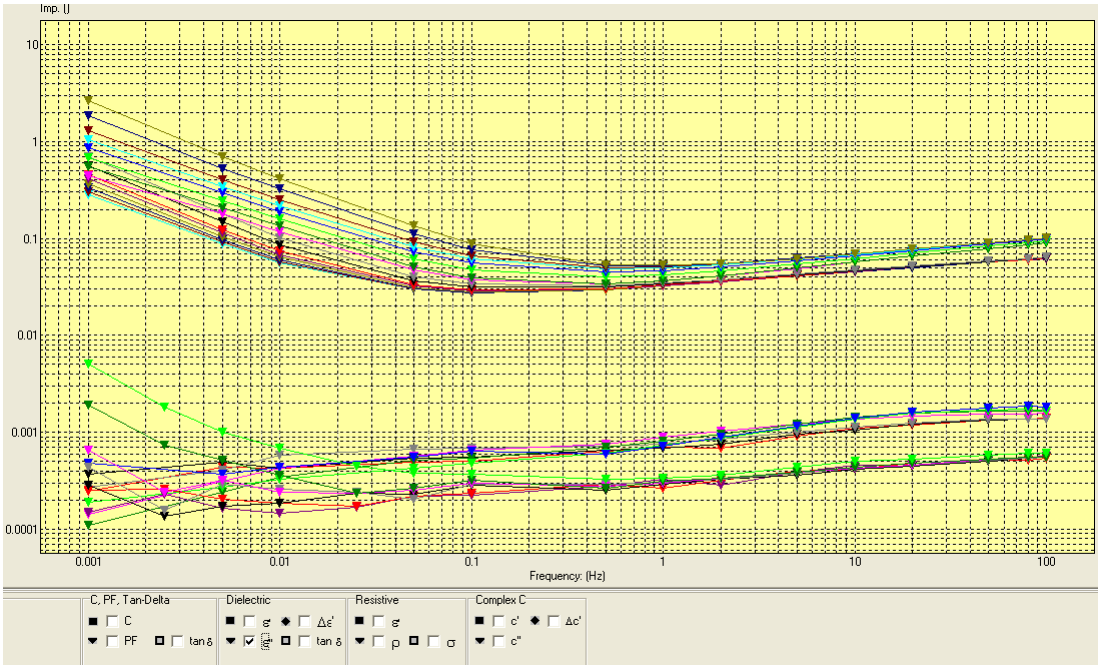

Figure 4.50: ϵ'' data for several voltages and test objects, direct screen-shot from IDA.

4.2.2 Dielectric Losses

As we recall from the theory section the $\tan\delta$ graphs shown in Figures 51(a) and 51(b) is used to show the dielectric losses. Here they are presented at two different RMS electric field intensities.

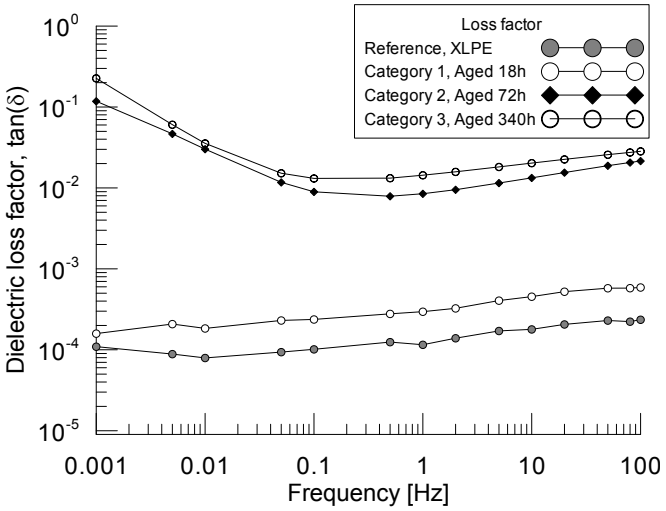

(a) 4kV/mm

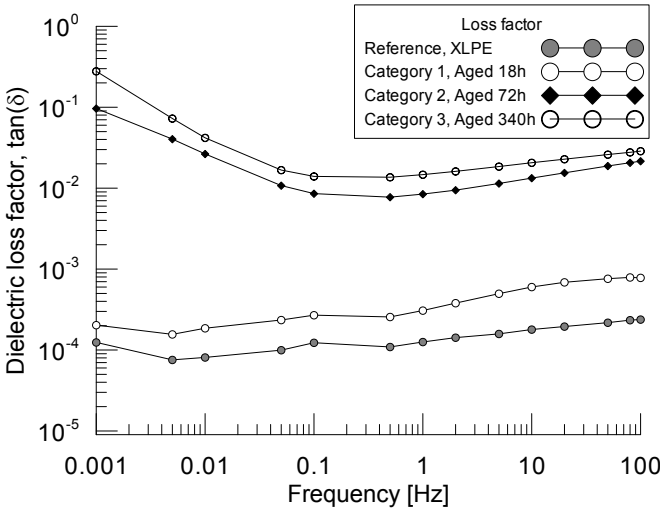

(b) 20kV/mm

Figure 4.51: Dielectric loss factor $\tan\delta$

4.2.3 Conductivity

The conductivity part of the experiments was limited by time and equipment. Ideally the experiments would include DC conductivity measurements using a stable AC current source with a sensitive pico-amperemeter. DC measurements trough the insulating material requires time and good instrumentation, which in this case was limited. So, dc conductivity was down prioritized. In stead of DC measurements, it is possible to use the low frequency part of the dielectric spectrum to estimate the DC conductivity.

The low frequency parts of the conductivity for the four categories of test objects are shown in in Figures 52(a) and 52(b). The conductivity has a certain dependence on the electric field, so they are shown at two different field intensities 4kV/mm and 20kV/mm.

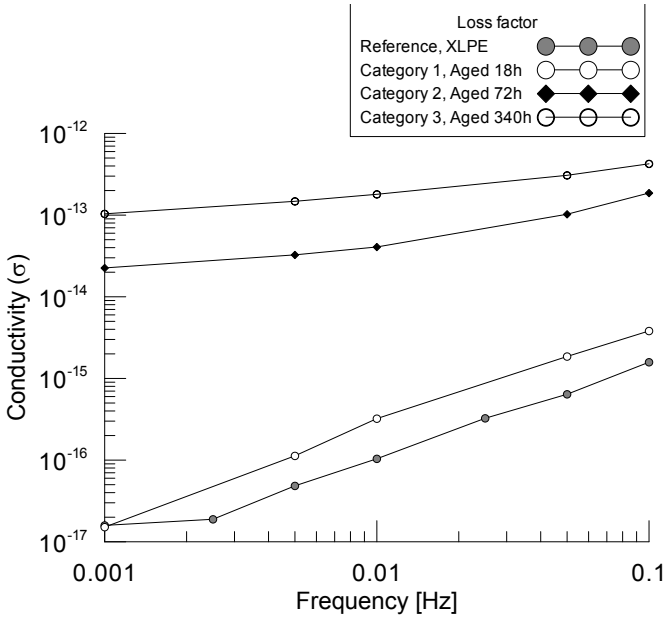

(a) 4kV/mm

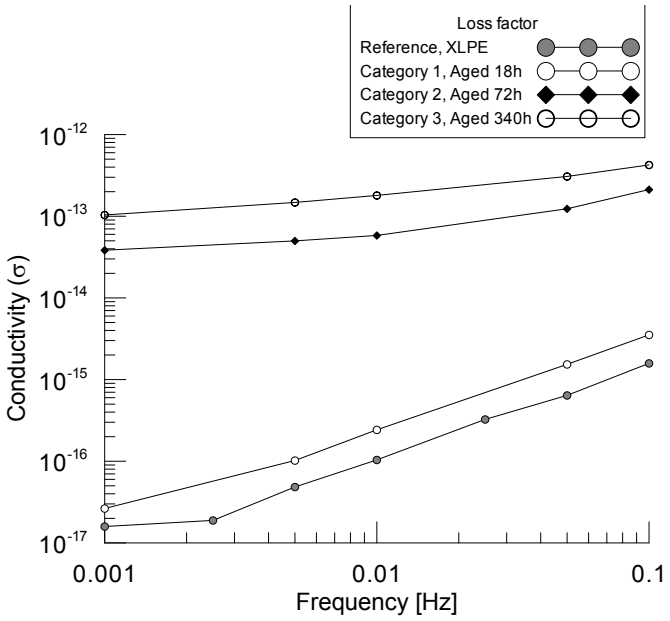

(b) 20kV/mm

Figure 4.52: Conductivity σ $[(\Omega\mathrm{m})^{-1}]$

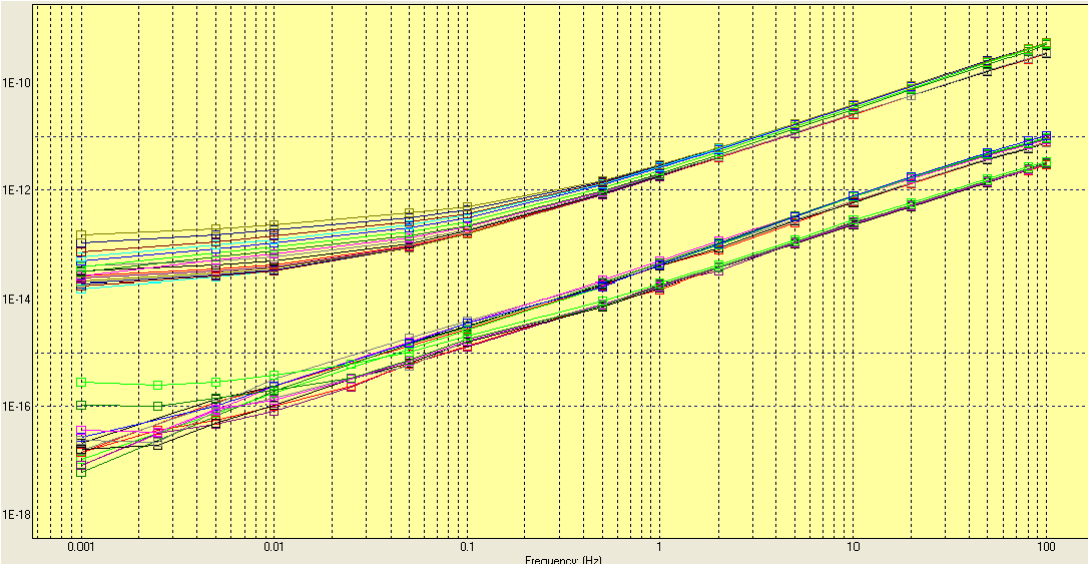

Figure 4.53: Conductivity data for several voltages and test objects, direct screen-shot from IDA.

4.3 Breakdown Measuremets

In table 4.7 the breakdown strengths are presented. The sample size is 5 test object per series. The standard deviation is marked σ.

Table 4.7: Electric breakdown strengths, in units of [kV/mm]

	d [mm]	E^{rms}_{Max}	E^{rms}_{Min}	$E^{rms}_{avg.}$	σ	Var (%):
Reference	0.25	64.71	28.84	55.31	6.93	12.53
Category 1	0.25	70.26	46.12	56.44	9.73	17.25
Category 2	0.25	46.20	28.84	36.03	7.22	20.03
Category 3	0.25	8.96	2.00	24.07	12.88	53.50

Photos of the breakdown sites in a selection of test-objects are shown in Figures 4.54, 4.55, 4.56 and 4.57. The photos was taken with an optical microscope. It is seen from the photos that the damage caused by the breakdown in the insulating material is increasing with the degree of oxidation. This is most likely because of the inferior mechanical properties of oxidized XLPE that arises from degradation processes like chain scission. However, it is also possible that the damage arises from increased heat development and partial discharge activity in oxidized material. Or a combination of these causes.

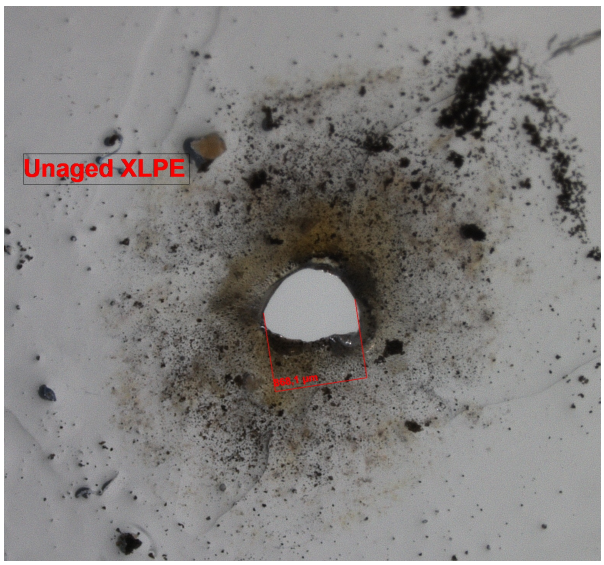

Figure 4.54: Microscope picture of the site of breakdown in a typical reference object.

.

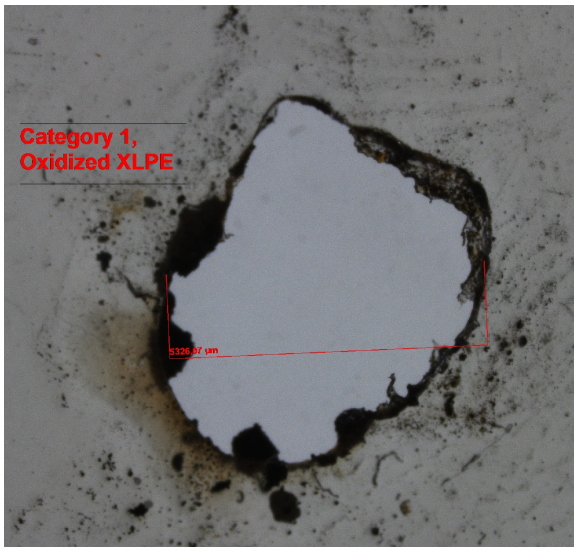

Figure 4.55: Microscope picture of the site of breakdown in a typical category 1 object.

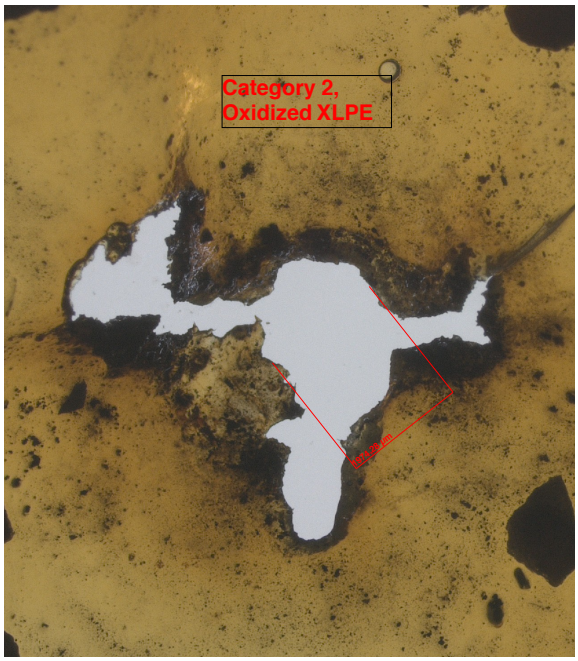

Figure 4.56: Microscope picture of the site of breakdown in a typical category 2 object.

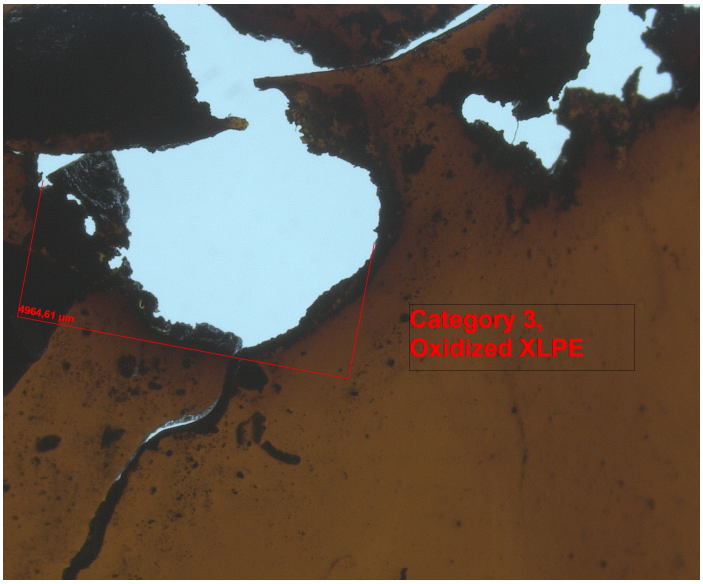

Figure 4.57: Microscope picture of the site of breakdown in a typical category 3 object.

5 Discussion

5.1 Carbonyl compounds

From the oxidation process it is produced organic chemical compounds that are generally of the carbonyl functional group, which is conveniently one of the most prominent absorption bands in FTIR spectra for oxidized organic compounds. In the contaminations studied in this work the most distinguished absorption peak from carbonyls is centered around wavenumbers of $k = 1721\text{cm}^{-1}$ which is assigned to ketones. Real contaminations has been categorized into three types, and one contamination from each category has been used as reference to investigate the thermal oxidization of XLPE samples. Samples that have been thermally oxidized at 170°C show a development of the same ketonic absorption peak at $k = 1721\text{cm}^{-1}$ as is found in the real contaminations. The FTIR absorption peak was used as a quantification of the degree of of oxidation. Thermal oxidation times was tuned in to match the same degree of oxidation. The absorption spectra of contaminations from category 1 and 2 shows a striking resemblance to that of the samples that are thermally oxidized at 170°C for respectively 18h and 72h within the region of interest ($k = 1500\text{cm}^{-1} - 2000\text{cm}^{-1}$). In addition to the ketonic absorption peak, the category 3 shows a deviation peak $k = 1610\text{cm}^{-1}$ which is not assigned to ketones, and this peak is not obtainable by thermal oxidation of XLPE which have been treated with peroxides an stabilizers. The $k = 1610\text{cm}^{-1}$ can possibly be assigned to carboxylate ions RCOO− (salts or esters -of carboxylic acid), this could only be obtained in heavily oxidized material i.e without peroxides and stabilizing additives.

5.2 Possible carboxylates

In category 3 contaminations there is in addition to the ketone absorption band located at $k = 1721\text{cm}^{-1}$ another absorption peak at about $k = 1610\text{cm}^{-1}$, see figure 4.45. This peak can not be assigned to the same ketonic compound that is found in category 1 and 2. The $k = 1610\text{cm}^{-1}$ is not possible to reproducible with XLPE samples, using the same thermal procedure as category 1 and 2 with longer oxidation times. The peak can possibly be assigned anti-symmetric stretching of carboxylate which is a salt or ester of a carboxylic acid [41] ,shown in figure 5.58. Or it could be carboxylic acid (R−COOH) anti-symmetric stretching [15]. To be exact in what the compound the peak represent is difficult, since the reported data of other experiment varies, and the typical absorption band of carboxylate and carboxylic acids i quite broad

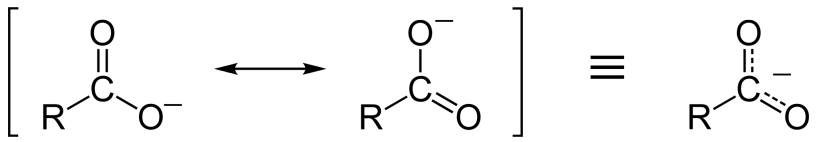

Figure 5.58: Carboxylate

5.3 Consequences of Contaminations

In order to set the properties of test-objects into context with a real insulation material, the effects that real contaminations might have on the insulating system will be discussed. The effects of different categories of particles (different degrees of oxidation) will also be discussed.

5.3.1 Electric Permittivity

Figure 5.59 shows the relative permittivity plotted as against the absorption factor A/d. Since the relative permittivity has a certain frequency dependence, the plot includes ϵ' for 100Hz, 50Hz, 1Hz and 1mHz. It is seen form the oxidized XLPE results, that the relative permittivity is increasing with increased degree of oxidation.

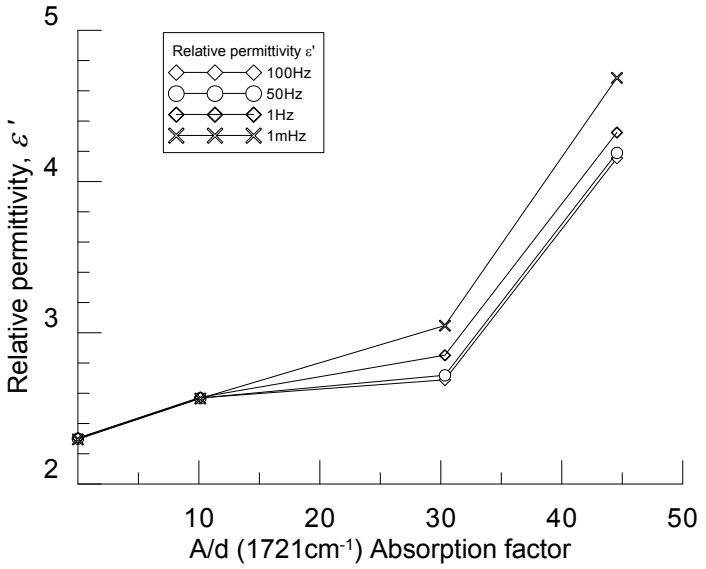

Figure 5.59: The relative permittivity vs. the carbonyl absorption factor A/d

The fact that the permittivity increases with the degree of oxidation

implies that the contaminations found in the insulating material will have a higher electric permittivity than the surrounding material.

5.3.2 Field Enhancement Factor

The electric field strength E is dependent on the permittivity of the material. A high permittivity material will induce a stronger electric field. For a linear material: $\vec{E} = \epsilon\vec{D}$. So when there are inclusions of different permittivity present in the insulating material there will be some electric field enhancement factor γ at the location of the inclusion (contamination).

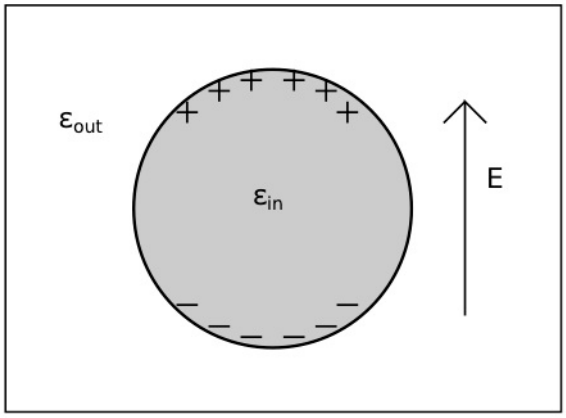

Figure 5.60: Interfacial charge accumulating because of the difference in permittivity.

$$\vec{E}_{in} = \gamma\vec{E}_{out} \tag{5.82}$$

If the electrical field can be approximated to be almost homogenous then the effect of the contamination can be modeled as perfect spherical dielectric inclusion placed in a homogeneous field. For the maximum field on (the outside of) such an inclusion, the field enhancement factor γ can be calculated compared to the homogeneous field strength.[36, 28].

$$\gamma = \frac{3\epsilon_{in}}{2\epsilon_{out} + \epsilon_{in}} \tag{5.83}$$

According to equation 5.83, the following observations can be made:

1. Maximum field occurs in the direction of the electric field
2. If the inside permittivity ϵ_{in} increases, the field enhancement increases, whereas if the outside permittivity ϵ_{out} increases, the field enhancement decreases. The latter effect is small since both the value and the relative change in the outside permittivity is small compared to the value inside.
3. the maximum field enhancement does not depend on the radius of the sphere.

The electric field enhancement factor can be an important parameter to evaluate the effect of the different categories of particles embedded

in the XLPE insulation. In table 5.8 the field-enhancement factor for spherical inclusions of contaminations is shown.

Table 5.8: Approximative field enhancement factor for contaminations.

Type	A/d	ϵ'(50Hz)	γ
Reference XLPE	0	2.3	1
Category 1	10.12	2.57	1.07
Category 2	30.34	2.69	1.11
Category 3	44.56	4.15	1.43

5.3.3 Dielectric Losses

The dielectric losses is as we have seen increasing with oxidation levels. The most dangerous effect of this is the lowered breakdown strength and increasing heat development because of energy dissipation through frictional and viscous molecular vibrations induced by the alternating electric field, and joule heating. This may leave weak spots in the cable that may be vulnerable to over voltages, partial discharges and impulses that may eventually lead to failure of the cable.

ϵ'' is plotted as a function og the carbonyl absorption index in Figure 5.61.

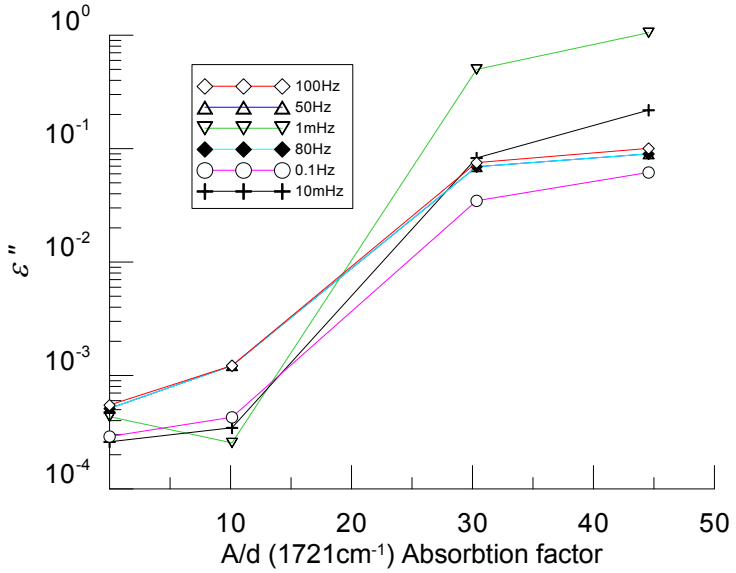

Figure 5.61: Lossy part of the dielectric function plotted against the carbonyl absorption.

5.3.4 Breakdown Strength

The electric breakdown strength can be plotted against the absorption factor measured in the thermally oxidized samples investigated by FITR to see the tendencies of the development of the breakdown strength as a function of carbonyl contents. Data presented inFfigure 5.62 shows the tendency of reduced breakdown strength of oxidized XLPE. The error bars represent standard deviations of the measured breakdown strength data for each category of contaminations.

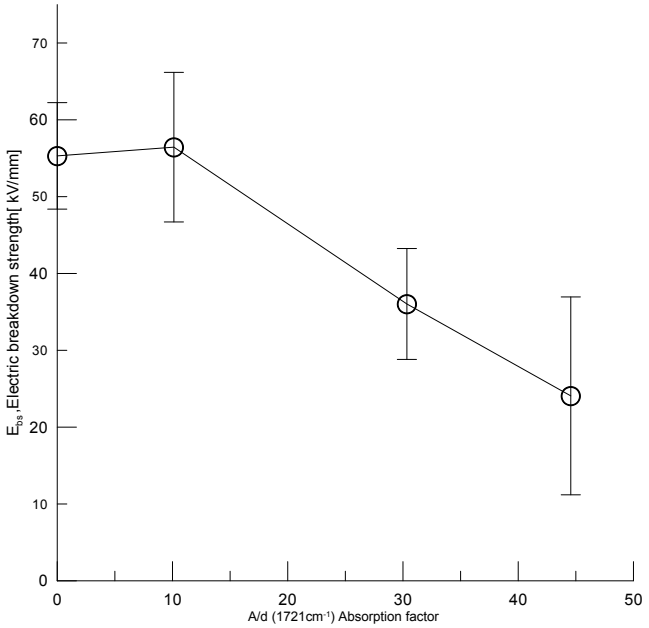

Figure 5.62: Breakdown strength vs. carbonyl contents.

Seen in context with elevated temperatures because of increased dielectric losses, higher conductivity and electric field enhancement factor, the lower breakdown strength introduced by the contaminations may cay be considered a significant reliability issue for the insulating material. And will most likely be the source discharges and eventually failure in case of over-voltages (lighting over-voltage or switching over-voltages). The contaminations may also reduce the life-time of the cable.

6 Conclusion

In dielectric insulating materials subjected to alternating electric fields there are energy losses associated with polarization mechanisms and resistivity. A typical dielectric material used for insulation of high voltage sub-marine cables is cross-linked polyethylene (XLPE) produced from polyethylene (PE). Under production, PE can stagnate in high temperature thermal zones and consequently be subjected to thermal oxidation that introduces polar carbonyl groups to the polyethylene chain, which leads to increased energy losses, inferior insulating properties and subsequent degradation and eventually breakdown and failure of the cable.

The oxidized polyethylene can contaminate the insulating material in the form of microscopic particles embedded in the material, that are difficult to detect and separate from the polyethylene granulate. In this work the focus have been on documenting the fundamental properties of the oxidized XLPE contaminations, such as complex permittivity, associated energy losses and breakdown strengths, compared to that of un-oxidized XLPE.

In this thesis the thermal oxidation process of XLPE and PE has been studied in order to determine the degree of oxidation and carbonyl contents, using Fourier transform infra red spectroscopy, to replicate the contaminations found in real contaminations . Three real contaminations was found and investigated. They were categorized and replicated through thermal oxidation at 170°C. Infrared absorption index per thickness([a.u./mm]) at $k = 1721\text{cm}^{-1}$ was used to quantify the carbonyl contents of the XLPE samples. Oxidation times of 18h, 72h and 340h was used to achieve carbonyl absorption indexes of 10.15 a.u./mm 30.43 a.u./mm and 45.9 a.u/mm, which are comparable to the real contaminations for the two first categories (18h, 72h). Category 3 contaminations deviates with an extra absorption peak located around $k = 1610\text{cm}^{-1}$, which is not present in 340h oxidized XLPE samples. From FTIR absorption-spectra in this work, it is seen that the $k = 1610\text{cm}^{-1}$ absorption peak might be reproducible in oxidized PE that does not contain additives such as stabilizers and peroxides.

The electrical properties of artificial contaminations has been investigated using dielectric spectroscopy and breakdown strength-tests. In dielectric spectroscopy the complex permittivity $\tilde{\epsilon} = \epsilon' - i\epsilon''$ is used characterize the dielectric properties of the material. It is found that the permittivity increases with oxidation. At 50Hz the real relative permittivities are $\epsilon' = 2.30$ for un-oxidized XLPE, $\epsilon' = 2.57$ for category 1 samples, $\epsilon' = 2.72$ for category 2 samples and $\epsilon' = 4.19$ for category 3 samples.

The lossy polarization process is characterized by the imaginary part of the permittivity ϵ''. It is seen that the dielectric losses are indeed increasing with the presence of polar carbonyl group, as expected from

theoretical considerations. It is also seen that ϵ'' in oxidized samples increases as the frequency decreases, which indicates that the conductive process dominates the low frequency domain, and that the DC conductivity is higher in contaminations than in un-oxidized XLPE. It was observed a decrease in breakdown strength in oxidized XLPE. The breakdown strengths decreased from (55.31±31)kV/mm in un-oxidized XLPE to (24.07±12.88) kV/mm in the most oxidized category 3 XLPE sample.

As a consequence of the theories and experimental results presented in this work, it can be said that there is a causal relation between dielectric losses and breakdown strengths in oxidized XLPE material, which can be summarized as follows: The introduction of polar carbonyl groups through thermal oxidation of polyethylene causes increased permittivities and dielectric losses. Subsequently there will be a decrease in electric breakdown strength of the XLPE insulation. Contaminations of oxidized material embedded in a solid insulation system may pose a reliability issue and may eventually be the cause of breakdown and failure of the cable.

7 Suggestions for further work

Because of the significant extent of the aspects of physical, chemical and system properties that can be studied related to the organic contaminations and oxidized XLPE, not all phenomena and considerations have been investigated in this thesis. The results presented in this thesis represent a significant part of understanding the dielectric behavior and properties of oxidized XLPE, however there are still interesting experiments that could have been done if time allowed it. If further investigations on the topic is to be done, here are some suggestions on what experiments and considerations that may be relevant:

- DC conductivity is an important parameter that can be put into direct relation to the dielectric response measurements done in this thesis. The DC conductivity dependence on electrical stress or temperature is of significance for the insulating properties of the XLPE and contaminations.[20]
- Dielectric response measurements at different temperature levels. Thermal breakdown depends on the temperature dependence of the dielectric losses $\tan\delta$, so $\tan\delta$ expressed as a function of temperature, would make it possible to calculate the thermal breakdown voltage of oxidized XLPE, and then make comparisons to the experimental measurements. The set-up used in this thesis should be easily adaptable to a heating cabin. A larger frequency range could also be of interest, then with different instrumentation.[7, 47].
- Measuring the surface adhesion-cohesion (wetability) of the oxidized XLPE surface using a goniometer would provide interesting information about the surface energy of the contaminations and the intermolecular bonds at an interface between oxidized material and unoxidized material, which then again tells how well the contaminations will be embedded in the solid insulating material, i.e if it is possible of formation of voids in the insulation. [1].
- SEM and AFM microscopy of the morphological structure of the solid-solid interface in the polymer contaminations may reveal further details such as porosity and macro-molecular structure. SAXS (small angle x-ray scattering) would also be an effective way of finding out more about the macromolecular size and structure of the contaminations. Studying the effect of the solid-solid interface on breakdown strength would be of interest (like for instance [19]).
- The contaminations can also be the subject of more theoretical investigation related to the macromolecular dynamics and modelling of the oxidation process. [18].
- Doing multi-physical analysis with finite-element software implementing the various parameters which are measured, such as permittivity, dielectric losses, conductivity, thermal conductivity etc., together with realistic geometries may reveal the over-all effect of the contaminations.
- Making an test-cable with controlled artificial contaminations with properties similar to that of the real contaminations, for dielectric

response, polarization-depolarization and partial discharge measurements may be the ultimate way to test the effects of these contaminations.

List of Notations

α	Molar Absorptivity 13
α_p	Atomic polarizability [C·m^2·V^{-1}] 10
χ_e	Electric susceptibility 12
ΔH	Change in enthalpy 7
δ	Loss-angle 12
ϵ	Electric permittivity $\epsilon = \epsilon_r \epsilon_0$ 12
ϵ_0	Electric vacuum permittivity $\epsilon_0 \simeq 8.854187817620 \cdot 10^{-12}$F/m12
ϵ_r	Relative electric permittivity 12
$\langle \vec{p} \rangle$	Mean linear momentum [N·s] 9
$\langle \vec{v} \rangle$	Mean velocity [m/s] 9
ν	Frequency [Hz=1/s] 12
ω	Angular frequency [rad./s] $\omega = 2\pi\nu$ 12
σ	Electric conductivity 11
$\tan\delta$	Dielectric loss-tangent 12
τ	Transmittance [dimensionless] 13
τ_i	Mean free time between ionic collisions. 9
$\tilde{\epsilon}(\omega)$	Complex permittivity 13
$\tilde{C}(\omega)$	Complex Capacitance 13
$\vec{B}$	Magnetic field strength [50] 11
$\vec{D}$	Electric displacement field 11
$\vec{E}$	Electric field vector [V/m] 9
$\vec{H}$	Magnetic flux density, Magnetic induction [50] 11
A	Absorbance [dimensionless] 13
C	Capacitance [Farad] 13
c	Concentration 13
$d\vec{p}$	Infinitesimal amount of momentum [N·s] 9
H	Enthalpy - Total energy in a thermodynamic system 7
I	Current [A] 12
i	$\sqrt{-1}$ 12
I_{IR}	Beam-Intensity 13
J_f	Free current density 11
P_{loss}	Power-loss 12
q	Electric charge 9
R	Resistance [Ω] 12

List of Figures

List of Tables

References

[1] M. Ashraf Khan and R. Hackam. Surface properties of cross-linked polyethylene. In *Electrical Insulation and Dielectric Phenomena, 1998. Annual Report. Conference on*, pages 673 –677 vol. 2, oct 1998.

[2] Anthony Barlow. The chemistry of polyethylene insulation. *IEEE Electrical Insulation Magazine*, 1991-Vol.7(No. 1), 1991 Jan/Feb.

[3] T. C. Chapman and H. J. Wintle. Dielectric absorption currents and surface charge on polymeric insulators. *Journal of Applied Physics*, 51(9):4898–4904, 1980.

[4] John Coates. *Interpretation of Infrared Spectra, A Practical Approach*. John Wiley & Sons, Ltd, 2006.

[5] Kenneth S. Cole and Robert H. Cole. Dispersion and absorption in dielectrics i. alternating current characteristics. *The Journal of Chemical Physics*, 9(4):341–351, 1941.

[6] P. Debye. Part i. dielectric constant. energy absorption in dielectrics with polar molecules. *Trans. Faraday Soc.*, 30:679–684, 1934.

[7] S. Diaham, M.-L. Locatelli, T. Lebey, and S. Dinculescu. Dielectric measurements in large frequency and temperature ranges of an aromatic polymer. *The European Physical Journal - Applied Physics*, 49(01):null–null, 2010.

[8] Jeppe C. Dyre and Thomas B. Schrøder. Universality of ac conduction in disordered solids. *Rev. Mod. Phys.*, 72:873–892, Jul 2000.

[9] Bruno M. Fanconi. Chain scission and mechanical failure of polyethylene. *Journal of Applied Physics*, 54(10):5577–5582, 1983.

[10] H. Faremo and E. Ildstad. Diagnosis and restoration of water tree aged xlpe cable materials. In *Electrical Insulation, 1996., Conference Record of the 1996 IEEE International Symposium on*, volume 2, pages 596 –599 vol.2, jun 1996.

[11] R. Charles Bacon Frank M. Rugg, Joseph J. Smith. Infrared spectrometric studies on polyethylene. *Journal of Polymer Science*, XIII:545–547, 1954.

[12] H Fröhlich. *Theory of dielectrics: dielectric constant and dielectric loss*. Clarendon Press, Oxford, 2d ed edition, 1958.

[13] G. Gagnon, S. Pelissou, and M.R. Wertheimer. Oxidation dependence of breakdown strength of xlpe. In *Electrical Insulation and Dielectric Phenomena, 1989. Annual Report., Conference on*, pages 241 –246, oct-2 nov 1989.

[14] D.J. Griffiths. *Introduction to electrodynamics*. Prentice Hall, 1999.

[15] O. Hadžija and B. Špoljar. Quantitative determination of carboxylate by infrared spectroscopy: application to humic acids. *Fresenius' Journal of Analytical Chemistry*, 351:692–693, 1995. 10.1007/BF00323352.

[16] Svein Thore Hagen. *The effect of artificial inclusions and byproducts from the crosslinking process*. PhD thesis, NTH, 1993.

[17] J. O. Halford. Stretching force constant of the carbonyl bond in unconjugated ketones. *The Journal of Chemical Physics*, 24(4):830–833, 1956.

[18] H. Z. Y. Han, T. C. B. McLeish, R. A. Duckett, N. J. Ward, A. F. Johnson, A. M. Donald, and M. Butler. Experimental and theoretical studies of the molecular motions in polymer crazing. 1. tube model. *Macromolecules*, 31(4):1348–1357, 1998.

[19] S.M. Hasheminezhad, E. Ildstad, and A. Nysveen. Breakdown strength of solid|solid interface. In *Solid Dielectrics (ICSD), 2010 10th IEEE International Conference on*, pages 1 –4, july 2010.

[20] R. Hegerberg, L. Lundgaard, and E. Ildstad. Dielectric relaxation and dc conductivity of transformer pressboard and xlpe cable insulation. In *Conduction and Breakdown in Solid Dielectrics, 1992., Proceedings of the 4th International Conference on*, pages 47 –51, jun 1992.

[21] A. Helgeson and U. Gafvert. Dielectric response measurements in time and frequency domain on high voltage insulation with different response. In *Electrical Insulating Materials, 1998. Proceedings of 1998 International Symposium on*, pages 393 –398, sep 1998.

[22] Anders Helgeson. *Analysis of Dielectric Response Measurement Methods and Dielectric Properties of Resin-Rich Insulation During Processing*. PhD thesis, KTH, 2000.

[23] S.M. Helleso, V.C. Henoen, and S. Hvidsten. Simulation of water diffusion in polymeric cables using finite element methods. In *Electrical Insulation, 2008. ISEI 2008. Conference Record of the 2008 IEEE International Symposium on*, pages 595 –598, june 2008.

[24] Arne Holmström and Erling M. Sörvik. Thermooxidative degradation of polyethylene. i and ii. structural changes occurring in low-density polyethylene, high-density polyethylene, and tetratetracontane heated in air. *Journal of Polymer Science: Polymer Chemistry Edition*, 16(10):2555–2586, 1978.

[25] S. Hvidsten and E. Ildstad. Water causing a nonlinear dielectric response of water treed xlpe characterized by ftir microspectrometry. In *Electrical Insulation, 1998. Conference Record of the 1998 IEEE International Symposium on*, volume 1, pages 101 –104 vol.1, jun 1998.

[26] S. Hvidsten, E. Ildstad, and H. Faremo. Mechanisms causing nonlinear dielectric response of water treed xlpe cables. In *Conduction and Breakdown in Solid Dielectrics, 1998. ICSD '98. Proceedings of the 1998 IEEE 6th International Conference on*, pages 73 –78, jun 1998.

[27] Sverre Hvidsten and Frode Sætre. Dielectric response of spp and xlpe insulations at high temperatures and electric fields. In *2011 Annual Report Conference on Electrical Insulation and Dielectric Phenomena*. SINTEF Energy Research, 2011.

[28] Erling Ildstad. *High Voltage Insulating Materials*. NTNU, 2009.

[29] G. Iyer, R.S. Gorur, R. Richert, A. Krivda, and L.E. Schmidt. Dielectric properties of epoxy based nanocomposites for high voltage

insulation. *Dielectrics and Electrical Insulation, IEEE Transactions on*, 18(3):659 –666, june 2011.

[30] HH JENSEN. Carbonyl stretching force constant .1. a molecular orbital study. *Acta Chemica Scandinavica*, 23(9):3163–&, 1969.

[31] HH JENSEN and SJ CYVIN. Carbonyl stretching force constant .2. a normal coordinate treatment. *Acta Chemica Scandinavica*, 23(9):3168–&, 1969.

[32] A.K. Jonscher. *Dielectric relaxation in solids*. Chelsea Dielectrics Press, 1983.

[33] Andrew K Jonscher. Dielectric relaxation in solids. *Journal of Physics D: Applied Physics*, 32(14):R57, 1999.

[34] L. Acelrud J.V. Gulmine. Ftir characterization of aged xlpe. *Polymer Testing*, 25:932–942, 2006.

[35] K.C. Kao. *Dielectric Phenomena in Solids: With Emphasis on Physical Concepts of Electronic Processes*. Referex Engineering. Academic Press, 2004.

[36] Chonung Kim, Jingkuan Duan, Xingyi Huang, Soknam Kim, Pingkai Jiang, Hyeil Kim, and Sungil Hyon. Numerical analysis on water treeing deterioration of xlpe cable insulation using combination of fem and taguchi method. *European Transactions on Electrical Power*, 20(6):747–759, 2010.

[37] C. Kittel. *Introduction to solid state physics*. Wiley, 2005.

[38] T. Kurihara, T. Takahashi, H. Homma, and T. Okamoto. Oxidation of cross-linked polyethylene due to radiation-thermal deterioration. *Dielectrics and Electrical Insulation, IEEE Transactions on*, 18(3):878 –887, june 2011.

[39] D.R. Lide. *Handbook of chemistry and physics*. CRC Handbook of Chemistry and Physics. Taylor and Francis, 2009.

[40] Tong Liu, John Fothergill, Steve Dodd, and Ulf Nilsson. Dielectric spectroscopy measurements on very low loss cross-linked polyethylene power cables. *Journal of Physics: Conference Series*, 183(1):012002, 2009.

[41] Linette K. Martin and Charles Q. Yang. Infrared spectroscopy studies of the photooxidation of a polyethylene nonwoven fabric. *Journal of Polymers and the Environment*, 2:153–160, 1994. 10.1007/BF02074783.

[42] F. Mauseth, E. Ildstad, M. Selsjord, and R. Hegerberg. Quality control of extruded hvdc cables: Low frequency endurance testing of model cables with contaminations. In *High Voltage Engineering and Application (ICHVE), 2010 International Conference on*, pages 136 –139, oct. 2010.

[43] J.C. Maxwell and J.J. Thompson. *A treatise on electricity and magnetism*. Number v. 1 in Clarendon Press series. Clarendon, 1904.

[44] J. C. Maxwell Garnett. Colours in Metal Glasses and in Metallic Films. *Royal Society of London Philosophical Transactions Series A*, 203:385–420, 1904.

[45] I.W. McAllister and G.C. Crichton. Analysis of the temporal electric fields in lossy dielectric media. *Electrical Insulation, IEEE Transactions on*, 26(3):513 –528, jun 1991.

[46] J. McMurry. *Organic Chemistry*. International edition. Brooks/Cole, 2011.

[47] E Neagu, P Pissis, L Apekis, and J L Gomez Ribelles. Dielectric relaxation spectroscopy of polyethylene terephthalate (pet) films. *Journal of Physics D: Applied Physics*, 30(11):1551, 1997.

[48] Nexans. 60-500 kv high voltage underground power cables; xlpe insulated cables. *NEXANS France S.A.S au capital de 70 000 000 € - Headquarter 16 rue de Monceau 75008 PARIS FRANCE RCS PARIS 428 593 230 - APE 313*, 2004.

[49] Gerald Scott Norman Grassie. *Polymer Degradation and Stabilisation*. Cambridge University Press, 1985.

[50] C.Angell og B.E.Lian:. *Fysiske størrelser og enheter*. Universitetsforlaget, 2004.

[51] Lars Onsager. Electric moments of molecules in liquids. *Journal of the American Chemical Society*, 58(8):1486–1493, 1936.

[52] S.O. Pillai. *Solid State Physics*. New Age International, 2005.

[53] J A Reynolds and J M Hough. Formulae for dielectric constant of mixtures. *Proceedings of the Physical Society. Section B*, 70(8):769, 1957.

[54] Yukihiko Sato and Takamasa Yashiro. The effect of polar groups on the dielectric loss of polyethylene. *Journal of Applied Polymer Science*, 22(8):2141–2153, 1978.

[55] G Sawa and J H Calderwood. Dependence of surface conduction current in oxidized polyethylene on electric field at various humidities. *Journal of Physics C: Solid State Physics*, 4(15):2313, 1971.

[56] Yu. A. Shlyapnikov and I. A. Serenkova. High-temperature oxidation of polymers. *Die Angewandte Makromolekulare Chemie*, 114(1):1–11, 1983.

[57] W.T. Shugg. *Handbook of electrical and electronic insulating materials*. Van Nostrand Reinhold, 1986.

[58] A.H. Sihvola and Institution of Electrical Engineers. *Electromagnetic mixing formulas and applications*. IEE electromagnetic waves series. Institution of Electrical Engineers, 1999.

[59] John S. Toll. Causality and the dispersion relation: Logical foundations. *Phys. Rev.*, 104:1760–1770, Dec 1956.

[60] L. Audouin V. Langlois, M. Meyer and J. Verdu. Physical aspects of thermal oxidation of cross linked polyethylene. *Polymer Degradation and Stability*, 1991.

[61] A.S Vaughan, Y Zhao, L.L Barre, S.J Sutton, and S.G Swingler. On additives, morphological evolution and dielectric breakdown in low density polyethylene. *European Polymer Journal*, 39(2):355 – 365, 2003.

A Appendix A

A.1 FTIR spectra

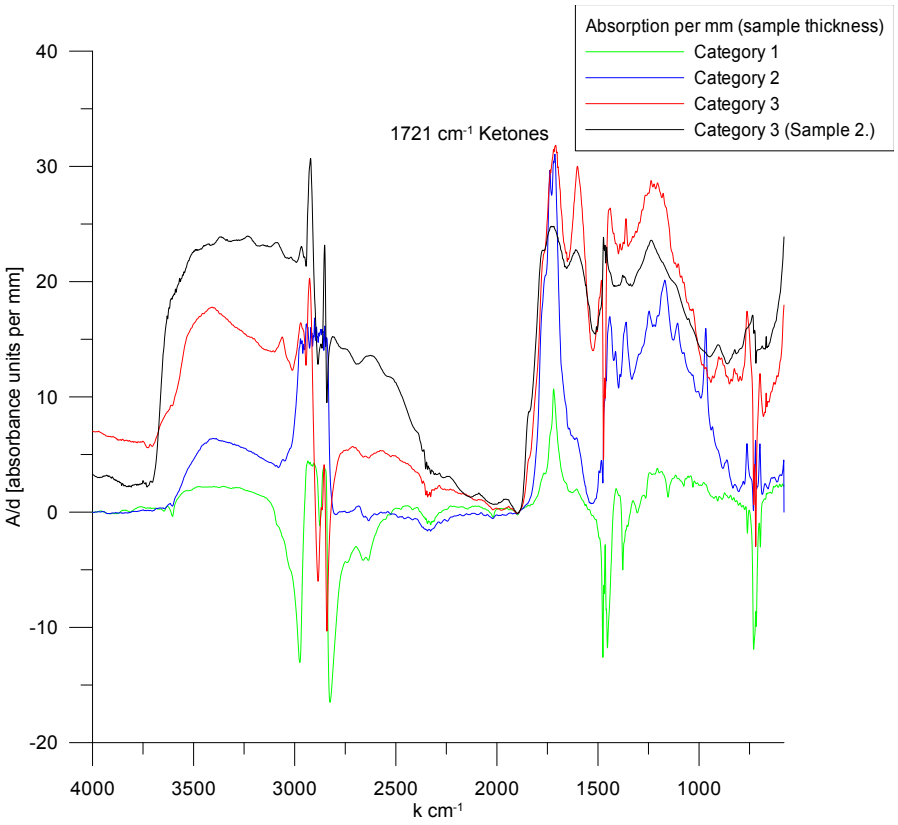

Figure 1.1: Absorption Spectra for all categories of contaminations, whole instrument range

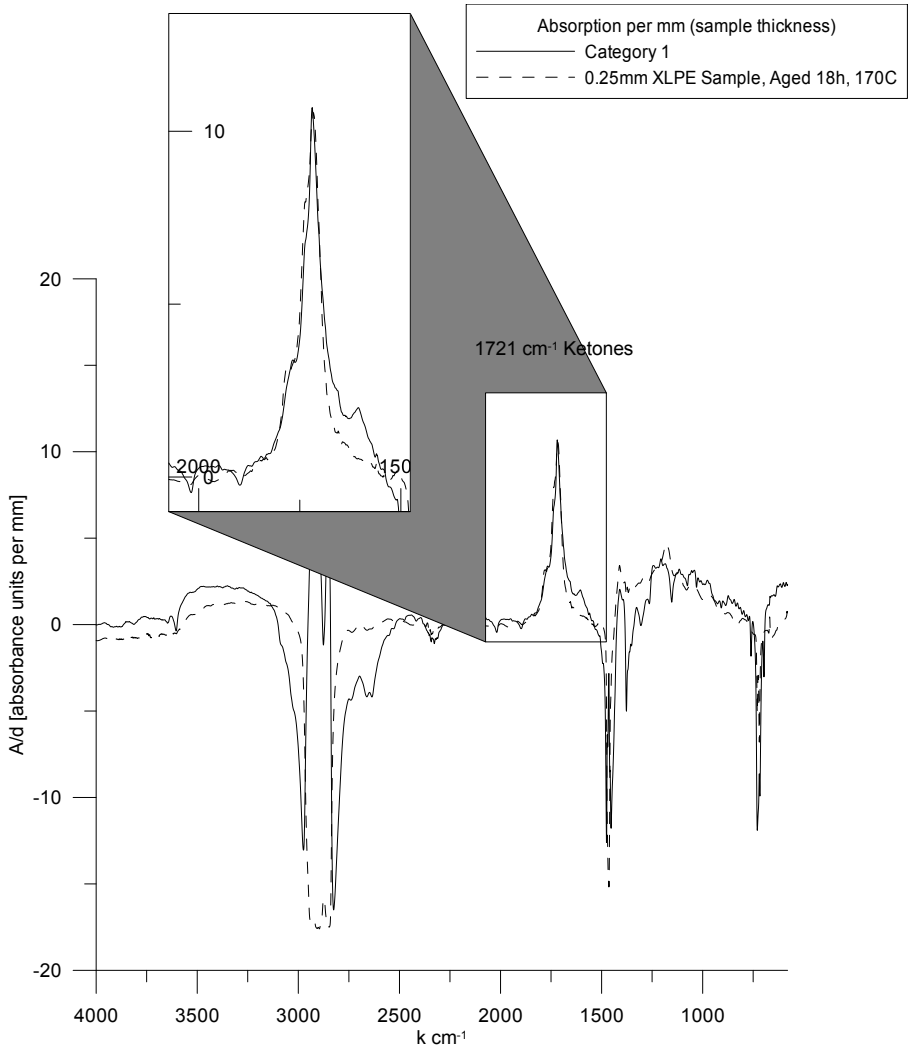

Figure 1.2: Comparison of Absorption spectra of category 1 contamination and 18h aged XLPE sample, whole instrument range

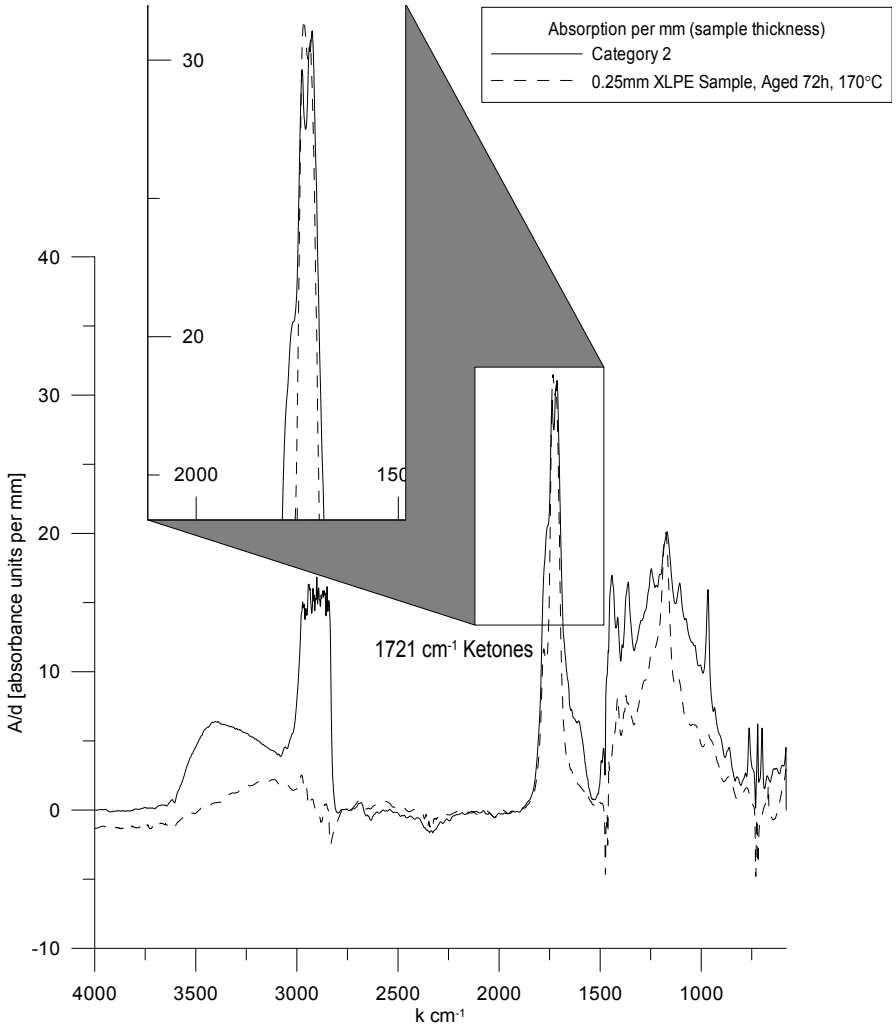

Figure 1.3: Comparison of Absorption spectra of category 2 contamination and 72h aged XLPE sample, whole instrument range

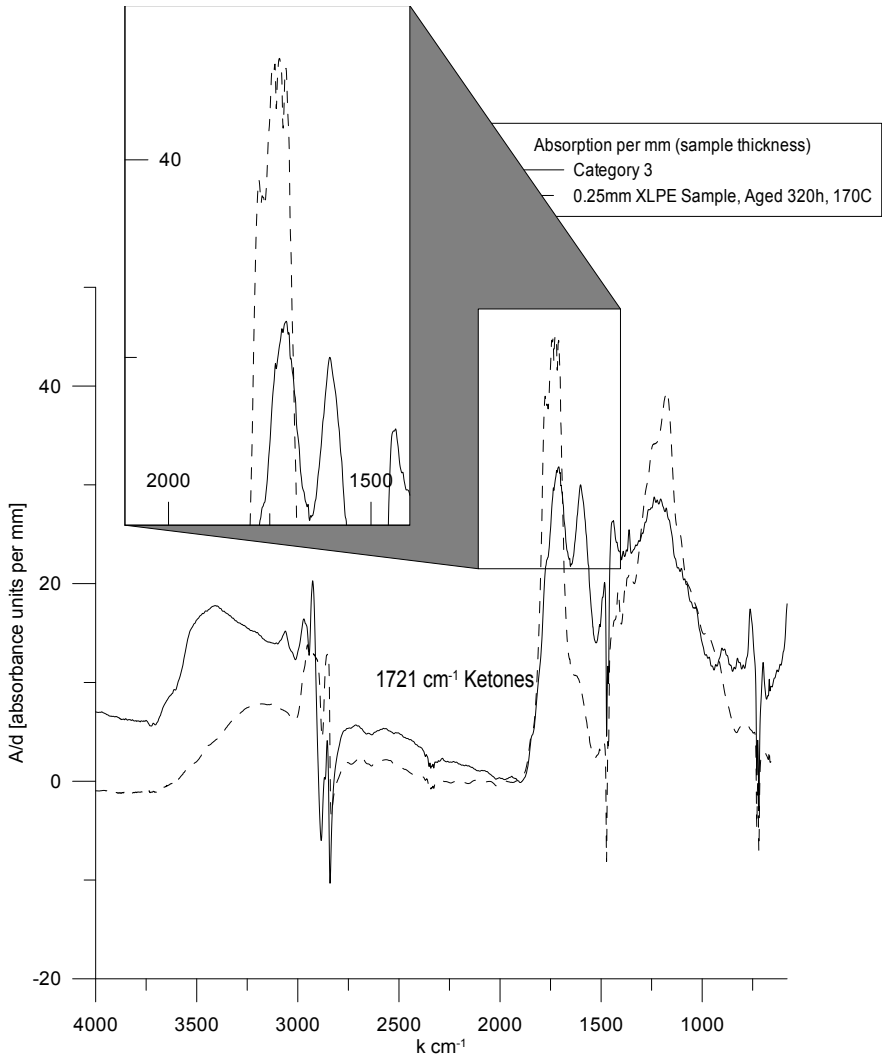

Figure 1.4: Comparison of Absorption spectra of category 3 contamination and 320h aged XLPE sample, whole instrument range

B Appendix B

Table 2.2: Breakdown strengths of all test objects

	Reference [kV]	Category 1 [kV]	Category 2 [kV]	Category 3 [kV]
1	16.18	13.95	10.06	8.13
2	14.02	25.31	7.56	8.96
3	14.59	17.56	7.21	7.91
4	12.61	11.53	8.66	
5	11.73	12.20	11.55	
	13.83	16.11	9.01	8.33
Variance	3.00	31.90	3.25	0.31
Standard Deviation	1.73	5.65	1.80	0.55

B.1 Effective Permittivity for Dielectrics with Inclusions

The following calculations on effective medium permittivity has been done, but is not seen to be particularly relevant to the purpose of this thesis. Effective medium approximations can be useful if there are numerous particles embedded in the insulation. I have not estimated how many contamination particles there will be in a cable.

The organic contaminations considered in this thesis are microscopic particles typically on a size-scale of 50μm - 200μm. The particles are characterized by physical properties that differs from those of the host material the particles is included in. Particularly they will have different dielectric properties, such as relative permittivity, conductivity and dielectric response. A theory of mixed dielectrics has to be established to account for the effects these inclusions has on the insulation capabilities of the material.
Historically, the problem of dielectric mixing and the effect of inclusions in dielectric material has been thoroughly studied and described, leading to many significant results both experimental and theoretical. Maxwells' treatise on Electricity and Magnetism has a whole chapter on lossy dielectrics[43, 44]. Theories and results from Maxwells' works and others will be presented in this chapter in order to describe phenomena related to the inclusions in dielectric insulation considered in this thesis. A collection of two-component dielectric mixing formulas has been reported by J A Reynolds and J M Hough in [53]. In this thesis I will, for mathematical simplicity consider the two simplest approximations of inclusions, spherical and ellipsoidal.

B.1.1 Spherical Dielectric Inclusions

The inclusions can for a reasonable approximation be modeled as a collection of randomly distributed spherical uniform inclusions in a isotropic host material. As mentioned in chapter 2.4.3 the molecular polarization of a single molecule can within the linear range be denoted with α, and the induced linear dipole moment is given by the following expression:

$$\vec{p}_m = \alpha \vec{E}_{local} \tag{2.1}$$

where $\vec{p}_m$ is the induced molecular dipole moment and $\vec{E}_{local}$ is the local electric field. The electric field $\vec{E}_{local}$ is the field at the location of the inclusion and is approximated by the following expression [37]:

$$\vec{E}_{local} = \vec{E} + \frac{\vec{P}}{3\epsilon_0} \tag{2.2}$$

This expression is known as the Lorenz relation [37]. Where $\vec{E}$ is the macroscopic average field in the host material. $\vec{P}$ is the polarization density associated with a uniformly polarized sphere, and ϵ_0 the permittivity of free space. The number density of such molecules N (number

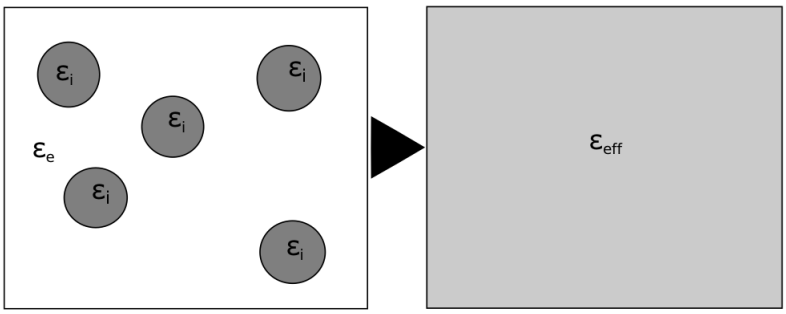

Figure 2.1: Effective medium with spherical inclusions

of molecules per volume) combined with equations 2.1 and 2.2 yields the dipole moment per unit volume $\vec{P} = N\vec{p_m}$:

$$\vec{P} = N\alpha(\vec{E} + \frac{\vec{P}}{3\epsilon_0}) \tag{2.3}$$

It is well known that in a isotropic medium $\vec{P} = (\epsilon_r - 1)\epsilon_0\vec{E}$, inserting this into equation 2.2, the formula known as the Lorenz-Lorenz or Clausius-Mosotti relation follows.[37]:

$$\alpha = \frac{3\epsilon_0(\epsilon_r - 1)}{N(\epsilon_r + 2)} \tag{2.4}$$

For a dielectric sphere of volume V, with relative permittivity ϵ_i embedded in a dielectric with relative permittivity ϵ_e, the polarizability will be given by the following expression:

$$\alpha = V(\epsilon_i - \epsilon_e)\frac{3\epsilon_0\epsilon_e}{\epsilon_i + 2\epsilon_e} \tag{2.5}$$

Combining equation 2.4 and 2.5 the expression for the final effective relative permittivity $\epsilon_{eff} = \epsilon_r$ of the mixture is obtained. This formulae is known as the Maxwell - Garnet mixing formulae. [44, 58], [45]

$$\epsilon_{eff} = \epsilon_r = \epsilon_e + \frac{3f\epsilon_e(\epsilon_i - \epsilon_e)}{\epsilon_i + 2\epsilon_e - f(\epsilon_i - \epsilon_e)} \tag{2.6}$$

Where $f = NV$ is the volume fraction of the inclusions in the overall volume of the dielectric.

B.1.2 The Drude Model of Conductors

If the conductor is placed in a electric field, the electric field will induce a current of electrons to oppose the the electric field. As the electrons make

their way trough the material they will scatter of the relatively immobile ions of the material. A simple classical model is used to describe the electronic properties of conductors and resistivity is the Drude model. The Drude model is explained as follows:

Assuming the ions to be hard immobile spheres. If an electron with charge q scatters of an ion and travels a mean time τ_i after its last collision it will accumulate a infinitesimal amount of momentum $d\vec{p}$ between the collisions, according to the electrostatic force law$\vec{F} = q\vec{E}$ given a constant electric field $\vec{E}$.

$$d\langle\vec{p}\rangle = q\vec{E}\tau \tag{2.7}$$

Since the electron does not remember its trajectory from before the last scatter (ie. random scattering). It will on average have a momentum $\langle\vec{p}\rangle$ given by the relation in eq. 2.8.

$$\langle\vec{p}\rangle = q\vec{E}\tau \tag{2.8}$$

Using the relations for current density and linear momentum, we can derive a relation between the current density and electric field. In these expressions m is the mass of the electrons, n is the number of scattered electrons, q is the charge of the electron and $\langle\vec{v}\rangle$ is the mean velocity of the electrons.

$$\langle\vec{p}\rangle = m\langle\vec{v}\rangle \tag{2.9}$$

$$\vec{J} = nq\langle\vec{v}\rangle \tag{2.10}$$

Derived from eq. 2.8, 2.9 and 2.10 is one of the most significant results of the Drude-model, which is the linear relation of current density and applied electric field, know as ohm's law 2.11.

$$\vec{J} = \left(\frac{nq^2\tau}{m}\right)\vec{E} = \sigma\vec{E} \tag{2.11}$$

Equation 2.11 also holds for a time-varying electric field.

C Technical Documents

Technical description

The system measures the complex impedance of a specimen at a variable voltage and frequency. A Digital Signal Processing (DSP) unit generates a test signal with the desired frequency. This signal is amplified with an internal amplifier and then applied to the specimen. The voltage over and the current through the specimen are measured with high accuracy using a voltage divider and an electrometer.

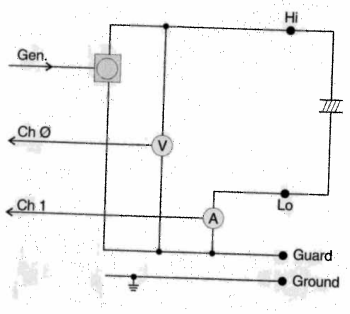

Schematic block diagram of the IDA 200-system.

For the measuring input, IDA 200 uses an advanced DSP unit that multiplies the input (measurement) signal with a reference sine voltage, and then integrates the results over a number of cycles. With this method, noise and interference is almost completely rejected - allowing IDA 200 to work with low voltage levels up to 200 V and still achieve high accuracy.

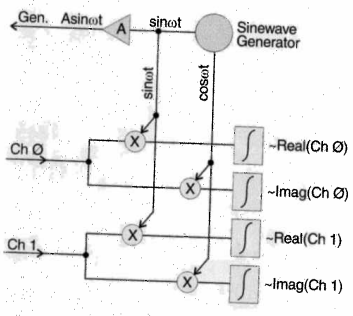

Principle of the sine correlation technique.

Specifications

General

Description	Portable, computerized insulation diagnostics system
Design	The instrument is intended for use in high-voltage substations and industrial environments
Measurement	Capacitance and dielectric losses in insulating materials at variable frequency
Application	Preventive maintenance - diagnostic measurements of electrical insulation in, eg: • Power transformers • Bushings • Instrument transformers • Cables

Measurement signal

Voltage / current	0 - 10 V_{peak} / 0 - 50 mA_{peak} (low range)
Voltage / current	0 - 200 V_{peak} / 0 - 50 mA_{peak} (high range)
Frequency	1000 Hz* - 0.0001 Hz

* Upper frequency current limited

Measurement ranges

Capacitance

Range	10 pF - 100 µF

Dissipation factor

Range	0 - 10 (with retained accuracy of capacitance - otherwise higher)

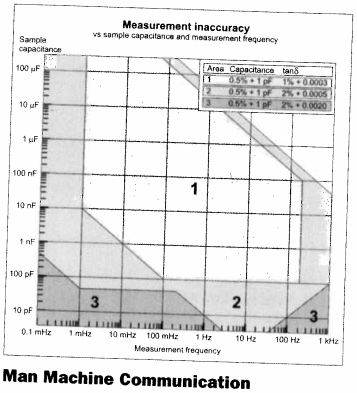

Man Machine Communication

IDA 200 includes an integrated PC and proprietary IDA 200 application software based on a Windows embedded NT platform.

Display screen	16 cm (6.4") TFT Color Monitor
Mouse / Keyboard	Included as standard accessory
Floppy Disk Drive	1.44 MB
USB port	For external keyboard
Ethernet	
Serial port	RS232
Parallel port	
Analog video port	SVGA

Figure 3.2: Technical specifications for IDA-200

EPOXY TECHNOLOGY

EPO-TEK® E4110

Technical Data Sheet

For Reference Only

Electrically Conductive, Silver Epoxy (formerly EP110)

Number of Components:	Two
Mix Ratio By Weight:	10:1
Specific Gravity:	
Part A	3.10
Part B	0.95
Pot Life:	4 Hours
Shelf Life:	One year at room temperature

Minimum Bond Line Cure Schedule*:

150°C	15 Minutes
100°C	1 Hour
80°C	3 Hours
60°C	6 Hours
23°C	3 Days

A heat cure is recommended to achieve optimum properties.

*Note: Container(s) should be kept closed when not in use. For filled systems, mix the contents of Part A thoroughly before mixing the two parts together. *Please see Applications Note available on our website.*

Product Description:

EPO-TEK® E4110 is an electrically conductive, silver-filled epoxy paste. This two component system is designed for low temperature curing from ambient to 80°C, although other heat cures can be used.

EPO-TEK® E4110 Advantages & Application Notes:

- Ease of use: smooth flowing paste allows for automated dispensing, stamping, brushing, or hand applications. In some cases, the low viscosity nature of the paste allows it to be sprayed onto targets.
- Suggested applications include: EMI and Rf shielding, ITO interconnects in LCDs, low temperature cryogenic cooling.
- Exhibits superior adhesion to a wide variety of substrates including most metals, ceramics, glass and plastics.
- Hybrid / Micro-electronic adhesive including die-attach and substrate attach for Rf and Microwave devices.
- Bright and shiny silver epoxy; provides a metallic-like layer after cure.

Typical Properties: *(To be used as a guide only, not as a specification. Data below is not guaranteed. Different batches, conditions and applications yield differing results; Cure condition: 150 °C/1 Hour ; * denotes test on lot acceptance basis)*

Physical Properties:	
*Color: Part A: Silver Part B: Clear/Colorless	Weight Loss:
*Consistency: Smooth flowing paste	@ 200°C: 0.70%
*Viscosity (@ 100 RPM/23°C): 800 – 1,600 cPs	@ 250°C:
Thixotropic Index: 2.1	@ 300°C:
*Glass Transition Temp.(Tg): ≥ 40°C (Dynamic Cure 20—200°C /ISO 25 Min; Ramp -10—200°C @ 20°C/Min)	Operating Temp:
	Continuous: - 55°C to 150°C
Coefficient of Thermal Expansion (CTE):	Intermittent: - 55°C to 250°C
Below Tg: 48 x 10^{-6} in/in/°C	Storage Modulus @ 23°C: 518,756 psi
Above Tg: 150 x 10^{-6} in/in/°C	Ions: Cl^- 151 ppm
Shore D Hardness: 60	Na^+ 23 ppm
Lap Shear Strength @ 23°C: 1,266 psi	NH_4^+ 23 ppm
Die Shear Strength @ 23°C: ≥ 5 Kg / 1,700 psi	K^+ 31 ppm
Degradation Temp. (TGA): 380°C	*Particle Size: ≤ 45 Microns
Electrical Properties:	
*Volume Resistivity @ 23°C: ≤ 0.0005 Ohm-cm	
Volume Resistivity @ 23°C (25°C/40-60%RH/3 Day cure): ≤ 0.007 Ohm-cm	
Thermal Properties:	
Thermal Conductivity: 1.37 W/mK	

EPOXY TECHNOLOGY, INC.
14 Fortune Drive, Billerica, MA 01821-3972 **Phone**: 978.667.3805 **Fax**: 978.663.9782
www.EPOTEK.com

Epoxies and Adhesives for Demanding Applications™

Rev. VII
Mar 2011

Figure 3.3: Data sheet for EPO-TEK E4110 conductive silver epoxy